A STUDY OF ISOELECTRONIC DEFECTS IN Si UNDER UNIAXIAL STRESS AND MAGNETIC FIELDS

by

Simon P. Watkins

B.Sc. Queen's University, 1980

M.Sc. Simon Fraser University, 1984

THESIS SUBMITTED IN PARTIAL FULFILLMENT OF
THE REQUIREMENTS FOR THE DEGREE OF
DOCTOR OF PHILOSOPHY

in the Department
of
Physics

SIMON FRASER UNIVERSITY

July 1986

Approval

Name: Simon P. Watkins

Degree: Doctor of Philosophy

Title of thesis: A Study of Isoelectronic Defects in Si Under Uniaxial Stress and Magnetic Fields

Examining committee:

Chair: Dr. D. Boal

Dr. M.L.W Thewalt
Senior Supervisor

Dr. J.C. Irwin

Dr. M. Plischke

Dr. B.P. Clayman

Dr. John Brebner
External Examiner
Professor of Physics
University of Montreal

Date approved: July 4, 1986

PARTIAL COPYRIGHT LICENSE

I hereby grant to Simon Fraser University the right to lend my thesis, project or extended essay (the title of which is shown below) to users of the Simon Fraser University Library, and to make partial or single copies only for such users or in response to a request from the library of any other university, or other educational institution, on its own behalf or for one of its users. I further agree that permission for multiple copying of this work for scholarly purposes may be granted by me or the Dean of Graduate Studies. It is understood that copying or publication of this work for financial gain shall not be allowed without my written permission.

Title of Thesis/Project/Extended Essay

A Study of Isoelectronic Defects in Silicon

Under Uniaxial Stress and Magnetic Fields

Author:

(signature)

Simon Watkins

(name)

31 July 86

(date)

Abstract

The photoluminescence spectra of isoelectronic bound excitons in quenched In- and Tl-doped Si are studied under uniaxial stress and magnetic fields. A tunable infrared laser system consisting of a dye laser-pumped optical parametric oscillator has been constructed, and used in conjunction with stress and Zeeman measurements to explain the excited state spectrum of the In-related photoluminescence emission. These excitons show several unusual features, including a configurational bistability, and a complete quenching of the hole orbital angular momentum for the case of one of the configurations. The binding centre symmetries and the detailed nature of the electronic states of the excitons are revealed by these data. A tentative model is proposed for the origin of the bistable behaviour.

TABLE OF CONTENTS

LIST OF TABLES

LIST OF FIGURES

List of Abbreviations

Abbreviation		Defining page
HTL	Hopfield, Thomas, Lynch	5
IBE	Isoelectronic bound exciton	1
OPO	Optical parametric oscillator	37
PL	Photoluminescence	1
PLE	Photoluminescence excitation	11

ACKNOWLEDGEMENTS

I would like to thank my supervisor Dr. Mike Thewalt for his support, encouragement, and guidance throughout this project. This work was supported by a grant from the National Sciences and Engineering Research Council of Canada (NSERC), obtained by Dr. Thewalt. I am indebted to NSERC for a post-graduate scholarship, and to Simon Fraser University for an Open Graduate Scholarship.

I am indebted to Sara Swenson for her encouragement and moral support, as well as for her help with some of the figures.

Chapter 1: Introduction

1.1: Overview

Isoelectronic impurities in semiconductors have been of great interest from both a technological and purely physical point of view. On the technological side, such defects are responsible for the intense electroluminescent emission exploited in commercially available visible light emitting diodes. A simple example of an isoelectronic dopant, and one which is used in such devices is N substituting for P, denoted N_p, in GaP or $GaAs_{1-x}P_x$. Since N has the same outer valence electron structure as P, all bonds to the neighbouring Ga atoms are satisfied, and it does not introduce an electrically active level in the usual manner familiar from shallow donors or acceptors, e.g. P or B in Si. Nevertheless, N produces a large perturbation in the GaP lattice, due to its considerably smaller atomic radius and its different atomic core structure. At low temperatures, ($T<100$ K) N is capable of binding an electron-holeh pair, or exciton by virtue of the short-range non-Coulombic potential which it introduces. The resulting bound state is called an isoelectronic bound exciton (IBE).

A convenient way to study the properties of IBE is the method of photoluminescence (PL) spectroscopy. In this technique electron-hole pairs are generated by light of a fixed energy, usually greater than the bandgap, and are rapidly captured onto the isoelectronic binding centres in a time scale of

less than a nanosecond. The recombination of the IBE generates a photon spectrum which is characteristic of a given impurity centre, and is analyzed by a spectrometer-photodetector system.

In addition to the single atom isoelectronic impurities such as GaP:N, and ZnTe:O, there exists a much larger class of defect "complexes" consisting of two or more constituents, which do not introduce extra carriers in the sense of Si:P, but which are similarly capable of binding an exciton. In some cases, for example Cd_{Ga}-O_P pairs in GaP, the short range potential introduced by the defect is sufficiently strong to bind an isolated electron or hole, in addition to the ability to bind an exciton. In other cases, the short range potential is too weak to bind a single particle, but the effects of electron-hole correlations and possible strain contributions to the binding energy, which are attractive to both particles, can result in the existence of a bound state for the exciton as a complete entity.

It is of interest from a physical point of view to determine the process whereby an isoelectronic defect binds free carriers without the benefit of the long-range Coulombic potential typical of simple donors and acceptors. Such questions belong to the study of so-called "deep" defects, in which highly localized interactions with a range of the order of a lattice constant, are responsible for the binding process (see e.g. Jaros, 1982). This is in contrast to the case of so-called shallow levels in which the binding processes are predominantly Coulombic and long-ranged, and the bound states are delocalized over several tens of lattices constants. Examples include the

shallow substitutional donors and acceptors e.g. Si:P, Si:B, GaP:Cd, and GaP:Te.

Prior to 1979, most of the work on isoelectronic defects involved the host lattice GaP (see Dean and Herbert, 1979). No examples had been reported in Si. Indeed, it was believed from simple theoretical arguments that there could be no bound states for any of the simple single-atom substitutional defects such as Si:C or Si:Sn, in agreement with experiment. Since 1979, however, a multitude of PL lines in Si have been shown to originate from multi-atom isoelectronic complexes. In many cases the exact nature of the constituents of these defects remains unclear.

This thesis details the study of two closely related isoelectronic defect complexes in Si associated with the deep acceptors In and Tl and some other as yet undetermined constituent(s). These two defects have been the subject of considerable phenomenological study since 1981 and 1982 respectively, but until the present work no specific model had been proposed for the nature of the electronic states. The work consists of two main sections. First the ground state spectrum of both the Si:In and Si:Tl defects is studied by means of conventional PL spectroscopy using above bandgap optical excitation in conjunction with uniaxial stress and magnetic field perturbations. These data give the symmetries of the defects responsible for the exciton binding in both cases. The Si:Tl centre is of particular interest from a basic physics point of view since it possesses the unique feature of existing in either of two

metastable configurations, each with a distinct spectral signature. The stress and Zeeman data show that these two configurations of the Si:Tl centre have completely different symmetries wwich give rise to the very different spectral properties. These data are used to show that, contrary to prior assertions (Sauer and Weber,1983), the exciton ground state splittings can be understood in terms of conventional models of isoelectronic bound excitons. An interesting feature of these excitons however is the effect of the low symmetry crystal defect field on the hole states, in particular the "quenching" of the hole orbital angular momentum in the case of the low energy configuration of the Si:Tl defect and the Si:In defect. In addition there is evidence for a weak Jahn-Teller effect in the high energy configuration of the Si:Tl defect, an unusual result for a bound exciton in a material with such a small bandgap.

The second main focus of the thesis concerns the construction and application of a tunable laser source for resonantly exciting the higher lying electronic states of the In-related IBE. These excited states are inaccessible to conventional PL with fixed energy excitation due to thermalization effects. The excited state spectrum of the In-related IBE had been previously observed by other workers (Wagner and Sauer, 1983) but no model was proposed to explain the apparently anomalous spectrum. In this work, the additional application of uniaxial stress and magnetic field perturbations in conjunction with tunable excitation are used to explain the excited state

spectrum. The data imply an impurity potential which is attractive to both electrons and holes, consistent with a charge independent "strain well" binding mechanism superimposed on a highly localized hole-attractive impurity potential.

Finally, a simple model for the bistable behaviour of the Si:In and Si:Tl isoelectronic defects is presented, based on the results of the Zeeman and stress data.

1.2: Isoelectronic binding mechanisms

The physical process whereby an electrically neutral defect in a semiconductor, for example N_p in GaP, can bind an electron-hole pair, to form an IBE, has motivated a great deal of study in past years. The simplest model, due to Hopfield, Thomas, and Lynch (1966) (HTL), assumes that such defects introduce a short-range potential which binds one of the particles in a highly localized state, with the other bound in turn by the Coulombic potential introduced by the primary particle. In this model the defect was referred to as an isoelectronic donor or acceptor depending on whether the loosely bound secondary particle was an electron or a hole. This picture essentially treats the last bound particle as a single particle state. Fig. 1.1 shows a simple energy level representation of the HTL model. The zero of energy E_c is taken to be the bare defect with no exciton, and is called the crystal ground state. The energy of a free electron and hole at infinite separation is given by the bandgap energy E_g. $E_g - E_{ex}$

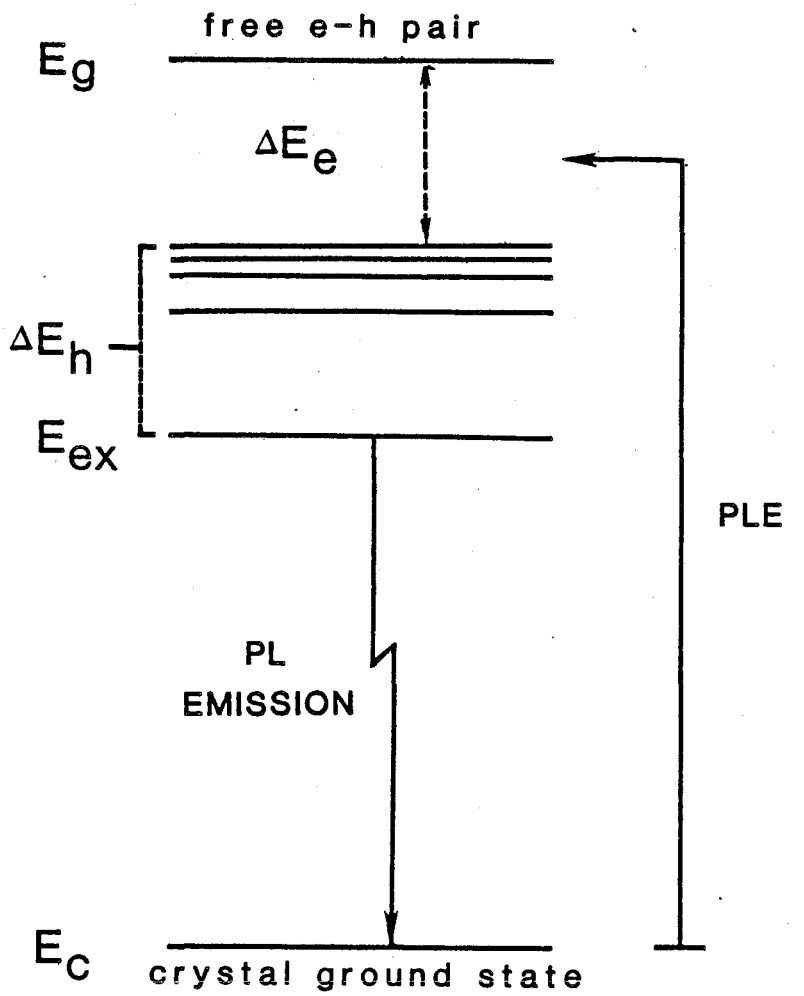

Fig.1.1: Energy level representation of an isoelectronic acceptor in the HTL model. For an isoelectronic donor, e and h are interchanged. E_c is the crystal ground state energy in the absence of an exciton. The energy of an electron-hole pair at infinity is given by the bandgap energy E_g, referred to the crystal ground state. E_g-E_{ex} represents the energy which the e-h pair loses by being captured on the isoelectronic impurity. E_{ex} is the energy of the photons measured experimentally in PL. ΔE_e represents the binding energy of the tightly bound electron. ΔE_h is the energy of the loosely bound hole, bound to the Coulomb field of the primary particle. In photoluminescence excitation (PLE) spectroscopy the PL emission is measured at E_{ex} as the excitation energy is tuned across the various excited state transitions with a tunable laser.

represents the binding energy of an exciton at the defect. $\Delta E_{h(e)}$ is the binding energy of the loosely bound hole(electron) to the tightly bound primary particle which has a single particle binding energy $\Delta E_{e(h)}$.

It is not the case that every isoelectronic trap can bind a single particle. GaP:N_p is a system which has been the subject of considerable theoretical and experimental work. It represents in many ways the epitome of the "deep" defect. In the simplest approximation, the N_p impurity potential is given by the difference between the unscreened core potentials for isolated N and P. Faulkner (1968) showed that this results in an electron-attractive potential with a predicted binding energy of ~1 eV, in complete disagreement with experiment. Indeed, while it is well known that N_p can bind an exciton, it is not clear whether a bound state exists for an isolated electron.

A more sophisticated approach, used by Jaros and Brand (1979) includes the effects of screening, by means of Green's function techniques. This has the effect of greatly reducing the binding energy from that of Faulkner, although the exact binding energy depends on the specific assumptions about the form of the impurity potential. The impurity potential is localized to the order of 0.1 nm, with the result that k-states from a wide region of the Brillouin zone are admixed into the wavefunction. In addition, their calculations show that the binding energy is considerably reduced when contributions from the lower lying s-like valence bands, and higher order conduction bands are included.

While efforts to observe the binding of an isolated electron at GaP:N_p have proved fruitless, direct evidence for such binding has been given in the case of GaP:Bi_p. From a simple comparison of the unscreened core potentials of Bi and P one expects a large isolated hole binding energy of the order of an eV, similar to the magnitude of the electron binding energy expected in the case of N_p. In this case however, it turns out that the effects of screening and the band structure effects observed by Jaros and Brand for the case of N_p do not completely cancel out the very large core potential, with the result that a single hole binding energy of 38 meV is observed (Dean et al., 1969). This value was deduced from the observation of luminescence due to the recombination of isolated holes bound to the Bi_p defects with electrons from deliberately introduced Te_p donors, whose binding energy is accurately known.

In addition, Bi can bind an exciton (Trumbore et al., 1966) with a binding energy of 107 meV relative to the GaP bandgap at 4.2 K. The energy gained in binding the extra electron is thus ~69 meV. This is of the order of the total exciton binding energy, and electron-hole correlation effects are thus expected to be large. In this case it is meaningless to talk about a single particle electron binding energy as envisioned in the HTL model.

It would appear from the above two examples that extreme differences between the host lattice and impurity core potentials are required in order to produce single particle bound states at simple substitutional impurities. In practice

however, by far the majority of isoelectronic defects observed to date in GaP, and all of the cases in Si belong to the class of multiatom "isoelectronic" complexes such as GaP:Cd_{Ga}-O_p and GaP:Zn_{Ga}-O_p. Such complexes are electrically neutral and introduce no free carriers, and are also referred to as isoelectronic defects. Substitutional O_p is known to introduce a very deep donor level with an electron binding energy of 895.5 meV (Dean et al., 1968). The presence of a nearest-neighbour Cd_{Ga} or Zn_{Ga}, which are shallow acceptors, greatly reduces the binding energy of O_p by an energy roughly given by $e/\varepsilon a_o$ where ε is an effective dielectric constant, and a_o is the equilibrium bond length of the Cd-O or Zn-O complex. The above energy can be thought of as the Coulomb interaction energy of the nearest neighbour Cd-O or Zn-O pair, which are essentially ionized donor-acceptor pairs. Consider a distant Cd_{Ga}-O_p donor-acceptor pair with no carriers bound at either impurity. The electrostatic energy of this configuration decreases with decreasing pair separation. If an electron is bound at the O_p, the electrostatic interaction is zero. The difference in total energy between this case and the case of the bare donor-acceptor pair is the binding energy of an electron at a Cd_{Ga}-O_p pair which can be seen to be a minimum for the nearest-neighbour case.

These two centres are known to bind an isolated electron because of the observation, similar to the case of GaP:Bi, of luminescence due to the recombination of electrons bound to the complexes, with holes bound to isolated Cd or Zn acceptors. In the case of Zn-O the electron binding energy, E_e is reduced from

the 895.5 meV value for O_p to 282 meV. In addition, Henry et al. (1968) have shown that this centre can bind an exciton with additional gain of 35 meV in binding energy, which is very close to the 40 meV binding energy of a shallow acceptor in GaP.

In the above case the 35 meV increase in binding energy associated with the capture of the hole is essentially the acceptor binding energy, E_h of a hole bound to the "point charge" distribution generated by the highly localized electron. Since the electron is highly localized by the Cd-O or Zn-O potential, and the hole is diffusely bound to this localized charge distribution, there is relatively little overlap of the electron and hole wavefunctions, and correlation effects are expected to be small. The excited state spectrum should resemble the well known hydrogenic series of nS-like excited states for a substitutional acceptor (see e.g. Ramdas and Rodriguez, 1981). This is indicated schematically in Fig. 1.1 by the Rydberg-like series of excited states converging to an energy ΔE_h above the exciton ground state. In practice, this is not observed in the case of Cd-O or Zn-O (Henry et al., 1968), presumably because phonon assisted transitions (Chapt. 1.1) have a much higher probability, due to the strong coupling of the exciton states to internal modes of the complex, and to low energy transverse acoustic modes of the GaP lattice. The absorption measurements of Henry et al. showed only broad bands and anti-Stokes phonon replicas of the exciton ground state transitions in the region of the expected excited states.

The exciton excited state spectrum has been observed for

the case of near-neighbour N_p-N_p pairs in GaP. Thomas and Hopfield (1966) showed that for high N concentrations, exciton binding can occur at near-neighbour pairs, denoted NN_i where i denotes the ith nearest neighbour pair. In their model the binding energy of the exciton increases with decreasing pair separation, due to the increasing strength of the total central cell potential. In conventional PL measurements, a series of spectral peaks corresponding to the ground state exciton transitions of the various pairs is observed, converging to the isolated N_p exciton binding energy as $i \rightarrow \infty$. The excited states are not observable in PL due to rapid thermalization by the emission of acoustic phonons at 4.2 K.

Cohen and Sturge (1977) used photoluminescence excitation spectroscopy (PLE) to probe the higher-lying excited states of the individual pairs species. In this technique, the excited state spectrum of the NN_i pairs with $1 \leq i \leq 10$ was obtained by selectively monitoring the ground state PL emission from a given pair species, while scanning to higher energy with a tunable dye laser (Fig. 1.1). At liquid He temperatures, excitons which are created in an excited state by this technique thermalize to the ground state in a time that is short compared to the radiative lifetime, so that the PL emission intensity is directly proportional to the absorption strength of the transition being excited. Using the PLE method, the excited state spectrum for a given N_p-N_p pair could be unambiguously determined. Cohen and Sturge observed in each case a hydrogenic series of nS-like excited states, with n up to 8, converging to a limit of 34-40

meV above the ground state transition. This energy is close to the ~40 meV binding energy of holes to shallow acceptors in GaP, and was taken as evidence for the HTL model, with the electron as the tightly bound particle. The difference between the ionization limit of the hole, as determined from the series limit of the excited states, and the exciton ground state (see Fig. 1.1) was found to vary from 120 meV for the NN_1 centres to 5 meV for the NN_7 centres, and was likely zero for $i \geq 8$. The above difference in energy was interpreted by Cohen and Sturge within the HTL model as the binding energy of the isolated electron at the centre. It is important to realize that in the case when $E_e \sim 0$, electron-hole correlations must represent a large portion of the exciton binding energy, and the excited state spectrum being measured is no longer due to single particle excitations, but to excitations of the two particle system. It is therefore remarkable that there is so little change in the "hole" binding energies deduced by Cohen and Sturge over such a wide range of exciton binding energies.

Allen (1970) proposed a completely different model of the binding process for GaP:NN_i in which the exciton as a whole is bound to a single N, and the strain field generated by the second N lowers the binding energy by an amount proportional to a strain energy $-\beta r_i^{-1}$ where r_i is the pair separation, and β is a constant. This strain field would be attractive to both particles, since it produces a local splitting of both the conduction and valence band extrema. The significant mismatch in size between N and P is expected to give a large strain field

in the vicinity of the defect. Allen's model provided a remarkably good fit to the exciton ground state energies for i>1, although this may be regarded as somewhat fortuitous considering the simplifications used in obtaining the above form of the strain perturbation. Jaros and Brand (1979) have extended the methods of their GaP:N calculations to the case of the pairs, and find a significant increase of the binding energy of electrons to pairs with decreasing separation based on the screened core potential approach. The true physical picture is almost certainly a combination of the above two models. Clearly, given the tendency of screening and band structure effects to reduce the binding energy of isoelectronic systems, lattice effects such as strain fields can be expected to contribute significantly to the binding of IBEs. This has been borne out by recent work on low symmetry Cu-related IBE in GaP (Monemar et al., 1982; Gislason et al., 1982), and will be shown to be the case for the Tl- and In-related IBE in Si.

Davies (1984) has recently produced a model in which the binding potential of the exciton is simulated by an axial internal strain associated with the axial deformation produced by such low symmetry IBE binding centres. Finite binding energies are obtained regardless of the sign of the strain field generated. However, his model completely ignores the other sources of binding, and must be considered a strictly phenomenological description which is useful only for predicting the general form of the exciton ground state splittings.

Enhancement of binding energy due to lattice relaxation

Lattice relaxation refers to the rearrangement of the host lattice or defect constituents accompanying capture of a carrier or exciton. This effect is especially large for deep defects, in which a high degree of localization of the bound carrier charge density can cause substantial deformation after capture. In this case, the wavefunction contains both vibrational and electronic, (i.e. "vibronic") contributions. In the absence of degeneracy, in the Born-Oppenheimer approximation (see Stoneham, 1975), the total wavefunction is written as

$$\Xi(r,Q)=\Psi(r;Q)\chi(Q) \qquad [1.1]$$

where r is the electronic coordinate, and Q is a coordinate for nuclear motions, associated with the wavefunction $\chi(Q)$. The form of [1.1] permits a separation of the wave equation for $\Xi(r,Q)$ into an electronic equation, which is evaluated at a fixed Q, and a vibrational equation which depends only on Q. The potential energy term in the wave equation for $\chi(Q)$ can be visualized in terms of a configuration coordinate diagram (Fig. 1.2). This represents the sum of the defect's vibrational potential energy, and the electronic energy evaluated at a fixed value of Q, plotted as a function of Q.

A simple example can be given to illustrate a mechanism for vibronic relaxation at isoelectronic defects. As discussed previously, the binding energy of the O_p donor in GaP is dramatically reduced by the presence of a nearest neighbour Zn_{Ga}

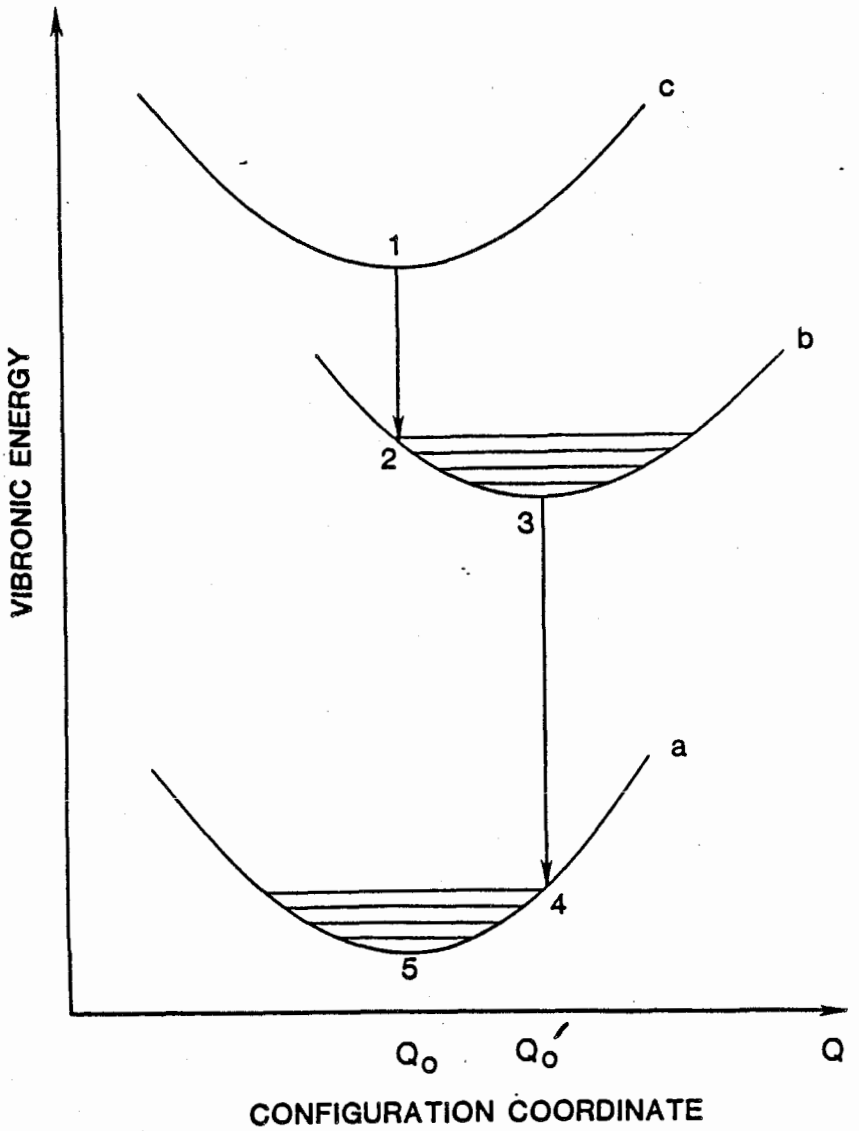

Fig. 1.2: Configuration coordinate diagram for a defect with strong vibronic coupling. In the case of exciton binding at an isoelectronic defect, the figure represents the electronic + vibrational energy surface for (a), the bare defect, (b), the bound exciton, and (c) the bare defect + free exciton. In the case where the isoelectronic defect can bind a single carrier, essentially the same curves apply, in which case (a), (b), and (c) are respectively the valence band, the trapping level, and the conduction band.

ion. Thus one expects the binding energy of the electron at a Zn-O complex to be extremely sensitive to axial displacements of the pair (Jaros and Brand, 1976). In the absence of an electron, the pair separation can be described by a vibronic energy surface (Fig. 1.2a) with an equilibrium coordinate Q_o which is determined by the balance of the Coulomb attraction of the oppositely-charged pair components, and the restoring force of the lattice. When an electron is localized at the defect, the Coulomb forces are considerably altered. The electron binding energy can be increased by a dilation of the pair bond length, but at the eventual cost of increased vibrational potential energy. The new vibronic energy surface will in general be displaced to some new coordinate, Q_o' (Fig. 1.2b). In the case of the Zn-O bound exciton, the above description is essentially unchanged, since the hole wavefunction is much more diffuse, and should not couple appreciably to the pair motions.

For the moment assume that the energy surface labelled (c) in Fig. 1.2 represents the vibronic energy of the free exciton + defect. Since the free exciton states are delocalized, this is identical to the curve for the bare binding centre (a) but shifted up by the free exciton formation energy. From Fig. 1.2 and the above discussion it is clear that a considerable portion of the binding energy of a free exciton at the defect can derive from vibrational relaxation. According to the Frank-Condon approximation (see Stoneham, 1975), capture of a free exciton at point 1 in Fig. 1.2 occurs with no change in the coordinate $Q=Q_o$. Subsequent to capture, the system relaxes to

the new equilibrium position, Q_o' by emitting S phonons of energy $\hbar\omega=(E_2-E_3)/S$ where S is the Huang-Rhys factor (see Stoneham, 1975).

It is important to realize that the energy $S\hbar\omega$ can represent a large fraction of the total binding energy. In some cases there can be no binding in the absence of relaxation and the exciton is essentially "self-trapped" (Toyazawa, 1983).

Since the configuration-coordinate surfaces for (c) and (a) are identical, S is also given by the energy $(E_4-E_5)/\hbar\omega$ in Fig. 1.2. S can therefore be determined from the lineshape of the exciton luminescence, which corresponds to optical transitions from (b) to (c). The horizontal bars in Fig. 1.2 represent the allowed phonon modes on a given surface. At liquid He temperatures all the excitons thermalize to the lowest (m=0) vibronic level on curve (b). The probability of decay of the exciton to the vibronic states in (a) is proportional to an electronic matrix element, multiplied by a factor which is proportional to the overlap of the initial (m=0) and final vibrational wavefunctions $\chi_i(Q)$ and $\chi_f(Q)$. The transition from the m=0 initial state to the m=0 final state is called the no-phonon transition. This line is typically very sharp, with a linewidth of 0.2 meV or less at liquid He temperatures, and permits a very accurate determination of the exciton ground state. In addition, one observes a series of broader Stokes phonon replicas of the no-phonon transition at lower energy. The excess vibrational energy of the final states in these transitions is rapidly dissipated by coupling to lattice

phonons, resulting in an appreciable broadening compared with the no-phonon transition. The strength of the Stokes phonon sideband is a direct measure of the strength of the vibronic coupling of the exciton to the defect coordinates. In the limit of strong vibronic coupling, the ratio of the no-phonon line to the total contribution from transitions to the $m \geq 0$ final states is given by

$$\frac{I_{n.p.}}{I_{total}} = e^{-S} \qquad [1.2]$$

In this limit the radiative lineshape function reduces to a Gaussian centred on the energy $(E_4-E_5)-S\hbar\omega$ (Fig 1.2b). For the GaP:Zn-O IBE, one obtains $S\hbar\omega \sim 190$ meV from the position of the maximum of the phonon assisted sideband observed in PL relative to the no-phonon line position (Henry et al., 1968). Thus, of the 282 meV exciton binding energy, over half is due to vibrational relaxation.

1.3: Breakdown of crystal momentum conservation

In above analysis, the phonon coupling was oversimplified by assuming coupling to local internal modes of the defect only. In an indirect gap semiconductor however, there is an additional complication due to the fact that the conduction band minima and the valence band maxima do not occur at the same value of crystal momentum $\underline{k}$. This reduces the effective electronic transition probability in the above analysis, compared with the

case of direct gap semiconductors.

Si and GaP are both indirect gap semiconductors, with respective conduction band minima at 0.85 and ~1.0 times the first Brillouin zone boundary wave vector, located along the ⟨001⟩ direction. For Si there are six equivalent minima, whereas for GaP this is reduced to three because the minima are at or very close to the zone boundary. Recombination of an electron at the conduction band minimum with a hole at the k=0 valence band maximum must be accompanied by the emission of a momentum-conserving phonon, with a subsequent reduction in the recombination energy of the order of 10 to 60 meV in Si, determined by the particular branch to which the phonon belongs. At liquid He temperatures, the dominant radiative decay channel for carriers in crystalline Si with very low impurity concentrations ($<10^{14}$ cm^{-3}) is the free exciton, which consists of an electron-hole pair weakly bound by virtue of their Coulomb interaction with a binding energy of 14 meV. In the free exciton the electron and hole are quite localized in k-space to the conduction and valence band extrema. The requirement that a momentum-conserving phonon be emitted upon recombination has the effect of greatly reducing the radiative transition probability of free excitons in indirect gap semiconductors compared with direct gap materials such as GaAs or InP.

When an exciton is bound to an isoelectronic defect, the high degree of real space localization of one of the particles results in a breakdown of this crystal momentum conservation condition because the wavefunction is no longer made up solely

of k-states derived from the band extrema. The calculations of Jaros and Brand (1979) indicate that the admixture of k=0 conduction band states for the GaP:N electron level is as high as 10% of the value at the band minimum. The small but significant overlap of the k-space wavefunctions of the electron and hole greatly enhances the radiative recombination rate compared with that of intrinsic processes like the free exciton. This effect is responsible for the high efficiencies of GaP:N electroluminescent displays. A characteristic signature of IBE optical spectra is the presence of a strong zero phonon line, with negligible coupling to momentum conserving phonon modes. The dominant observed phonon modes are the local internal modes of the defect described above, and non-momentum conserving lattice phonons. The former are seen as fairly sharp discrete replicas of the zero-phonon transitions, while the latter are observed as broad bands which generally reflect the lattice phonon density of states.

The case of IBE should be contrasted with that of excitons bound to neutral donors or acceptors. In this case the binding mechanism is largely Coulombic and therefore long-ranged. For example, the P donor bound exciton in Si:P consists of two electrons and a hole localized around the long-ranged 1/r Coulomb potential of the positively charged P ion. The exciton states are considerably more delocalized than the primary particle in an IBE, with the result that the k-space wavefunctions are largely confined to the minima. A small zero phonon line is observed for these excitons due to the small k=0

tails of the electron state wavefunctions, but it is often weaker than the momentum-conserving phonon replicas.

1.4: Effects of stress and Magnetic fields

Stress dependence

The effect of stress perturbations on the free electron and hole states of Si is well known (e.g. Laude et al., 1971). For shallow donors and acceptors the treatment is very similar (e.g. Ramdas and Rodriguez, 1981) since these states are relatively localized in k-space near the band extrema. The effects of stress on deep states are much more difficult to calculate, since the stress dependence of different points in k-space is not well known and a detailed knowledge of the k-space distribution of the defect wavefunction is required. The usual approach with isoelectronic defects has been to treat the electron and hole states as in the shallow case, and to attribute differences in the observed deformation potentials to the deep nature of one of the particles.

In cubic crystals, such as Si or GaP, the lowest valence band is p-like and would be six-fold degenerate, including spin, in the absence of the spin-orbit interaction. The stress perturbation can be written quite generally in the form

$$V=\sum_{ij} A_{ij}\sigma_{ij} \qquad [1.3]$$

where σ_{ij} is the stress tensor and A_{ij} are experimentally determined constants. The effect of the above perturbation on the three p-states can be expressed by a 3×3 matrix (see e.g. Davies, 1984) which on symmetry grounds can depend on only three parameters in a cubic crystal. These are the a, b, and d deformation potentials of, for example, Laude et al. (1971).

In the absence of stress, the hole states are split into a four-fold (including spin) $j=\frac{3}{2}$ band and a two-fold $j=\frac{1}{2}$ split-off band, 44 meV higher in hole energy, by the spin-orbit interaction (Fig. 1.3). The eigenfunctions of the spin-orbit Hamiltonian, $\xi \underline{L}\cdot\underline{s}_h$ are linear combinations of the product states, $p_i\uparrow$ etc. In this basis it is straightforward to calculate the off-diagonal matrix elements of the above stress Hamiltonian. For small stresses along each of the three principal crystal axes the $j=\frac{3}{2}$ band splits with shift rates defined by the following relations (e.g. Chandrasekhar and Ramdas, 1975):

$$\Delta E_{001} = K_{001}T \quad , K_{001}=2b(S_{11}-S_{12})$$

$$\Delta E_{111} = K_{111}T \quad , K_{111}=\frac{d}{\sqrt{3}} S_{44} \qquad [1.4]$$

$$\Delta E^2_{110} = \frac{1}{4}(K^2_{100}+3K^2_{111})T^2$$

where S_{11}, S_{12}, and S_{44} are the non-zero compliance constants of Si, and T is the applied force per unit area along the direction indicated. Note that the response to <110> stress is determined

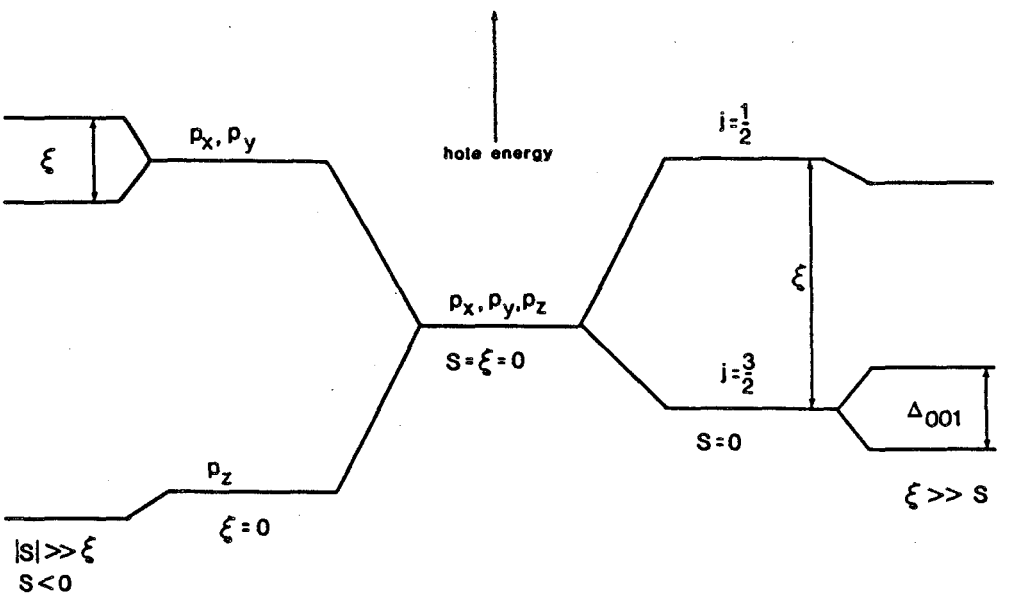

Fig. 1.3: Splitting of the hole states under ⟨001⟩ stress in two limiting cases. On the right is the splitting for the case in which the stress splitting energy Δ_{001} is much smaller than the spin orbit coupling energy, ξ. In this limit the hole states resemble those of the free hole $j=\pm\frac{1}{2}$ and $j=\pm\frac{3}{2}$ bands, but with the $j=\frac{3}{2}$ band split by an amount Δ_{001}. On the left is the case of a stress which is large compared to the spin-orbit energy, such that the lowest hole state is a single degenerate orbital p-state with a negligible spin-orbit admixture of the other two p-states.

by the response to tetragonal (<001>) and trigonal (<111>) stresses. While these splitting rates are quite different in principal, it turns out that for Si and GaP the small stress splittings are within 20% of each other regardless of the stress direction. In addition to the above splitting terms, there are also hydrostatic shifts of both valence bands which depend on the parameter a (see Laude et al.). The above expressions remain valid only in the limit $\xi >> \Delta$, for which case there is negligible mixing between the $j=\frac{1}{2}$ and $j=\frac{3}{2}$ valence band states. More general expressions have been derived by Chandrasekhar et al. (1975) for the case of large strains.

When the strain energy exceeds the spin-orbit coupling energy ξ, it is more convenient to think in terms of the p_i basis, with the spin-orbit interaction added as a perturbation. If for example, a large compressive stress is applied along the <001> axis, the p_z level is lowered with respect to the degenerate p_x and p_y levels. For sufficiently large splittings the spin-orbit interaction can no longer mix the p_x and p_y states with p_z, and the state of lowest energy is just the p_z state multiplied by a spin function (Fig. 1.3). This limit is not reached in practice for externally applied stresses, but it turns out that the internal strain field introduced by a defect, in conjunction with a possible reduction of the spin-orbit coupling energy at the defect, can produce the above situation. The implications of this result to IBE will be shown in Chapts. 4 and 5.

The conduction band minima of Si are s-like and lie along

the ⟨001⟩ axis, at 0.85 times the zone boundary wavevector. On symmetry grounds (see e.g. Ramdas and Rodriguez, 1981), the stress perturbation of a given band extremum depends on two parameters, the dilational and shear deformation potentials, labelled Ξ_d and Ξ_u. Subtracting a hydrostatic shift term which depends upon Ξ_d, one obtains the following expression (e.g. Tekippe et al., 1972):

$$\delta E_j = \Xi_u T(S_{11}-S_{12})(\hat{\underline{k}}_j \cdot \hat{\underline{T}}) \qquad [1.5]$$

where $\hat{\underline{k}}_j$ is a unit vector along the direction of the band minimum j, and $\hat{\underline{T}}$ is a unit vector in the direction of the applied force, and T is the magnitude of the applied force per unit area. T is negative for compressive stresses. Under a ⟨001⟩ stress, the bands shift by an amount

$$\delta E_{(1,2)} = -\frac{2}{3}T\Xi_u(S_{11}-S_{12})$$
$$\delta E_{(3,4,5,6)} = \frac{1}{3}T\Xi_u(S_{11}-S_{12}) \qquad [1.6]$$

where the indices 1 and 2 refer to the bands which lie along the stress axis.

The above shift rates describe the behaviour of free electron states. The case for bound electrons is complicated by the valley-orbit interaction. A shallow impurity such as P with a long ranged 1/r Coulomb potential can bind an electron in a hydrogenic orbit which extends over several tens of lattice constants. Because of the diffuse nature of such states, the

wavefunction is relatively localized to the k-space minima. However, the electron is no longer confined to one band since the impurity potential removes the full translational symmetry of the lattice and can scatter electrons among the six equivalent valleys. The six-fold degeneracy of the 1S-like donor state can be lifted by the T_d crystal field of a substitutional impurity in Si, and the ground state can split into levels which transform as the representations Γ_1, Γ_3, and Γ_5 in the notation of Koster et al. (1963), with degeneracies of 1, 2, and 3 respectively (Kohn and Luttinger, 1955). Spin has been excluded from the above discussion.

The ordering and energy splittings of the three valley-orbit states depend on the detailed nature of the binding potential, which is often poorly known. The details of the physical process responsible for the valley-orbit splittings are generally lumped into two experimentally determined constants equal to the matrix elements of the impurity potential with respect to the various valleys (see e.g. Wilson and Feher, 1961). For electron attractive central cell potentials, the totally symmetric Γ_1 state lies at lowest electron energy. The splitting of the Γ_3 and Γ_5 levels is usually small because these states vanish at r=0 where the impurity potential is strongest. In this case the splitting of the Γ_1 and $\Gamma_{3,5}$ states is given by $6\Delta_c$ where Δ_c represents the matrix elements of the impurity potential between any two of the conduction band valleys.

The valley-orbit eigenstates consist of different linear combinations of the six conduction band minima. Since the

stress dependence of these six bands is defined by [1.6] it is straightforward to obtain the stress dependence of the valley-orbit states (see Wilson and Feher, 1961).

For <111> stresses, all six bands are equivalent and there is no interaction between the Γ_1, Γ_3, and Γ_5 states, resulting in a linear shift rate. Under compressive <001> stress two of the bands are lowered with respect to the other four. This has the result of inducing mixing between the Γ_1 and Γ_3 levels resulting in nonlinear shift rates given by

$$\Delta E_{\Gamma_1} = \Delta_c[-2 + \frac{1}{2}x - \frac{3}{2}(x^2 + \frac{4}{3}x + 4)]^{1/2} \qquad [1.7a]$$

$$\Delta E_{\Gamma_3} = \Delta_c[-2 + \frac{1}{2}x + \frac{3}{2}(x^2 + \frac{4}{3}x + 4)]^{1/2} \qquad [1.7b]$$

where $x=\Xi_u s/6\Delta_c$, and s is the strain, given by $s=2(S_{11}-S_{12})T$, and the zero stress Γ_3 to Γ_5 splitting has been assumed equal to zero. For <110> compressive stress four of the bands are lowered with respect to the other two with the result that the shift rates are given by the above expression with the replacement $T \rightarrow -T/2$.

Exciton states

A simple approach to the modelling of axial IBE under stress was derived by Morgan and Morgan (1970) for the case of <111> oriented defects such as GaP:Cd-O. This model assumes that the exciton is composed of weakly interacting single particle electron and hole states that are essentially those of

shallow donors and acceptors, i.e. that they are derived from the conduction and valence band minima. The axial nature of the excitons was attributed to a small internal strain which was presumed to split the $j=\frac{3}{2}$ band into two bands at energies $\pm\varepsilon$ from the zero strain value. The electron states were assumed to belong to the nondegenerate Γ_1 valley-orbit state, and any mixing effects with higher electron states was neglected.

The fine structure of the exciton ground state was modelled by Morgan and Morgan in a phenomenological way without regard for the detailed mechanisms of exciton binding, or of the perturbations which result in the splittings. The model thus makes no predictions about absolute energy positions, but only about zero field and stress-induced splittings of the ground state. Residual dipole-dipole interactions, as well as the effects of correlation and exchange, between the the bound electron and hole were accounted for by a j-j coupling term of the form $-\Delta \underline{j}_h \cdot \underline{j}_e$ where $\underline{j}_h$ and $\underline{j}_e$ are the hole and electron total angular momentum operators respectively. This term is often loosely referred to as the "exchange interaction" term. If we neglect the defect strain field splitting ε then, assuming spherical symmetry, the exciton eigenstates produced by the above term are just the eigenstates with total angular momentum J=1 and 2. j-j coupling causes the J=1 and J=2 states to shift by $+\frac{3}{8}\Delta$ and $-\frac{5}{8}\Delta$ respectively relative to the unperturbed exciton energy (Fig. 1.4). Dipole selection rules imply that transitions from the J=2 level to the crystal ground state are dipole forbidden, while transitions from the J=1 level are dipole

allowed.

In the basis of the product states $|m_e, m_h\rangle$, where m_e and m_h are the magnetic substates of the total orbital angular momentum for the electron and hole states respectively, the complete zero-stress Hamiltonian is of the form (Morgan and Morgan, 1970; Gil et al., 1982):

$$
\begin{array}{c}
\begin{array}{cccccccc}
|\frac{1}{2},\frac{3}{2}\rangle & |\frac{1}{2},\frac{1}{2}\rangle & |\frac{1}{2},-\frac{1}{2}\rangle & |\frac{1}{2},-\frac{3}{2}\rangle & |-\frac{1}{2},\frac{3}{2}\rangle & |\frac{1}{2},\frac{1}{2}\rangle & |\frac{1}{2},-\frac{1}{2}\rangle & |\frac{1}{2},-\frac{3}{2}\rangle
\end{array} \\
\left|\begin{array}{cccccccc}
-\frac{3}{8}\Delta-\varepsilon & 0 & 0 & 0 & 0 & 0 & 0 & 0 \\
0 & -\frac{1}{8}\Delta+\varepsilon & 0 & 0 & -\frac{1}{4}\sqrt{3}\Delta & 0 & 0 & 0 \\
0 & 0 & \frac{1}{8}\Delta+\varepsilon & 0 & 0 & -\frac{1}{2}\Delta & 0 & 0 \\
0 & 0 & 0 & \frac{3}{8}\Delta-\varepsilon & 0 & 0 & -\frac{1}{4}\sqrt{3}\Delta & 0 \\
0 & -\frac{1}{4}\sqrt{3}\Delta & 0 & 0 & \frac{3}{8}\Delta-\varepsilon & 0 & 0 & 0 \\
0 & 0 & -\frac{1}{2}\Delta & 0 & 0 & \frac{1}{8}\Delta+\varepsilon & 0 & 0 \\
0 & 0 & 0 & -\frac{1}{4}\sqrt{3}\Delta & 0 & 0 & -\frac{1}{8}-\Delta+\varepsilon & 0 \\
0 & 0 & 0 & 0 & 0 & 0 & 0 & -\frac{3}{8}\Delta-\varepsilon
\end{array}\right|
\end{array}
$$

Since at most two states are coupled in the above matrix, diagonalization is trivial. For a tensile defect strain field, i.e. for $\varepsilon>0$, the lowest lying exciton state is the $|\frac{1}{2},\pm\frac{3}{2}\rangle$ state. The other states are mixtures of the basis states used in the above matrix. The exact eigenvalues are given in Fig. 1.4 together with the levels to which they correspond. In the $|J,m_J\rangle$ basis, m_J remains a good quantum number, as shown in Fig. 1.4. In this representation, the ground state is the $|2\pm2\rangle$ substate from which transitions to the crystal ground state remain dipole forbidden. Transitions from the next lowest

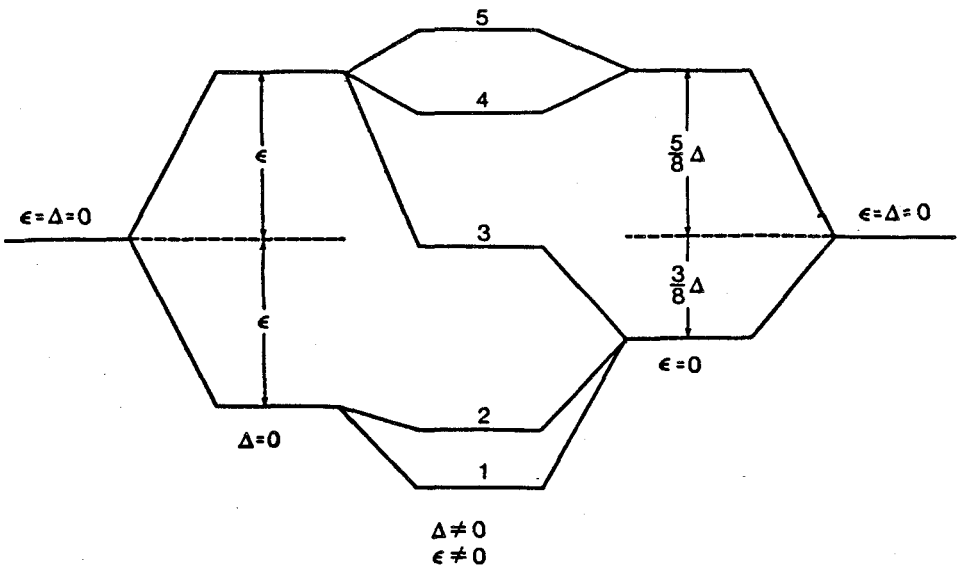

	Exciton state	Energy
(5)	$\|1,0\rangle$	$\varepsilon + \frac{5}{8}\Delta$
(4)	$\|1,\pm1\rangle$	$\frac{1}{8}\Delta + (\varepsilon^2 - \frac{1}{2}\varepsilon\Delta + \frac{1}{4}\Delta^2)^{1/2}$
(3)	$\|2,0\rangle$	$\varepsilon - \frac{3}{8}\Delta$
(2)	$\|2,\pm1\rangle$	$\frac{1}{8}\Delta - (\varepsilon^2 - \frac{1}{2}\varepsilon\Delta + \frac{1}{4}\Delta^2)^{1/2}$
(1)	$\|2,\pm2\rangle$	$-\varepsilon - \frac{3}{8}\Delta$

Fig. 1.4: Zero field energy splittings for an exciton bound to axial defect with an internal strain splitting of the hole states, ε and an electron hole j-j coupling energy Δ. The energy eigenvalues are from Morgan and Morgan (1970) and refer to the $|J,m_J\rangle$ basis where J and m_J refer to the total exciton angular momentum.

state, the $|2,\pm1\rangle$ substate become partially allowed due to strain-induced admixture of the dipole allowed $|1,\pm1\rangle$ substate. These remarks apply in the case where vibronic coupling effects can be neglected, an assumption which is not always valid.

Gil et al. (1981) used the above technique to fit the zero field splittings of several of the NN_i pairs in GaP. They generalized the zero-applied-stress results of Morgan and Morgan to include the effects of a more general biaxial crystal field perturbation, such as exists in the case of centres with C_{2v} symmetry for example NN_1, for which case the strain component of the above matrix is no longer diagonal. Another defect to which the above approach has been applied is the axial isoelectronic defect GaP:Li-Li-O (Dean, 1971).

The above matrix is useful in the case in which the internal strain energy ε is small compared with the spin-orbit interaction energy, ξ . When this is no longer true, the approximation that the higher-lying $j=\frac{1}{2}$ split-off valence band states can be neglected is no longer valid (Fig. 1.3, right side). Davies (1984) has generalized the above treatment to include these states. The inclusion of the split-off hole states involves the addition of 4 extra basis states, and necessitates the solution of a 12×12 matrix.

Since the behaviour of the hole states under externally applied stress is determined by [1.3] it is straightforward to generalize the above matrix and Davies' expanded version (1984) to the case of external stress. In all of these analyses, the internal and externally applied stresses are assumed to be

uniform and linearly additive. The deformation potentials are entered as adjustable parameters, but must clearly not differ much from the shallow donor and acceptor values for the assumptions of the model to remain valid.

It is worth pointing out that the above formalism is rather incompatible with the standard HTL description of isoelectronic binding in which one of the particles has large amplitudes at points in k-space away from the band extrema, and is more in line with a longer-ranged process such as Allen's strain field model (1972).

In cases where there is a definite breakdown in the k-space localization assumption for one or both particles, the form of the stress dependence of the exciton as a single entity can be argued on symmetry grounds. The following example illustrates this technique and will be useful for discussing the later stress data. Take the case of a nondegenerate Γ_1 exciton ground state derived from a totally symmetric Γ_1 electron and hole, neglecting spin. In this case the stress dependence of the full exciton state can be written in the form [1.3]. Suppose the defect symmetry is C_{2v}, corresponding say to a second-nearest-neighbour substitutional impurity pair aligned along a ⟨110⟩ axis. The symmetry operations of such a defect consist of a two-fold axis Z along a ⟨001⟩ or equivalent direction, and two reflection planes whose normals, labelled X and Y, are perpendicular to that axis and lie along the ⟨110⟩ and ⟨1$\bar{1}$0⟩ or equivalent axes. There are six equivalent orientations of such a defect in an unstrained cubic host lattice.

Under external stress some of these orientations become inequivalent. The stress is then said to have removed the six-fold orientational degeneracy of the defect. For ⟨111⟩, ⟨110⟩, and ⟨001⟩ stresses there are respectively two, three, and two inequivalent classes of defects.

The stress potential in [1.3] can be rewritten in the form

$$V = \sum_{\Gamma,r} A_{\Gamma r}\sigma_{\Gamma r} \qquad [1.9]$$

where the $\sigma_{\Gamma r}$ is the stress tensor component which transforms as the basis function r, of the irreducible representation Γ, of C_{2v}. The four representations of C_{2v} are one dimensional, and transform as the products $(X^2+Y^2+Z^2)$, XY, YZ, and XZ, where the coordinate axes are referred to the defect C_2 axis. [1.9] can therefore be written as

$$V = A_1\sigma_{XX} + A_1'\sigma_{YY} + A_1''\sigma_{ZZ} + A_2\sigma_{XY} + A_3\sigma_{YZ} + A_4\sigma_{XZ} \quad . \qquad [1.10]$$

The stress perturbations to the Γ_1 ground state are given by the matrix elements $\langle\Gamma_1|V|\Gamma_1\rangle$, and hence only the first three terms, which transform as Γ_1, will contribute a nonzero matrix element. Thus the stress splittings will depend on only three parameters. Transforming from the X, Y, Z coordinates of the defect to the x, y, z crystal coordinates, it is straightforward to show that the linear shift rates of the Γ_1 state under stresses along the three principal crystal axes are given by the values listed in

Table 4.1, in which the parameters A_i are linear combinations of the first three coefficients in [1.10]. Kaplyanski (1964) has compiled tables of such splitting rates for nondegenerate electronic states at low symmetry defects imbedded in cubic crystals. The above procedure is readily extended to cases with electronic degeneracy (Hughes and Runciman, 1967). The number of stress-split components together with the observed shift rates provide a useful way of unambiguously determining the defect symmetry.

Effects of magnetic fields

The treatment of the magnetic field perturbations on the exciton states is qualitatively similar to the above procedures. For a single electron the leading term in the Zeeman Hamiltonian is the linear term

$$H_{LZ} = \mu_B \underline{H} \cdot (\underline{L} + g_e \underline{s}_e) \qquad [1.11]$$

For the 1S donor states which will be of interest here, the orbital part does not contribute. For a many-valleyed indirect gap semiconductor like Si, the electron g-factor for a free electron or shallow donor is somewhat altered by band structure effects (e.g. Stoneham, 1975). For electrons in a single valley one obtains different g-factors $g_{\parallel}$ and $g_{\perp}$ for magnetic fields parallel and perpendicular to the direction of the valley, resulting in a slight anisotropy of the splittings. A 1S

valley-orbit state consists of an average over the six band edge states, with the result that the g-value is given by the isotropic value $g^*=(g_{\parallel}+2g_{\perp})/3$. In practice small deviations from the values obtained from the free electron data are observed in Si and GaP and have been attributed to the localization of the donor wavefunction.

The general treatment of the magnetic field perturbations on the band-edge hole states is very complicated due to the effects of the degenerate k=0 band extremum (Luttinger, 1955; Balderschi and Lipari, 1971). For the purposes of modelling the experimental data one can write down a simple linear Zeeman Hamiltonian similar to [1.11] of the form

$$H_{LZ}=\mu_B \underline{B}\cdot(\gamma \underline{L}+g_h \underline{s}_h) \qquad [1.12]$$

where the factor γ is an orbital angular momentum reduction factor, and g_h is the purely spin part, which should remain close to 2.0. The hole Bloch functions are derived from p-like orbitals, and hence even though the hole envelope function will in general be s-like, the $\underline{B}\cdot\underline{L}$ term will in general be non-zero for bound holes.

The factor γ can be reduced from unity in systems with strong vibronic coupling of the hole states. In such a case, the electronic states must be replaced by product states involving the vibrational functions. Ham (1965) has shown that the expectation value of electronic operators like $\underline{L}$ amongst the full vibronic basis functions can be significantly reduced in

the case of strong vibronic coupling to a degenerate mode. This effect is included in [1.12] as the reduction factor γ.

In addition to the reduction in γ, the orbital part of [1.12] can vanish if the low symmetry defect field is of sufficient strength and of the appropriate sign to ensure that the lowest hole state is a single p-state coupled with spin as discussed earlier (Fig. 1.3, left side). In this case, the expectation value of $\underline{L}\cdot\underline{B}$ is zero and the Zeeman splittings are those of a pure spin $\frac{1}{2}$ particle. This case will be discussed further in Chapters 4 and 5.

Chapter 2: Experimental Methods

2.1. Photoluminescence and data acquisition system

Much of the PL data acquisition apparatus has been described in some detail previously (Watkins, 1983; Steiner, 1986). The luminescence was usually detected with a Varian VPM159A photomultiplier tube cooled to -100°C. In addition, a liquid nitrogen-cooled intrinsic Ge detector (North Coast, E0817L) was available for these measurements. This detector does not suffer from the rapid drop in quantum efficiency of the photomultiplier beyond 1.2μm, but for shorter wavelengths it is considerably less sensitive than that device. Luminescence was dispersed by a 3/4 m Spex Czerny-Turner double spectrometer with 600 lines/mm gratings, blazed for 1 μm. The minimum energy resolution of this spectrometer was approximately 0.1 meV. In practice the useful resolution of the system was somewhat larger than this, due to a certain amount of jitter in the tracking of the grating mechanism. The photomultiplier signal was digitally processed in photon counting mode by means of the previously described experimental system (Watkins, 1983). The Ge detector signal was processed with standard lock-in amplification techniques.

The excitation source for the above gap PL measurements was a Spectra Physics 171 Ar ion laser. The 514.5 nm line was used for these measurements at a total power of no greater than 200 mW. For PLE measurements in the 1.0-1.2 μm region of Si, a

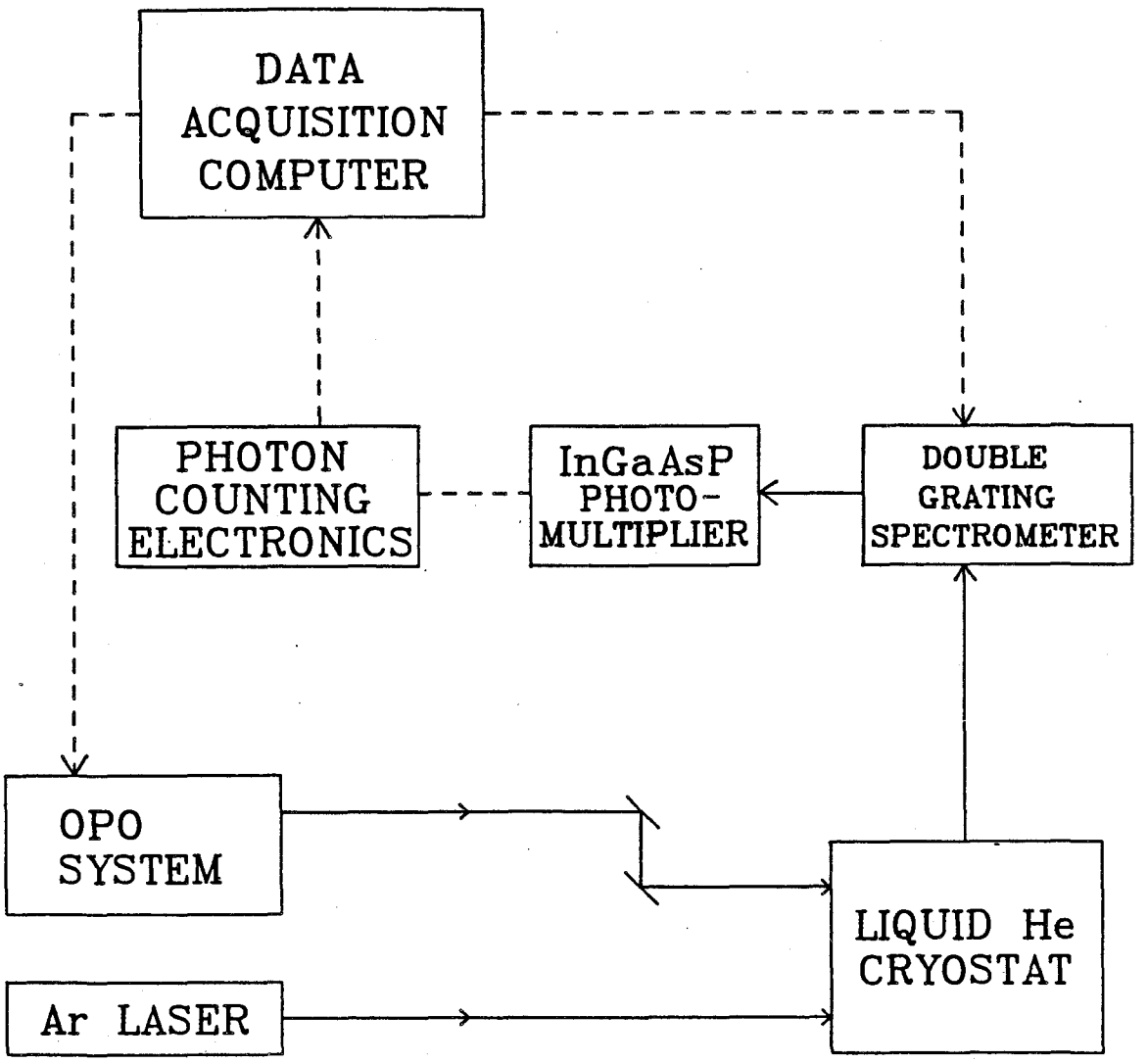

Fig. 2.1: Block diagram of the experimental apparatus employed in this study.

tunable optical parametric oscillator (OPO) system was constructed as a part of this study, the details of which will be given in Chapt. 2.4.

A custom-built computer system (see Steiner, 1986) provided the capability to do PL spectral scans, in which the wavelength of the spectrometer was advanced by a computer-controlled stepping motor. The system provided the ability to average successive spectra, in order to minimize errors due to drift in either the response of the detection apparatus or the intensity of the laser. By making modifications to the control program, it was possible to use the same program to control the energy of the tunable OPO for PLE measurements, in which the emission intensity of a given PL line was monitored as the OPO excitation wavelength was varied up through the excited states.

A block diagram of the complete experimental apparatus used in this study is shown in Fig. 2.1.

2.2. Cryostats and stress and Zeeman apparatus

Three different liquid He cryostats were available for this work. A standard Janis immersion dewar with an approximate optical aperture of ~f/3 was employed for stress measurements from 1.4 K to 4.2 K. For stress measurements above 4.2 K, an Andonian variable temperature dewar was employed. In this cryostat, a flow of He gas from a reservoir is used to cool the sample, which is mounted in the jaws of the stress rig (Fig. 2.2). The temperature was sensed by a Si diode sensor

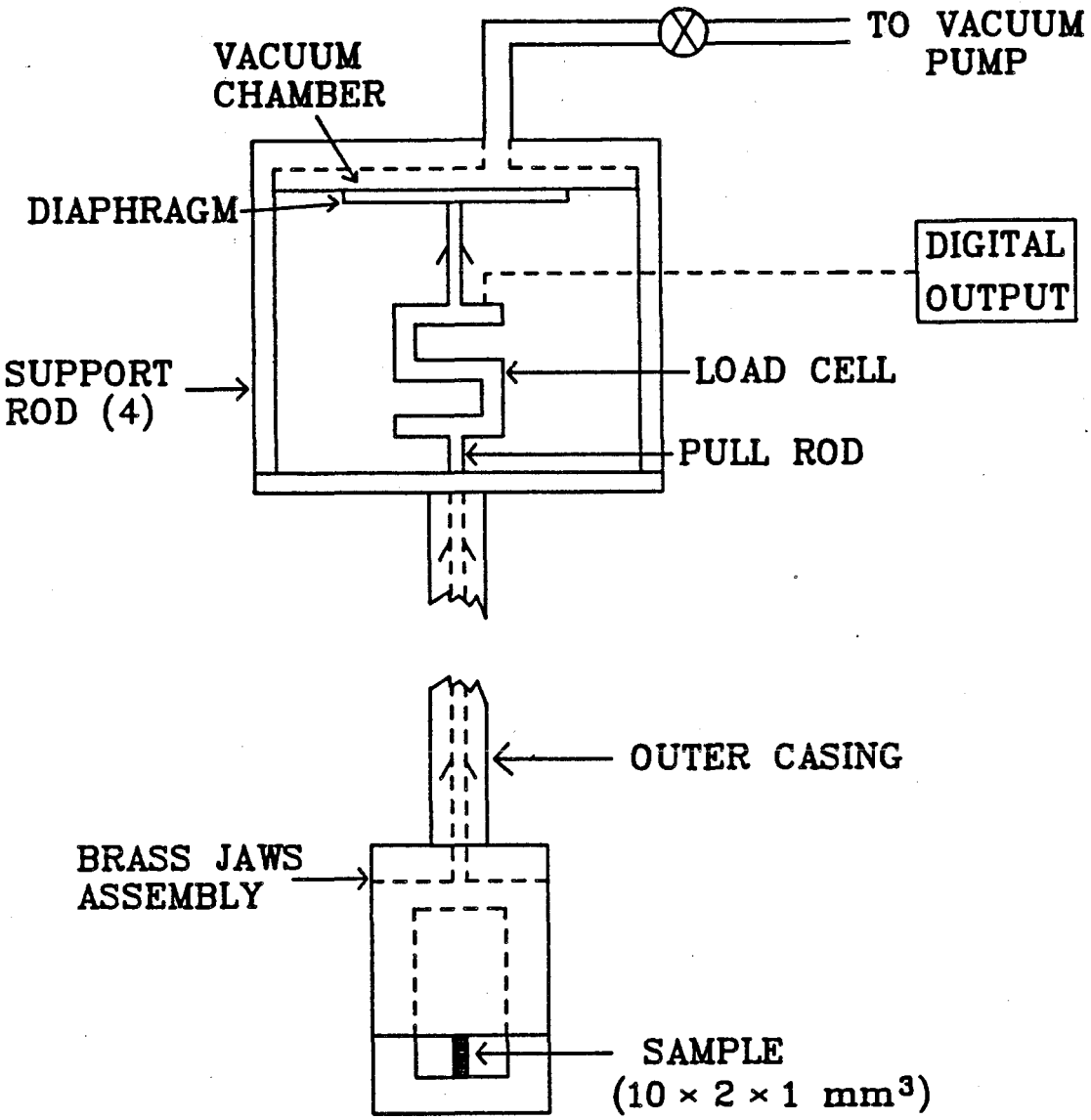

Fig. 2.2: Schematic diagram of the vacuum-actuated device for applying uniaxial stress to the Si samples.

(Lakeshore DT-500-CU-36) mounted in close proximity to the sample. The diode signal was monitored by a Lakeshore DRC-80C temperature controller. Temperature control was provided by a heater consisting of nichrome wire wrapped around the stress rig jaws.

Stress was applied to the samples by the vacuum diaphragm activated arrangement shown schematically in Fig. 2.2. In this arrangement a tensile force is applied to the brass stress rig jaws, which are such that they transmit a compressive force to the sample. The force is applied by a low volume vacuum chamber, and was varied manually by a needle valve. The tensile force was monitored by a 250 kg load cell connected directly to the stress rig pull rod. The load cell output was monitored on a digital output calibrated in kg. The maximum applied "force" was limited by the diameter of the diaphragm to 100 kg. From a knowledge of the sample cross-section, the true stress at the sample was calculated. The only sources of friction between the load cell and the sample were an O-ring at the top of the outer casing, and the jaws mechanism itself. The sliding surfaces of the stress rig jaws were lubricated with graphite powder. Judging by the lack of hysterisis in the spectral line positions any friction effects were negligible.

Sample mounting was somewhat of a hit and miss process at times. Double sided tape was attached to the stress bearing ends of the sample in order to assist in sample placement within the jaws. Occasionally, improper sample alignment resulted in poor quality spectra, due to inhomogeneous stresses at the end

faces. These were immediately recognizable by virtue of their very broad linewidths and, in some cases by the presence of additional spurious structure. The spectral linewidths of properly mounted samples remained close to the spectrometer resolution of 0.1 meV right up to maximum stress, confirming a high degree of stress homogeneity.

Zeeman measurements were carried out in a custom-built split-pair 10 T superconducting magnet cryostat designed by Dr. M. Thewalt. The optical throughput of ~f/6 was considerably reduced from that of the other two dewars. Luminescence was observed along a direction perpendicular to the magnetic field in all cases. In this particular cryostat, the sample chamber was completely separate from the magnet He reservoir. For $T \leq 4.2$ K, the sample chamber was filled with liquid He. For temperatures above 10 K, a crude but effective system was used whereby He gas was transferred into the sample chamber using a transfer siphon. The flow rate was adjusted to balance the 200 mW or so thermal input from the Ar laser. Since the Si sensors employed in this study were useless in magnetic fields, the temperature was estimated from the ratios of the various lines whose zero field thermal behaviour was known.

For the angular Zeeman measurements, samples were mounted on a rotating holder which could be rotated from outside by a simple gear arrangement. The samples were mounted with a <110> axis parallel to the rotation axis and to the observation axis. This geometry assured that the principal crystal axes, <001>, <111>, <110>, and <112> could all be aligned parallel to the

field.

For the Si:In Zeeman excitation spectroscopy measurements, it was found that very high count rates ($\sim 10^6$/s) could be obtained by mounting <110> stress samples end-on along the rotation axis in order to take advantage of the long penetration depth of the near infrared excitation. In this arrangement, samples were excited through one face, and the luminescence output was observed from the other face, 1 cm distant. Above-bandgap excitation in this geometry typically yielded count rates two orders of magnitude lower than with resonant excitation, with its much larger absorption length.

Polarization measurements were only undertaken for the PLE stress and Zeeman measurements. Such measurements are notoriously difficult for ordinary PL measurements due to the many internal reflections which the luminescence can undergo prior to escape from the crystal. This is an especially severe problem in Si with its refractive index of ~3.5 at 1.1 μm. In addition, in PL the polarization data are complicated by the fact that the initial state of the transition (i.e. the exciton) is generally at local thermal equilibrium, with the result that the splitting patterns tend to thermalize, at least if the degeneracy is purely electronic. In PLE, the exciton is the final state, and there are no thermalization effects, since PLE is essentially an absorption technique. The problems of internal reflection now apply to the excitation radiation, whose geometry is better defined and less susceptible to such reflections.

For the PLE measurements the polarization of the OPO

output was rotated by a quartz half-wave plate. The excitation radiation was then further analyzed using a Glan-Thompson polarizing prism. By passing a laser beam of known polarization through the axis of the magnet dewar, it was verified that the dewar windows did not alter the polarization state of the incident beam.

2.3. Material and preparation

The In-doped Si was obtained from a boule of commercial bulk-doped Czochralski-grown material ($\sim 2\times10^{16}$ In/cm^3). The starting material for most of the Si:Tl samples was Czochralski-grown P- or B-doped Si ($\sim 1\times10^{15}$ P/cm^3 and 1×10^{14} B/cm^3 respectively). The stress samples were X-ray oriented to within $\pm 1°$ and cut with a diamond saw into parallelopipeds of dimensions $\sim 10\times1\times2.5$ mm^3. Most of the Tl samples were prepared by diffusion of the above material in an evacuated quartz ampoule into which a small piece of Tl metal had been placed. Diffusions were carried out at 1100°C for two weeks. Even with such large diffusion times, it is unlikely that the Tl penetrated more than a few tens of microns into the bulk. For the purposes of PL measurements utilizing above bandgap excitation, with its short penetration depth, this was not a problem. In addition, samples that had been ion-implanted with both In and Tl in the same wafer were available for this study, although the signal levels were much lower than in the best diffusion-doped samples. All samples were quenched in a 1:1

ethanol:H_2O solution from ~1100°C in order to greatly increase the IBE luminescence intensity. The Si:In samples were etched in a standard HF:HNO_3 solution prior to heating and quenching. The Si:Tl samples were etched in pure HF prior to reheating and quenching, in order to remove the surface oxides introduced by the long furnace treatment, but not the diffused Si layer.

In addition some small samples of commercial Czochralski-grown bulk-doped Si:Tl were available for this study, with resistivities of 6.7 Ωcm (2×10^{15} Tl/cm^3) and 3.6 Ωcm (3.6×10^{15} Tl/cm^3). These showed PL intensities at least as good as those of the diffusion-doped material, and it was hoped that the bulk doping might enhance the chances of obtaining excitation spectra from this material. Unfortunately this was not the case.

2.4. Tunable optical parametric oscillator system

A considerable portion of this research involved the design and construction of a tunable optical parametric oscillator system for PLE measurements on the Si:In isoelectronic system. Before describing the details involved in the design and operation of this system it is useful to review some of the theory behind optical parametric oscillators in general.

Outline of OPO theory

The theory and design of OPO systems has been reviewed in detail by Byer (1975). Optical parametric amplification and

oscillation is a result of the second order nonlinearity of the induced polarization of materials under high optical excitation. In a crystalline solid under high excitation conditions, the i'th component of the induced polarization contains a nonlinear term

$$P_i^{NL}(\omega)=\varepsilon_o \sum_{jk} d_{ijk}E_j(\omega)E_k(\omega) \qquad [2.1]$$

where d_{ijk} is the second order nonlinear susceptibility, and E_j is the electric field at a frequency ω. Substitution of [2.1] into Maxwell's equations results in the addition of a driving term to the usual wave equation for the electric field, of the form

$$\mu\frac{\partial^2}{\partial t^2} P_i^{NL}$$

where P_i^{NL} will in general contain extra frequency components due to the fact that E_i appears in [2.1] to second order.

Consider the nonlinear interaction of three collinear beams of frequencies ω_1, ω_2, and ω_3, such that each is described by a plane wave propagating along the z axis:

$$E_z(\omega_1)=\frac{1}{2}\left[E_z(z,\omega_1)e^{i(k_1z-\omega_1t)} + c.c \right]$$

$$E_z(\omega_2)=\frac{1}{2}\left[E_z(z,\omega_2)e^{i(k_2z-\omega_2t)} + c.c \right] \quad \text{etc.}$$

The induced nonlinear polarization contains product terms of the form

$$d\mu E_z(\omega_1)\cdot E_z(\omega_2)e^{i[(\omega_1+\omega_2)t-(k_1+k_2)z]}$$

$$d\mu E_z(\omega_3)\cdot E_z(\omega_2)e^{i[(\omega_3-\omega_2)t-(k_3-k_2)z]}$$

where the nonlinear susceptibility tensor d_{ijk} has been reduced to a scalar, d for the case when z is a high symmetry axis of the crystal. If $\omega_3=\omega_1+\omega_2$, then the nonlinear polarization terms will drive each other, resulting in an exchange of energy between the three beams. By means of some algebraic manipulations it can be shown (Byer, 1975) that the three waves can be described by a set of coupled equations,

$$\begin{aligned}
\frac{d}{dz}E_z(\omega_1) &= i\kappa E_z(\omega_3)E_z^*(\omega_2)e^{i\Delta kz} \\
\frac{d}{dz}E_z(\omega_2) &= i\kappa E_z(\omega_3)E_z^*(\omega_1)e^{i\Delta kz} \\
\frac{d}{dz}E_z(\omega_3) &= i\kappa E_z(\omega_2)E_z^*(\omega_1)e^{i\Delta kz}
\end{aligned} \qquad [2.2]$$

where $\Delta k=k_3-k_2-k_1$, and $\kappa=\omega_i d/(n_i c)$. In general Δk is nonzero for three arbitrary waves due to the nonlinear dispersion relations (k vs ω) in solids. These equations lead directly to the "photon conservation relations" (Byer, 1975; Yariv, 1985) :

$$\frac{1}{\omega_1}\frac{d}{dz}I_1 = \frac{1}{\omega_2}\frac{d}{dz}I_2 = -\frac{1}{\omega_3}\frac{d}{dz}I_3 \qquad [2.3]$$

where I_i is proportional to $E_z(\omega_i)E_z^*(\omega_i)$. This relation implies that growth of the fields at frequencies ω_1 and ω_2, labelled the signal and idler in the language of parametric interactions, is at the expense of the field at ω_3.

It turns out that the presence of a strong pump field at

ω_3 results in amplification of a weak field at ω_1 if there exists a third frequency $\omega_2=\omega_3-\omega_1$ such that the phase mismatch factor Δk in [2.2] is close to or equal to zero. In the case of negligible depletion of the pump beam, in the low gain limit, the single pass gain, G, for such a wave of frequency ω_1 is given by (Byer, 1975)

$$G(\ell)=\Gamma_1^2\ell^2\ \frac{\sin^2(\Delta k\ell/2)}{(\Delta k\ell/2)^2} \qquad [2.4]$$

where ℓ is the length of the material over which the interaction takes place and $\Gamma_1=\omega_1\omega_2 d^2|E_3|^2/(n_1n_2c^2)$. Equation [2.4] pertains in the case where the incident idler intensity I_2 is zero. Γ describes the dependence of the gain on the nonlinear coefficient of the crystal, while the factor involving Δk represents the penalty for operating away from the phase matched condition, $\Delta k=0$. In this low gain limit, the gain bandwidth is given simply by the condition $\Delta k\ell/2\sim\pi$. In this study a 5 cm crystal was used, implying a gain bandwidth of the order of 1-2 cm^{-1}. This places a rather severe restriction on the linewidth of the pump laser.

When a material with sufficient parametric gain is placed inside a Fabry-Perot resonator, parametric oscillation can occur if the mirror coatings are reflecting for ω_1, or ω_2, or both. Since there are always noise photons present, no external field apart from the pump frequency need be supplied providing that the crystal properties are such that the energy conservation and phase matching conditions are satisfied for the three frequen-

cies ω_1, ω_2, and ω_3. The simplest configuration is the singly resonant oscillator, in which one of the beams, arbitrarily called the idler, is made to resonate, while the other, the signal, is extracted. The doubly resonant oscillator, in which the coatings are made reflecting to both beams offers a much reduced threshold pumping power, but suffers from a severe frequency stability problem due to the extra restriction that both ω_1 and ω_2 can only have discrete frequencies determined by the longitudinal mode spacing (Smith, 1973). Provided enough gain can be achieved, the higher threshold of the singly resonant cavity is not a severe drawback in practice. Conversion efficiencies of up to 70% have been reported from singly resonant oscillators at very high excitation levels.

Phase matching and tunability

The idler and signal frequencies are uniquely determined by the energy and phase matching restrictions, which for a collinear geometry can be summarized as

$$\omega_3 = \omega_1 + \omega_2 \qquad [2.5a]$$

$$n_3\omega_3 = n_1\omega_1 + n_2\omega_2 \ . \qquad [2.5b]$$

In crystals without birefringence one generally has $n_3 > n_2 > n_1$, if $\omega_3 > \omega_2 > \omega_1$ and hence the above conditions cannot be satisfied for such materials. Now consider a uniaxial birefringent crystal such as $LiNbO_3$ (Fig. 2.3). For an arbitrary wave vector $\underline{k}$, one

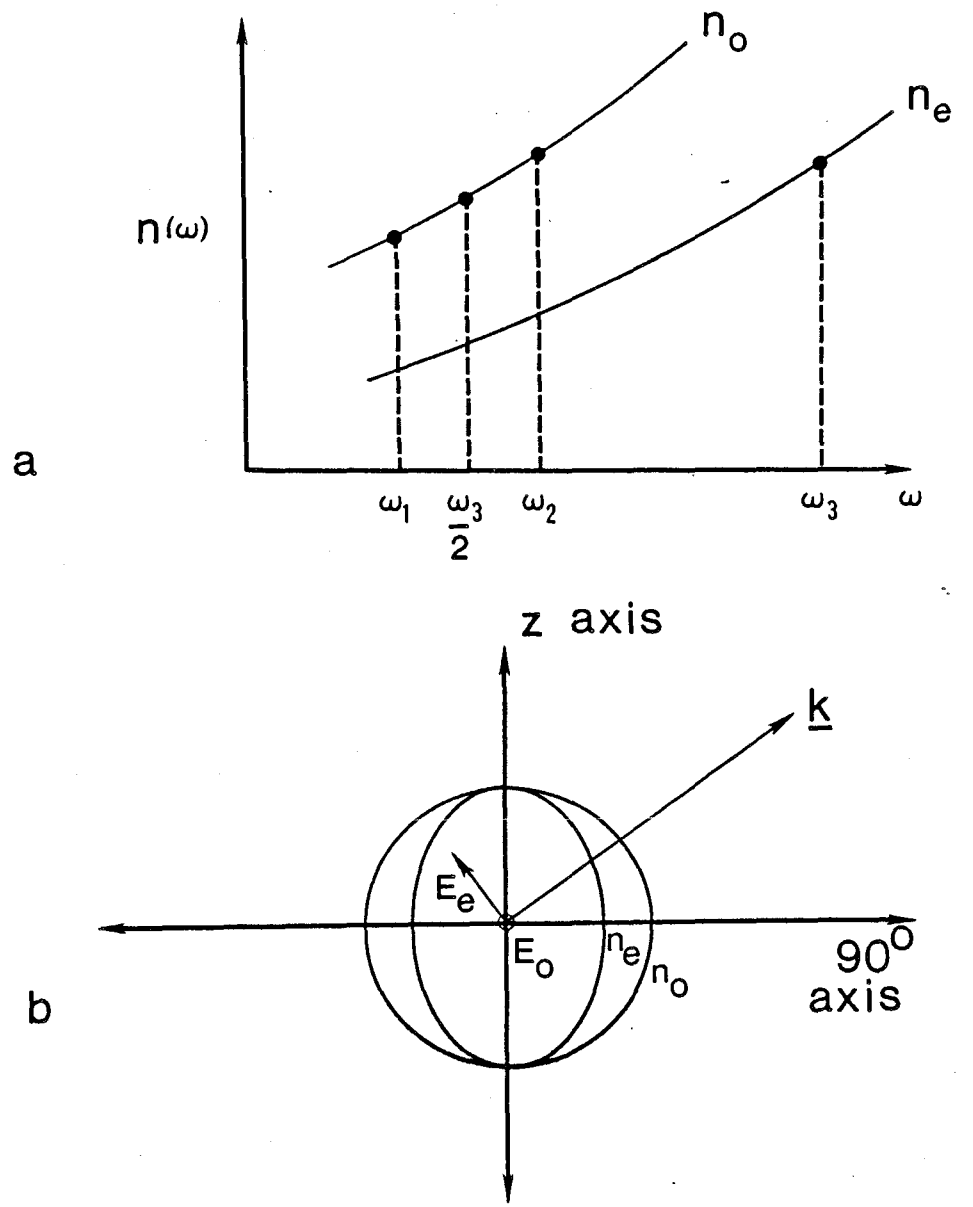

Fig. 2.3: (b) shows the index surface for a negative-uniaxial, birefringent crystal such as $LiNbO_3$. The ordinary surface corresponds to the E vector out of the page, while the extraordinary surface has E in the page. (a) shows how phase matching is possible in such a crystal if the pump beam is the extraordinary ray and the signal and idler are the ordinary rays.

can define two index ellipsoids (see Yariv, 1985) depending on whether the electric vector is in the plane defined by $\underline{k}$ and the optic axis, $\underline{z}$ (ordinary ray), or perpendicular to it (extraordinary ray). At a wavelength of 532 nm the ordinary and extraordinary indices n_o and n_e for $LiNbO_3$ are respectively 2.24 and 2.16. The ordinary index ellipsoid is a sphere with a constant value $n_o(\underline{k})=2.24$. For the extraordinary ray one has an ellipsoid with a minor axis given by $n_e(\underline{k})=2.16$ for $\underline{k}$ perpendicular to the optic axis, and a major axis which is identical to n_o. For an arbitrary direction of propagation, the extraordinary ray can have any value between the above. Thus for some angle, one should in principle be able to satisfy [2.5] by making the pump beam the extraordinary ray, and the signal and idler the ordinary rays (Fig. 2.3a). Whether or not this is possible depends on the detailed nature of the wavelength dependence of the two index surfaces. In addition it is highly desirable to achieve this phase matching condition for $\underline{k} \perp \underline{z}$, since only for this case will the Poynting vectors of the three waves remain collinear, due to the fact that the group velocity, and hence, the Poynting vector, point in the direction of the gradient of the index surface. This situation is referred to as 90° phase matching. This explains why it is possible to exploit $LiNbO_3$ crystal lengths of up to 5 cm, as opposed to many other nonlinear materials, where such matching is not possible.

Early work on $LiNbO_3$ demonstrated the feasibility of 90° phase matching. An initial problem was the formation of optically induced inhomogeneities in the refractive index, but these

were found to be self-annealing at temperatures above 180°C (Byer, 1975). $LiNbO_3$ is ferroelectric and exhibits a large variation of the refractive indices with temperature. This is exploited in practical devices as a slow but simple tuning mechanism. A much more rapid tuning method is to vary the frequency of the pump beam with the result that the signal and idler must in turn vary to satisfy [2.5]. Fig. 2.4 shows the form of the tuning curves that result for 90° phase-matched $LiNbO_3$ at various temperatures. In practice the crystal must be mounted in a very stable oven. In addition, a small flow of O_2 gas must be maintained in order to prevent oxygen depletion of the crystal. With different choices of the oven temperature, a wide range of signal wavelengths can be rapidly tuned by varying the pump wavelength.

Inspection of the tuning curves in Fig. 2.4 shows a drawback of operating the OPO with $\omega_i \sim \omega_s$. The condition $\omega_i = \omega_s$ is referred to as degeneracy, and it is clear from Fig. 2.4 that a small change in the pump frequency near degeneracy will result in a large change in the signal and idler frequencies. If linewidth is an important consideration it is therefore expedient to operate the device somewhat away from the degenerate condition. There is a trade-off however due to the fact that the parametric gain is reduced in going away from degeneracy by a factor $(1-\delta^2)^2$ where δ is defined by $\omega_i = \omega_o(1-\delta)$ and $\omega_s = \omega_o(1+\delta)$, and $\omega_o = \omega_p/2$ (Boyd, 1968). If a narrow linewidth is required close to degeneracy it is clear that the linewidth of the pump laser is the limiting factor.

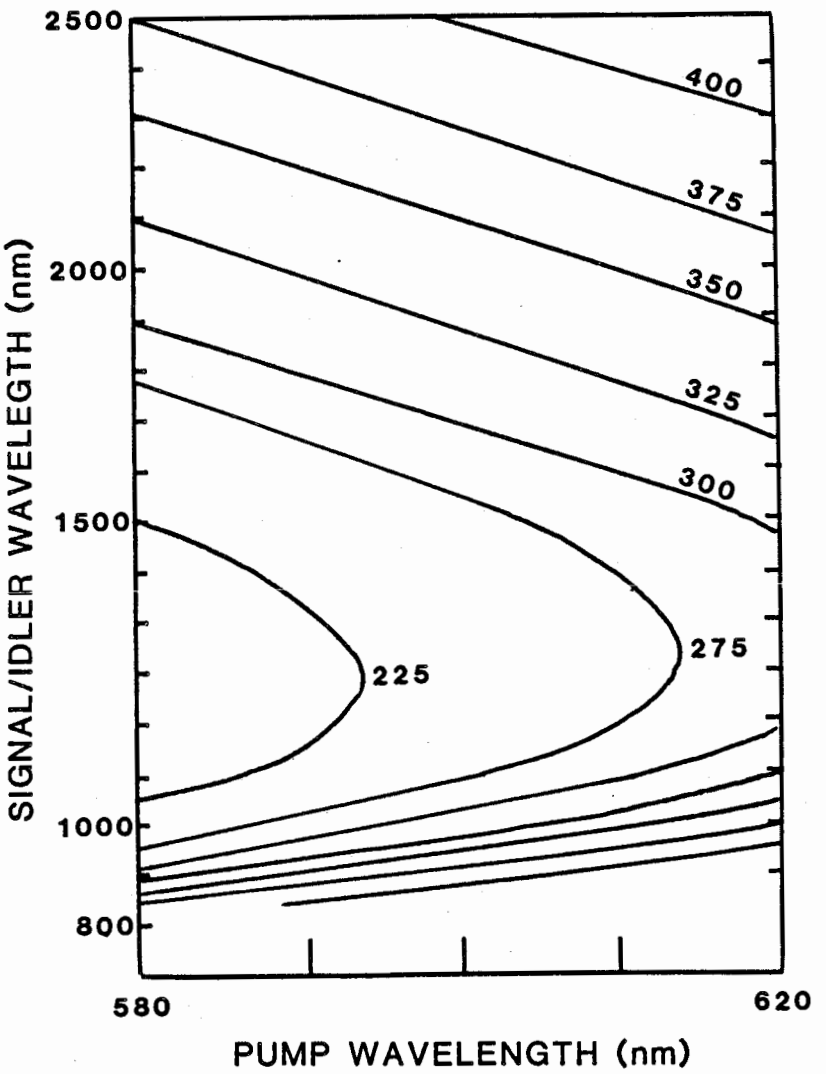

Fig. 2.4: Phase matching curves for $LiNbO_3$ for various operating temperatures in degrees C, as given in the Chromatix CMX-4/IR reference manual.

Design and construction of the OPO pump laser

The optical parametric oscillator used in this study was a commercially produced device (Chromatix CMX-4/IR). This unit was designed to be pumped by a commercial flashlamp-pumped dye laser (Chromatix CMX-4). The dye laser was limited to a repetition rate of 30 Hz and produced an average power output of a few tens of mW, with the result that the OPO power was the order of a mW or less, which was found to be inadequate for the study of many isoelectronic defects. In addition, the dye laser output was subject to unacceptable fading after ~30 minutes.

The original work on dye laser pumping of an OPO was done by R. Wallace (1972). In a brief note Wallace described a pumping scheme which employed a continuously-pumped, frequency-doubled, Q-switched Nd:YAG laser to pump a tunable dye laser which in turn permitted rapid tuning of a 5 cm $LiNbO_3$ OPO. In order to achieve the required OPO acceptance linewidth of ~1 cm^{-1}, four high dispersion Brewster prisms were employed in the dye laser. The laser cavity also employed a telescopic resonator in order to fill as large a portion of the prisms as possible, and thus decrease the spectral linewidth. Such resonators are notoriously difficult to align, and it is remarkable that Wallace was able to achieve a 5% total conversion efficiency (OPO power/Nd:YAG power) from a relatively low Nd:YAG power of 500 mW. Not surprisingly, this arrangement was deemed unsuitable for commercial production, and so the much simpler flashlamp-pumped dye laser arrangement was subsequently

developed by Wallace at Chromatix. There have been no reports in the published literature of other attempts to utilize the Nd:YAG pumping arrangement subsequent to Wallaces's note.

In the intervening years since Wallace demonstrated the Nd:YAG pumping scheme there have been some important developments in both Nd:YAG frequency doubling crystals and in dye laser resonators. Diffraction gratings have been used for several years as frequency selective devices in dye laser cavities, but they have generally been used in conjunction with telescopic resonators. The idea is to use an internal telescope to expand the beam in order to fill the grating and increase the frequency selectivity. The grating is mounted in the Littrow configuration, in which the angle of the grating is adjusted so that the grating acts like a mirror, diffracting the desired order back onto the incident beam. In addition to the difficulties in aligning such a resonator, they suffer from poor beam quality and very stringent tolerances on the rotation mechanism, as well as the need for frequent focussing adjustments.

A much simpler method for filling the grating was first demonstrated by Shoshan et al. (1977). In their arrangement the grating was filled by placing it at grazing incidence with respect to the laser beam, as in Fig 2.5. In addition to the dye cell and the grating the only other components were two highly reflecting mirrors. Rather than using the Littrow mounting, the feedback was provided by positioning one of the mirrors such that the strongest diffraction order was reflected back onto the grating. The output was provided by the zero order diffraction

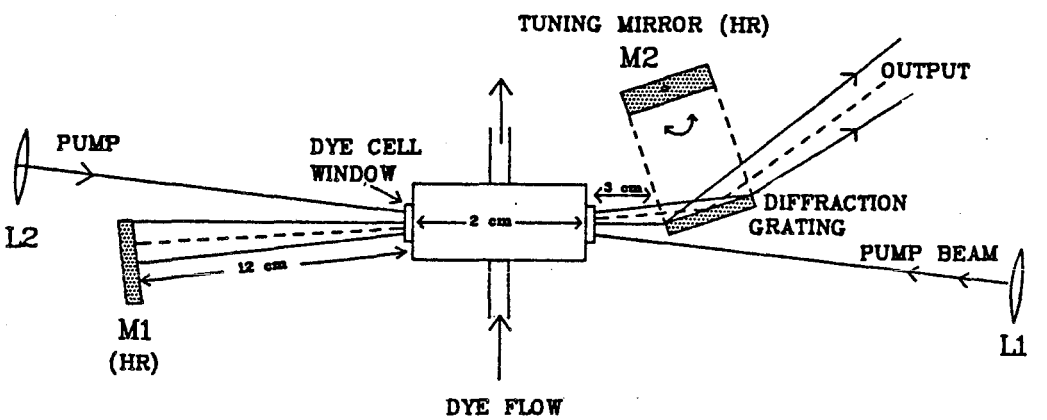

Fig. 2.5: Schematic diagram of the layout of the off-axis, longitudinally-pumped, grazing incidence dye laser constructed as a part of this study in order to excite the optical parametric oscillator (OPO). The laser cavity is formed by mirrors M1 and M2. The holographic diffraction grating provides feedback by diffracting the first order beam onto M2 at normal incidence. The output is taken from the strong zero order beam.

beam. Only a small fraction of the internal cavity radiation is fed back into the laser (<10%) because of the inefficiency of the gratings at such angles, but this is adequate for extremely high gain media such as dyes. Since the beam is diffracted twice per round trip, the angular dispersion is twice as large as in the Littrow case. In addition, it is possible to achieve very short cavity lengths, a feature which has made it possible for subsequent workers to achieve single longitudinal mode oscillation with no additional line-narrowing components (Littman, 1984).

With this system Shoshan et al. obtained linewidths of ~0.1 cm^{-1} at 570 nm with nitrogen laser pumping. Subsequent workers (see e.g. Hung, 1985) have improved on the above specifications by means of a number of refinements. Holographic gratings with very narrow ruling spacings (1800-2500 lines/mm) allow one to obtain very high angular dispersion, with remarkably high efficiency. Other workers reported further linewidth narrowing by replacing the feedback mirror (M2) with a Littrow mounted grating (Shoshan, 1978; Littman, 1978). Linewidths of 0.04-0.1 cm^{-1} have been reported, but with rather low conversion efficiencies of 3-10%. These results were obtained with very high peak power, low repetition rate pump sources such as N_2 or flashlamp-pumped Nd:YAG lasers with peak powers of 50-100 kW or greater. For such applications, a transverse pumping geometry is generally desirable in order to avoid damaging the dye cell windows. In this geometry, the laser radiation is focussed into a line onto one of the dye cell windows by means of a cylin-

drical lens. Lasing then occurs along the length of the line of optically excited dye which this generates.

The linewidths required to pump a $LiNbO_3$ OPO are less than the results quoted above, but it was not clear whether the required 1-2 cm^{-1} linewidth could be achieved with suitable conversion efficiency from the dye laser in order to achieve parametric oscillation. The dye laser pump source was a modified Control Laser model 514QT Q-switched Nd:YAG laser. This device is continuously pumped by means of a 5.2 kW Kr arc lamp. The laser was originally supplied with a $LiIO_3$ frequency doubling crystal, cut for phase matching at the 532 nm second harmonic of the fundamental 1.064 μm transition of Nd:YAG. The maximum green output obtained with this crystal was approximately 1.5 W at 5 kHz. In order to achieve higher dye laser powers for pumping the OPO, this crystal was replaced by a recently developed KTP ($KTiOPO_4$) doubling crystal (Airtron, 1984; Belt et al., 1985). This crystal immediately resulted in a greater than two-fold increase in green output from essentially the same laser cavity. Further modifications were made to the cavity in order to extract the backwards propagating 532 nm beam, which is normally lost in conventional Nd:YAG designs. These modifications are summarized in Fig. 2.6. With these modifications the laser produced a total power from both beams of 2.5-3.0 W at a reduced repetition rate of 2 kHz. Lower repetition rates tend to shorten the laser pulses by increasing the gain storage of the Nd:YAG crystal, with the result that the peak power increases, and with it the chances for reaching OPO

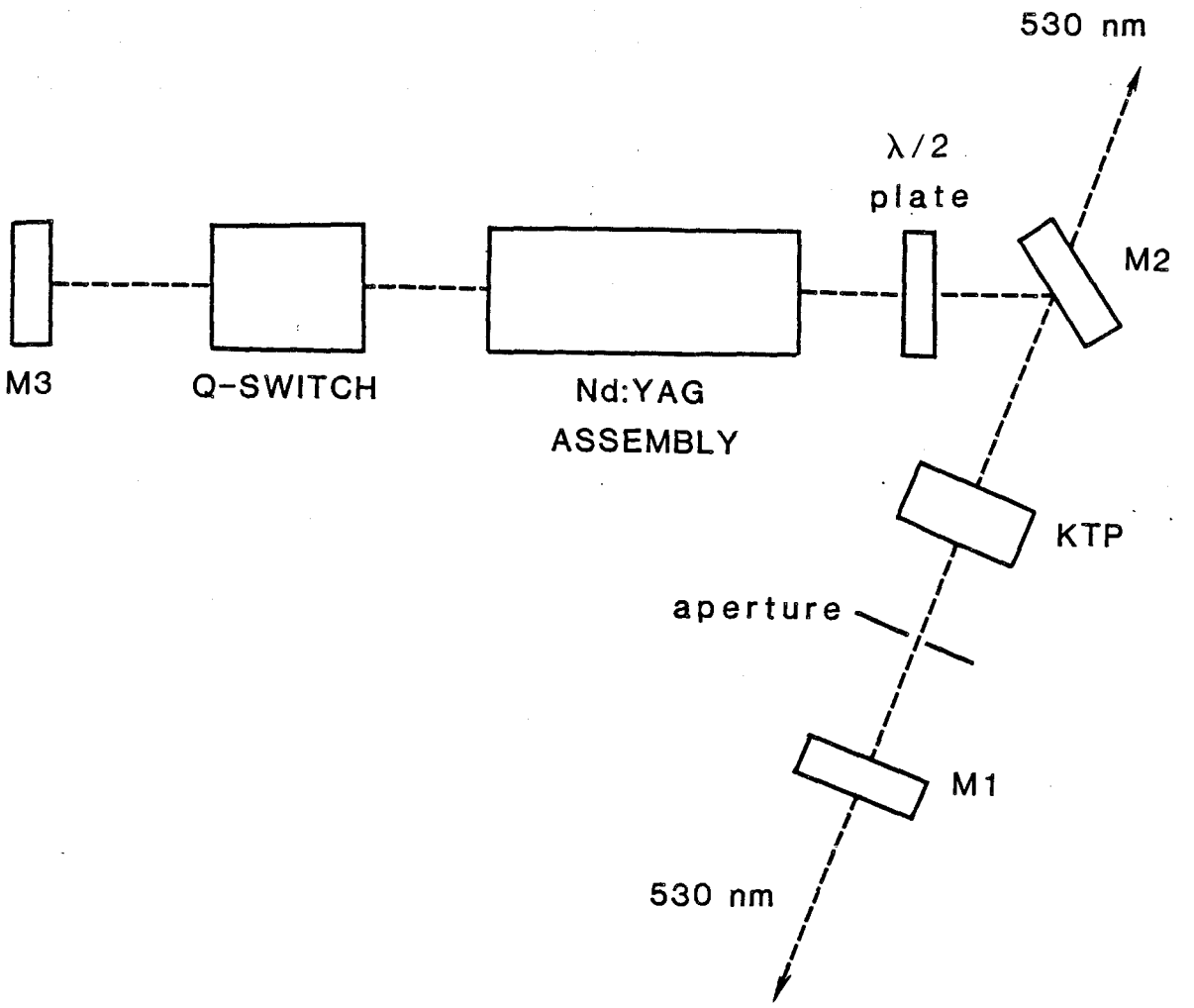

M1: HR @ 1.06 μm, HT @ 0.53 μm, @ 90°

M2: HR @ 1.06 μm, HT @ 0.53 μm, @ 45°

M3: HR @ 1.06 μm, @ 90°

HR= high reflecting, HT= high transmitting

Fig. 2.6: Modified Nd:YAG pump laser. The $LiIO_3$ frequency doubling crystal was replaced by a KTP crystal. The folded cavity configuration allows output coupling of the backward propagating 532 nm wave through the 45° folding mirror. This beam was previously absorbed in the Nd:YAG crystal in the earlier linear cavity configurations.

threshold. The laser pulse width was measured by a Si photodiode to be roughly 100 ns. At a total power of 2 W and a repetition rate of 2 kHz this would imply a peak power of 10 kW.

A simple schematic of the dye laser used in this work is shown in Fig. 2.5. This particular cavity configuration was arrived at after considerable experimentation with a variety of other possible options. The cavity is similar to that of Shoshan et al. (1977) in its simplicity. The major difference involves the choice of an off-axis longitudinal pumping arrangement rather than the more conventional transverse pumping scheme commonly employed in other systems. The transverse geometry was briefly attempted, but the beam quality and divergence properties were inferior to those of the longitudinal setup. The optically excited area overlaps the lasing volume much more closely in a longitudinal setup, and this is expected to become more important at the relatively low peak powers produced by the continuously-pumped Nd:YAG laser. The off-axis pumping geometry has the advantage that no restrictive coatings are required to couple the pump radiation into the cavity as is the case for a truly collinear longitudinal geometry. The dye laser power was surprisingly insensitive to the off-axis angle. The two counterpropagating Nd:YAG beams, each with a power of ~1.5 W were coupled in from opposite dye cell windows.

Both the end mirror and the feedback mirrors were planar broadband dielectric coated mirrors. Experiments with concave mirrors yielded high output powers but very poor beam divergence, unsuitable for efficient coupling into the OPO. A 5 cm

long holographic grating (American Holographic) with a ruling spacing of 2400 lines/mm was used. The angle of the first order diffraction maximum is given by the grating equation, $d(\sin\alpha+\sin\beta)=\lambda$, where $\alpha\sim87°$ is the angle of incidence, and β the diffraction angle, with the convention that both angles are measured with respect to the grating normal. At this ruling spacing one has $\beta=30°$. At an incidence angle of $\alpha\sim87°$ (Fig. 2.5) most of the grating was filled albeit rather nonuniformly.

The dye cell was machined out of brass and provided a 2 cm optical path length with the dye flow perpendicular to the lasing axis. It was found that a shorter path length of 2 mm caused severe fading problems due to the buildup of deposits on the inside surface of the dye cell windows. This correlated with the higher dye concentration required in this case. The dye cell windows were made of quartz and were antireflection coated. Rhodamine 640 and sulforhodamine 640 (Exciton Chemical Company) were the dyes used in this work. These have nominal tuning ranges extending as far as 620 and 640 nm respectively under flashlamp-pumped Nd:YAG excitation. Under the conditions of this study however a usable long wavelength limit of ~625-630 nm was observed for both dyes. Methanol was initially tried as a solvent but caused severe dye fading problems. In addition, the dye radiation became depolarized with respect to the pump beam, possibly because of the relatively low viscosity of ethanol. The use of ethylene glycol circumvented both of these problems. Typical dye concentrations of approximately 0.07 g/1000 ml were employed. By increasing the concentration

somewhat the tuning range could be extended a few nm into the red.

Dye laser performance

Power levels of 400-450 mW at 625 nm and 2 kHz were readily obtained with this cavity configuration. The laser is initially aligned with a single pump beam of ~1.5-2.2 W. Coupling of the second beam typically produced a 5-fold or greater increase in the output power. Accurate measurement of the dye laser linewidth was not possible with the grating spectrometer used in this study. At a dye laser wavelength of 625 nm an upper limit of ~0.1 meV was measured with the grating spectrometer, which is close to the instrumental resolution.

The polarization of the dye laser output was in the horizontal plane. No internal components were required to achieve the required well defined polarization, which was the same as that of the Nd:YAG pump laser.

Beam quality is a crucial factor for efficient pumping of the OPO, and is usually defined in terms of deviations from the diffraction limit. The dye laser output was fairly close to diffraction limited judging by the fact that it was possible to collimate the beam to a diameter of approximately 2 mm over a 10 m path length.

OPO pumping and OPO performance

A simple block diagram of the OPO system is shown in Fig. 2.7a. A schematic of the Chromatix $LiNbO_3$ OPO is given in Fig. 2.7b. The 450 mw dye laser output was first collimated by a single lens and then passed through an optical delay line consisting of three mirrors, which introduced an optical path length of 9.4 m. The delay line was a necessary feature in order to ensure that back reflections from the front mirror of the OPO were not reflected back into the dye laser while it was still lasing. The feedback provided by the grazing incidence grating is so low that such back reflections, which are not frequency selective, would allow the laser to oscillate independently of the grating. This is overcome by delaying the arrival of these back reflections until the Nd:YAG excitation pulse is over. The 9.4 m delay line gave a 60 ns delay of the arrival of the back-reflected pulse at the dye laser.

The dye laser radiation was coupled into the $LiNbO_3$ crystal by a 35 cm focal length lens. Given a beam diameter of d~2 mm at this lens the pump beam diameter at the focus is approximately given by the diffraction limit of $f\lambda/d \sim 100$ μm. At a pump power of 10 kW peak power this implies a power flux of 8 MW/cm^2 which is considerably lower than the $LiNbO_3$ damage threshold of 80 MW/cm^2 (Byer, 1975).

The Chromatix OPO consists of a 5 cm $LiNbO_3$ crystal mounted in a temperature controlled oven. The optic axis of the crystal, which is normal to the long axis, was oriented in the

a

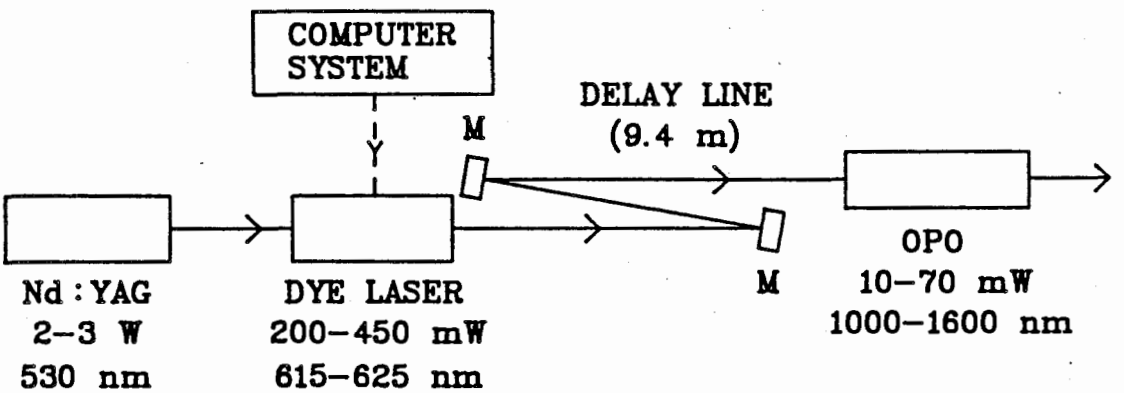

b

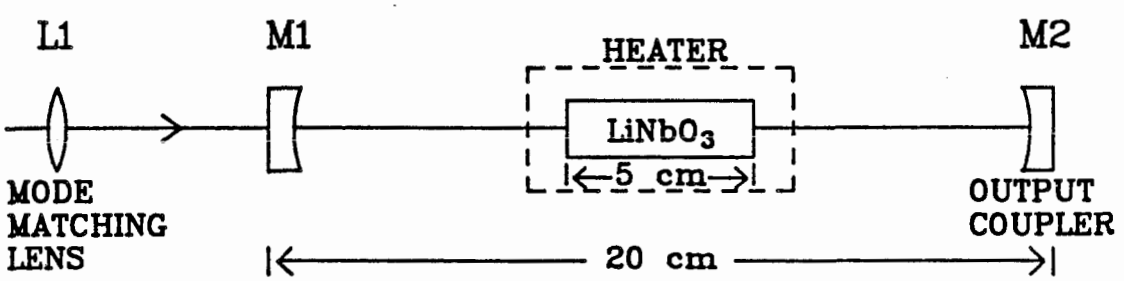

Fig. 2.7: (a): Schematic of the principle subcomponents of the entire OPO system. The purpose of the delay line is to ensure that back reflections do not reach the dye laser until after the Nd:YAG pulse is over, thus ensuring that oscillation does not occur at a wavelength other than that determined by the grating. (b):Schematic of the main components of the CMX-4/IR OPO. Excitation from the dye laser is focussed into the $LiNbO_3$ crystal by lens L1. Mirrors M1 and M2 are reflecting at the idler wavelength, but transmitting at the signal wavelength. The output emerges from M2.

vertical plane i.e. perpendicular to the plane of the dye laser polarization. The cavity is a stable nonconfocal resonator with input and output mirrors of identical 25 cm radii of curvature. The coatings on both mirrors were designed to be highly reflecting at the idler wavelength, and highly transmitting at the signal wavelength. In addition the pump mirror must transmit the pump beam with high efficiency. These are fairly stringent restrictions and are satisfied to a greater or lesser degree depending on the exact operating wavelengths. In practice, near degeneracy, there was appreciable reflection at both the signal and idler wavelengths.

With pump levels of 450 mW the OPO produced power levels of between 30 and 70 mW for a conversion efficiency (OPO power/ dye laser power) of between 7 and 16%.. 450 mW of dye power at 2 kHz implies approximately 2.3 kW of peak dye power, which is well above the typical 300-600 W threshold for oscillation reported by other workers (Byer, 1975). Oscillation was achieved over the range 1.0 to 1.180 μm with a single set of mirrors and at a single oven temperature. The pulse-to-pulse stability of the OPO was excellent, and far better than that of the flashlamp-pumped dye laser arrangement. Angular fluctuations in the beam axis of the Nd:YAG laser were the biggest single factor in determining the stability of the OPO output. These fluctuations were passed on to the dye laser and were magnified somewhat by the long delay line.

The OPO linewidth varied considerably, and the exact cause of this was not determined. Under optimum conditions

linewidths of ~0.3 meV were obtained for a signal wavelengths near 1000 nm. By changing to a different set of mirrors, oscillation was obtained at a wavelength of 1.6 μm, although at a much reduced power level of ~5 mW. As expected, the linewidth became considerably greater as degeneracy was approached ($\omega_i \rightarrow \omega_s$). For this reason it was generally preferable to work as far from degeneracy as possible by shifting the pump frequency as far into the red as possible. A puzzling feature of the broadening of the OPO pulses was that the broadening appeared to be the result of a superposition of regularly spaced lines with a spacing of ~0.2 meV. This spacing is approximately 100 times the expected longitudinal cavity mode spacing of either the dye laser or the OPO, which is given by $c/n2\ell \sim 0.002$ meV where ℓ is of the order of 20 cm in both cases. The origin of this broadening is not clear at the moment.

Computer control of the OPO

The tuning mirror adjustment micrometer of the dye laser was driven by a stepping motor (Airpax K82331-P2) in order to allow computer control of the OPO wavelength for the purpose of collecting spectra (Fig. 2.1). Since the OPO output wavelength is in general a nonlinear function of the pump frequency, there does not exist a linear relationship between the micrometer setting and the OPO wavelength. In addition the wavelength calibration was completely different for different operating temperatures. The spectrometer control program was therefore

modified to calculate a least squares fit to the OPO wavelength versus micrometer position based on a series of known calibration points which were obtained prior to startup using the spectrometer. This internal calibration was subsequently used to advance the dye laser stepping motor to provide constant increments of wavelength for the spectral scans. A least squares fit to a simple quadratic was found to give a very good fit to the calibration points. The program was capable of alternating between OPO and spectrometer control.

An additional feature that was occasionally useful was an option which normalized the photomultiplier signal against the output of Si photodiode which monitored the OPO intensity. Usually however, fluctuations in the OPO power were small enough that this feature was not required.

Chapter 3: Review of the Si:In and Si:Tl centres

A great deal of phenomenological data has been aquired regarding the In- and Tl-related isoelectronic bound excitons in Si. The work contained in this thesis has determined the detailed nature of the electronic states and symmetries of these particular defects, which had been somewhat of a mystery. It is useful at this point to review some of the previous work that has been done in the area of IBE in Si. Much of the literature on these defect systems has been summarized previously (Watkins, 1983; Watkins et al. 1984). For the sake of brevity, the discussion will be limited to those cases for which the excited state structure has been observed by means of PLE.

The first observation of an isoelectronic defect in Si was made by Weber et al. (1979). These authors performed lifetime and Zeeman measurements which showed that the level structure was similar to that observed in several previously reported axial IBE in GaP. The defect symmetry was C_{3v} and exhibited relatively small ground state splittings of the type described by the model of Morgan and Morgan (1970). The defect was later found to incorporate N in addition to another as yet unidentified constituent. By using the recently developed tunable F_2^{+*} colour centre laser (Mollenauer, 1980), Wagner and Sauer (1982) were able to perform excitation spectroscopy on this centre. A tunable laser was required because of the extremely low concentration of binding centres which precluded the possibility of absorption measurements. A series of acceptor-like

hydrogenic excited states was observed to converge to a limit 36.7 meV above the ground state, similar to the results of Cohen and Sturge (1977). From this, and the spectroscopic binding energy, an electron binding energy of 9.2 meV was deduced.

Henry et al. (1981) reported the observation of a similar axial defect in Be-doped Si. In this case the defect is believed to be a Be-Be intersticialcy, i.e. two Be atoms covalently bonded at a substitutional lattice site. Stress measurements performed by Colley indicated a C_{3v} symmetry for the defect (see Davies, 1984). Earlier Zeeman measurements by Killoran et al. (1982) indicated a D_{2h} symmetry, but there is some question as to the meaningfulness of the group theoretical procedures used in their analysis.

The PLE spectra of these excitons was recently obtained by Thewalt et al. (1982a) using a white light source filtered through a monochromator. In this case a tunable laser was not required because of the high concentration of binding centres ($\sim 10^{16}$ cm^{-3}). This excited state spectrum was subsequently interpreted by the far-infrared studies of Labrie et al. (1983) in which the states were also shown to correspond to those of a hole bound in a Coulombic potential with a binding energy of 43 meV. This implied a binding energy for the isolated electron of 50 meV.

Recently Thonke et al. (1985) have interpreted PLE transitions observed from the 790 meV defect in irradiated Si as being due to shallow donor-like excited states of an IBE. This case is interesting because of the very deep nature of the hole

state which is bound by an energy of the order of a third of the bandgap, while the electron is bound by only 38.3 meV. A thermally-induced defect observed by Wagner et al. (1985) in O-rich Si showed very similar behaviour. All of the above cases were consistent with the HTL model of IBE.

The In-related "P,Q,R" photoluminescence emission near 1118 meV was one of the first of a growing list of emission lines to be identified as due to the recombination of IBE in Si (Mitchard et al., 1979), principally on the basis of the long 230 μs luminescence decay times at 4.2 K. The spectroscopic binding energy of an exciton to this defect is just 22 meV larger than the relatively shallow In acceptor bound exciton binding energy. The luminescence intensity of the defect was found to be greatly enhanced by rapidly quenching the samples from 1100°C to room temperature (Thewalt et al., 1981a). A typical PL spectrum, obtained at 20 K with above gap excitation is shown in Fig. 3.1 from Thewalt et al. (1982b). The 20 K PL emission consists of an intense, narrow no-phonon line at 1118 meV, the P line, and a strong band of non-momentum-conserving phonon replicas, indicative of a highly localized electronic state. Unlike the In acceptor bound exciton the spectrum shows no evidence of any coupling to momentum conserving phonons. Distinctive spectral features are the broad local mode replica R, which has the same initial state as P, and the excited state transition Q, which, as determined from thermal activation measurements, originates on an initial state 3.8 meV above that of P. The 4.2 K spectrum is identical except for the absence of

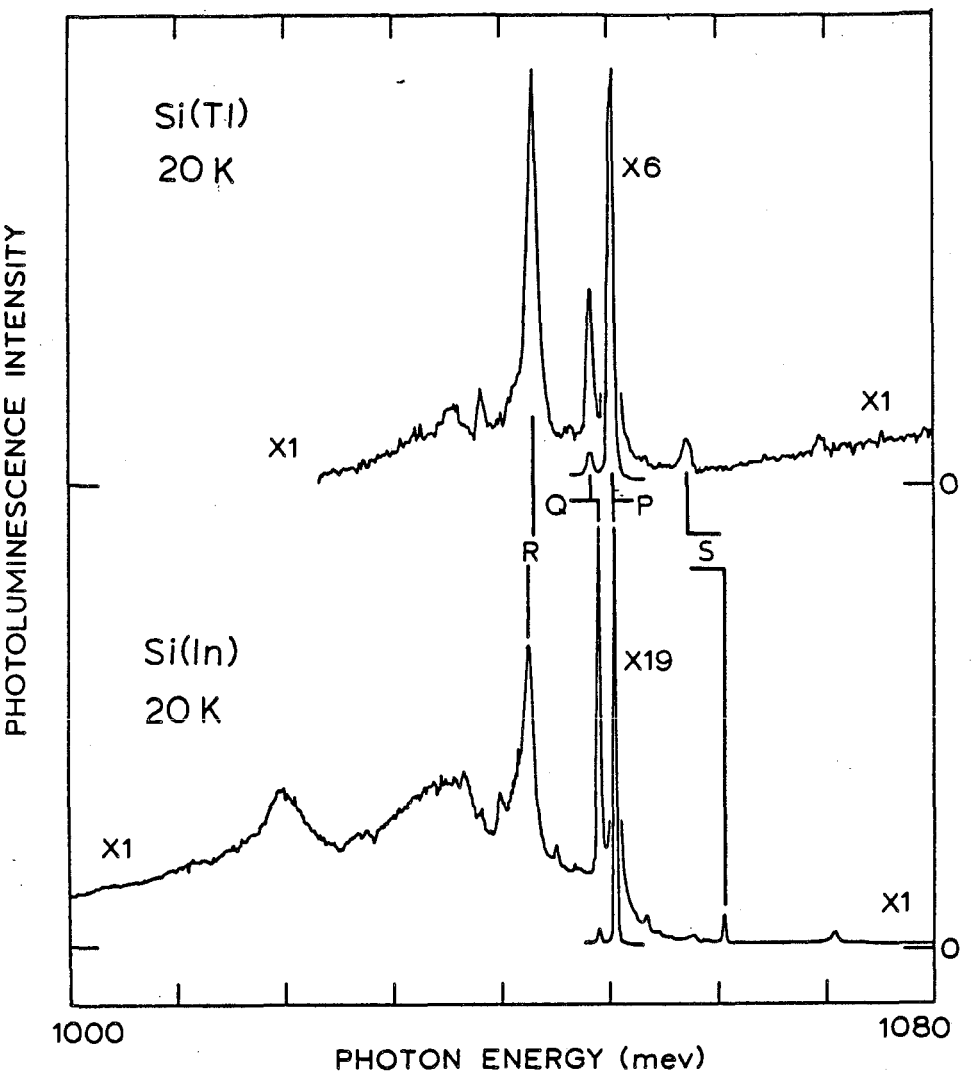

Fig. 3.1: PL spectra of the Si:In and Si:Tl isoelectronic centres recorded at 20 K. The Si:In spectrum has been shifted down in energy by 67.4 meV in order to align the principal no- phonon P lines and thus emphasize the spectral similarities. From Thewalt et al. (1981a).

the excited state transition Q. The transition Q has an energy just below that of P, which can only be explained if it terminates on an excited final state, most likely a local mode of the bare centre (Thewalt et al., 1981a). It is an unusual and distinctive feature that a no-phonon transition is not observed between the initial state of Q and the final state of P. Presumably this is the result of some selection rule. The PL properties of this centre have have been thoroughly investigated by a variety of techniques including transient excitation, thermal activation, uniaxial stress, and Zeeman measurements (Thewalt et al., 1982b; Watkins et al., 1984; Watkins and Thewalt, 1985).

The role of the central cell of the In acceptor was established by Thewalt et al. (1981b) who applied the same sample quenching procedure to samples doped with the deeper acceptor Tl. This was observed to produce a very similar set of lines at 20 K, displaced down in energy by 67 meV, which is a large fraction of the 91 meV difference in binding energy between the In and Tl acceptors. The striking similarity of the 20 K Si:In and Si:Tl spectra is shown in Fig. 3.1 in which the energy scales of the two spectra were shifted so as to bring the no-phonon P lines into coincidence. The similarity of the spectral features led to the use of the same labelling conventions. The unusual Q line feature is also observed in the 20 K Si:Tl spectrum, as well as the broad local mode replica R. The similarity of these spectra led to the use of the term P-centre to describe the defect responsible for both sets of PL lines.

Whereas the Si:In P,Q,R... luminescence system does not change significantly over the 1.6-25 K range, the Si:Tl P,Q,R luminescence vanishes completely below 12 K and is replaced by a new set of lines denoted A,B,C... for which the ground state to ground state transition (A line) lies 36.8 meV above the Si:Tl P line. The temperature dependence of this novel changeover is shown in Fig. 3.2. The long lifetimes (53 μs at 4.2 K) of these new lines was also suggestive of IBE recombination. At 4.2 K an intricate set of local mode phonon replicas B,C,D,E... of the dominant no-phonon transition A are observed, not all of which are well resolved in Fig. 3.2. All of these have identical thermal behaviour showing that they share the same initial state. A series of monotonically decreasing replicas of the A line, of which the line labelled B is the first, are generated by coupling to a 5.3 meV final state mode. The C line also generates a series of monotonically decreasing set of replicas, of which D is the first, with the same 5.3 meV spacing. The C line is itself a replica of the A line, generated by a 6.5 meV final state local mode.

The 15 K spectrum in Fig. 3.2 reveals an excited state transition labelled X at an energy 2.9 meV above A. This transition has an excited initial (exciton) state, but the same final state as A as confirmed by the existence of replicas Y,Z,Z'... generated by coupling to the same local phonon modes which couple to A.

The total broad-band phonon coupling generated by non-momentum conserving phonons is much greater for the A,B,C...

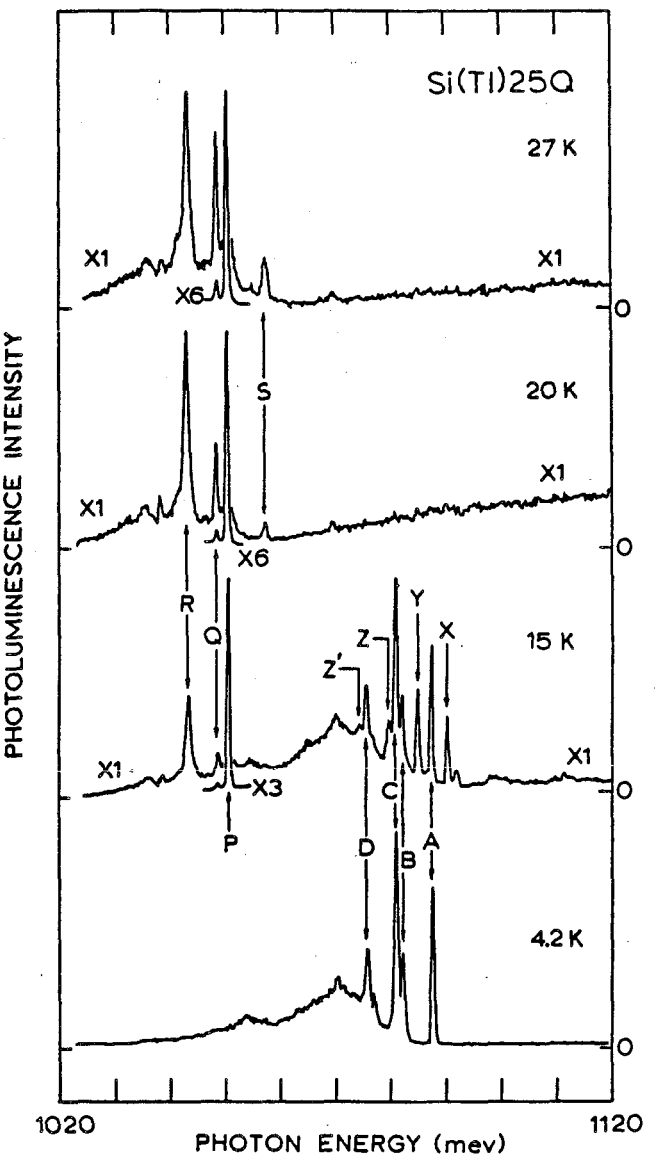

Fig. 3.2: PL spectra of the Si:Tl isoelectronic centre recorded at various temperatures, showing the changeover in the spectral features. From Thewalt et al. (1982b).

luminescence system than for either the Si:In or Si:Tl P,Q,R... systems, as summarized in Fig. 3.3 from Thewalt et al. (1982b). These data were obtained with an intrinsic Ge detector, which has a fairly flat response over this wavelength region. The magnitude of the sidebands in Fig. 3.3 is not evident in Figs. 3.1 and 3.2 since those data were obtained with the photomultiplier detector, which has a rapidly falling response below 1 eV.

The observation that the integrated luminescence intensity of all Si:Tl lines does not change appreciably in passing through the changeover temperature, and that no sample dependence of the relative line intensities is observed, suggested that the P,Q,R... and A,B,C... luminescence systems are due to the recombination of excitons at different configurations of the same binding centre, which can undergo some form of thermally induced reorientation (Thewalt, 1982b). The kinetics of this rearrangement process was investigated by Watkins et al. (1984) and Watkins (1983) by means of transient PL spectroscopy. In their model, excitons are initially captured in a high energy exciton configuration labelled the A-centre which is responsible for the A,B,C... lines, but can reorient to a lower energy configuration at T>14 K, the P-centre, by thermally overcoming a small energy barrier.

The changeover rate $1/\tau_c$ was found to obey a simple exponential behaviour of the form

$$\frac{1}{\tau_c} = \frac{1}{\tau_o} e^{E_B/kT} \qquad [3.1]$$

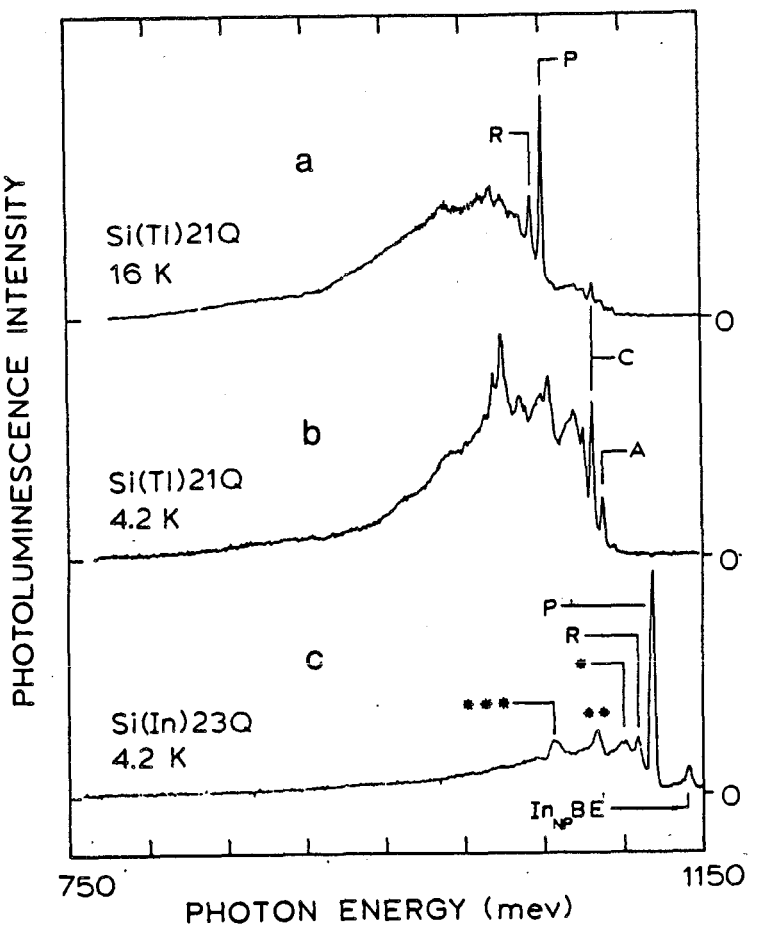

Fig. 3.3: Si:In and Si:Tl IBE spectra obtained with an intrinsic Ge photodiode detector, showing the strong coupling to phonons of the three principal luminescence emissions. Note that the ratio of the no-phonon oscillator strength to that of the vibronic sidebands is much larger for the A,B,C... system than for either of the P,Q,R... systems. From Thewalt et al. (1982b).

with a barrier energy E_B=20.5 meV and τ_o=1x10^{-12} s. The extremely short value of τ_o was consistent with a phonon-mediated rearrangement process. Such a process is completely unprecedented among IBE in any semiconductor. Qualitatively similar bistable effects have been observed for deep levels in Si (e.g. Bains and Banbury, 1985), GaAs (e.g. Levinson, 1983) and InP (e.g. Stavola et al., 1984) by deep level transient spectroscopy , but all of these cases involved very large barrier energies of a large fraction of the gap energy, in and it is not clear whether the underlying mechanism is the same.

In addition, evidence from the transient PL studies of the Si:In system was presented (Watkins et al., 1984) that a similar bistability exists for this system, with the difference that one of the defect configurations is non-radiative, and is inferred from the double exponential behaviour of the transient luminescence (Watkins, 1984). These transient data were explained by a model similar to that used for the Si:Tl data. Similar values of τ_0 and E_B were derived. In this case however it was assumed that the relaxed exciton energies of the A- and P-centre configurations were equal, and that changeover could therefore proceed in both directions at temperatures above 10 K.

An important piece of information which has been provided by the work in this thesis is the determination of the symmetries of the two Si:Tl defect configurations by means of stress and Zeeman measurements. These are found to be quite different, as would be expected for a configurational rearrangement process. In addition these data give detailed information about

the nature of electron and hole states responsible for the ground state fine structure. Prior to the results of this thesis, the nature of these states was not known. The defects were attributed to isoelectronic binding centres chiefly on the evidence of the long luminescence decay times, which are a well known feature of IBE in indirect gap semiconductors like Si and GaP and distinguish them from excitons bound to neutral donors or acceptors, in which the recombination energy of the exciton can be transferred nonradiatively to the remaining particle with high probability. In addition, the lowest lying exciton state is often dipole forbidden, resulting in very long luminescence decay times (Chapt. 1.4).

Prior to this study it was believed that the energy level structure of the Si:Tl and Si:In centres did not fall into the usual systematics for isoelectronic binding of excitons at low symmetry defects. From the stress and Zeeman measurements it was concluded that the symmetry of the low energy Si:Tl configuration was C_{3v}, and that the ground state spectrum was quite well explained by the axial IBE model of Morgan and Morgan (1970), contrary to the claims of Sauer and Weber (1982).

The hypothesis that the Si:In IBE and the high energy configuration of the Si:Tl IBE correspond to the same defect configuration, but differ only in the presence of Tl or In (Thewalt et al., 1982b; Watkins et al., 1984), is strongly supported by the uniaxial stress and Zeeman data obtained in this study. The stress data showed that the defect symmetry was in both cases C_{2v}. The ground state line of both centres was

observed to be split by a magnetic field into an isotropic triplet, with the g-factor of a pure spin triplet. This is unusual, in that it implies a complete quenching of the hole orbital angular momentum. This is a recently recognized phenomenon in low symmetry hole attractive isoelectronic centres in GaP (Monemar et al., 1982; Gislason et al., 1982), but has been observed in only one other IBE in Si, the four Li defect in electron-irradiated Si (Lightowlers et al., 1984).

A major portion of the thesis involved the design and construction of a tunable laser system in order to probe the excited state structure of both the Si:In and Si:Tl defects. The concentration of binding centres is so low for these systems that absorption measurements have not been possible. Wagner and Sauer (1983) have reported the PLE spectrum of the In-related isoelectronic defect in the absence of external perturbations using a colour centre laser. They reported a set of three strong, widely spaced absorption lines, P_0^0, P_2^0, and P_3^0 with a markedly non-hydrogenic energy spacing. Their P_0^0 transition corresponds to the previously discussed Si:In P line transition (exciton ground state to crystal ground state transition) observed in PL. The P_2^0 transition corresponds to the very weak PL excited state transition labelled S in Fig. 3.1. Prior to the work described in this thesis no model had been provided as to the anomalous character of this PLE spectrum, which does not fit into the expected systematics for a hydrogenic excited series of states.

In this study the previously discussed tunable OPO system

was used in conjunction with uniaxial stress perturbations to explain the electronic excited states seen in PLE. It was shown by selective excitation that the stress splittings of the two lowest lying states are purely orientational and consistent with the C_{2v} designation obtained from the PL measurements. Zeeman measurements were used to show that the exciton ground state is split by j-j coupling into a ground state triplet (P_0^0 line) and a singlet (P_2^0 line), from which an unusually large j-j coupling splitting energy of 11.4 meV was deduced. This splitting is much larger than previously reported values in Si, which were of the order of 2-3 meV, and indicates considerable electron-hole overlap arising from an electron that is more deeply bound than in the usual HTL case. In this respect, the excited state spectrum resembles that of the recently reported IBE in GaP:Cu (Monemar et al., 1982; Gislason et al., 1982). The polarization dependence of the magnetic field results for the two lowest-lying exciton states is explained by making simple assumptions about the symmetries of the electron and hole wavefunctions.

An interesting feature revealed by the stress data is the presence of extra degeneracy in the highest-lying exciton transition, P_3^0. It is proposed that this level is due to an excited state of the electron, which is in a 1s Γ_3 (T_d) valley-orbit state. The unperturbed electron states of the two lowest lying exciton levels are assumed to derive from the 1s Γ_1 (T_d) valley-orbit states. The observed nonlinearity of the <001> stress splittings of the lowest lying exciton levels is thus modelled by a stress-induced mixing of the Γ_1 and Γ_3 1s electron states

assuming a somewhat reduced value of the electron deformation potential, Ξ_u. The large value of the 1s Γ_1-to-Γ_3 splitting is also consistent with the conclusion that the short-range potential of this defect is attractive for electrons as well as for holes.

No sharp-line excitation spectrum was observed for the Si:Tl defects, despite the availability of bulk-doped Si:Tl material with relative high Tl concentration. Nevertheless, from the similarity of the stress and Zeeman behaviour of the Si:In and Si:Tl P,Q,R... luminescence systems, it is clear that many of the conclusions arrived at for the former apply to the latter.

Chapter 4.: Ground state stress and Zeeman splittings: Si:In and Si:Tl centres

4.1: Zeeman results: Si:Tl A-centres

The magnetic field splittings of the Si:Tl A line were briefly reported by Sauer and Weber (1983). In Fig. 4.1 the strongly anisotropic splitting of the A-line is shown at a representative field of 3.3 T. These curves agree with those obtained by Sauer and Weber. The X line showed no splitting within the resolution of the experimental apparatus, although there is a suggestion of a small splitting for $\underline{B} \| \langle 001 \rangle$. These data were obtained by rotating a $\langle 110 \rangle$ oriented slice about a $\langle 110 \rangle$ axis normal to the magnetic field. Luminescence was observed along the rotation axis. As a support for their model that the Si:Tl isoelectronic defect consists of an interstitial Fe-substitutional Tl pair (Fe_i-Tl_s), Sauer and Weber proposed that these lines resulted from transitions from an $m_J = \pm\frac{3}{2}$ upper to an $m_J = \pm\frac{1}{2}$ lower state, with the Fe_i supplying the additional half-integer j. Dipole selection rules would allow only two transitions for centres of a given orientation. They stated that the splitting pattern was consistent with a $\langle 111 \rangle$ oriented C_{2v} defect. Unpublished thermalization results were cited as further evidence for the above energy level designations.

It is shown in this work that the angular dependence of the Zeeman data shown in Fig. 4.1, together with thermalization measurements in Fig. 4.2, and the uniaxial stress results which follow this section, clearly demonstrate that the A and X lines

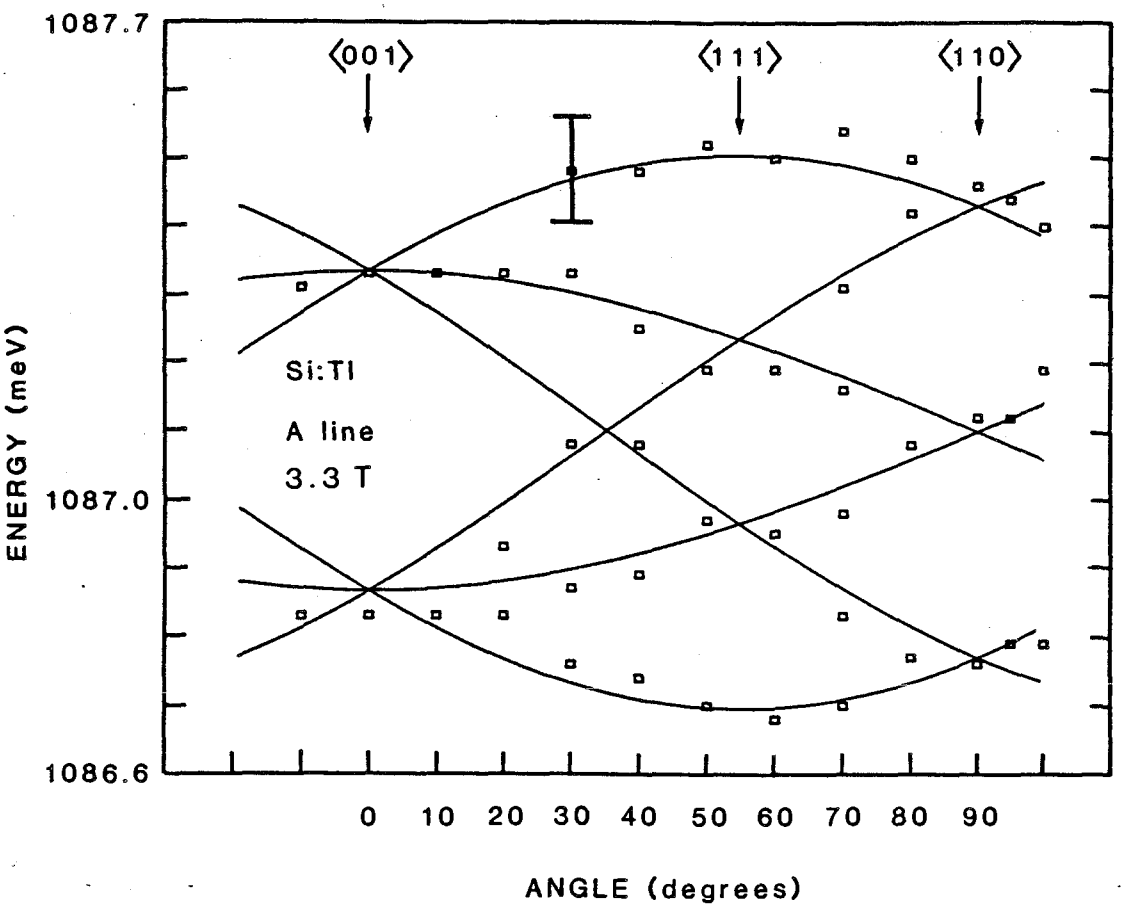

Fig. 4.1: The splitting of the Si:Tl no-phonon A line transition as a function of angle measured relative to a ⟨001⟩ axis, as the sample is rotated about a ⟨110⟩ axis normal to $\underline{B}$. The solid lines represent a fit using [4.4] with $g_{eff}=(\gamma+g_e+g_h)=2.2$. The bar represents the full width at half maximum of a resolved component.

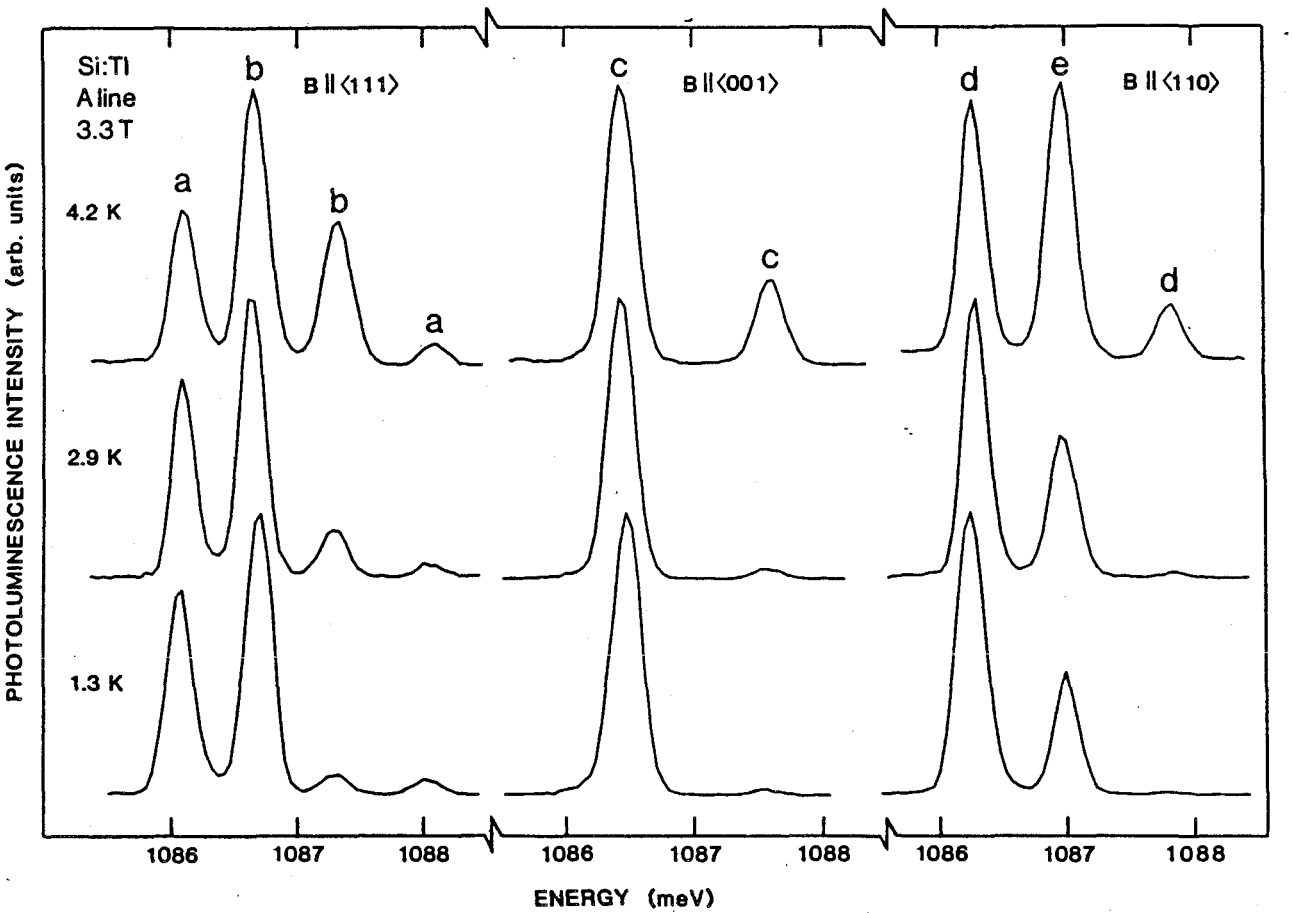

Fig. 4.2: The splitting of the Si:Tl no-phonon A line transition in a 3.3 T magnetic field for $\underline{B}$ aligned along the three principal crystal axes. The splitting is simplest for $\underline{B} \parallel \langle 001 \rangle$, as expected for a ⟨111⟩ oriented axial defect. Note the thermalization of the different subcomponents. Each letter labels a distinct subclass of C_{3v} defects with a common orientation with respect to the field. Thermalization of the subcomponents only occurs within a given subclass of defects as expected.

are consistent with IBE transitions at an axial defect which induces an internal tensile strain, and is aligned along a <111> axis. This is an agreement with the observation of long luminescence lifetimes for these centres (Thewalt et al., 1982) which are often observed in axial IBE with a dipole forbidden ground state as described in Chapt. 1.4.

It is proposed here that the A and X lines correspond to transitions from the $m_J=\pm 2$ and $m_J=\pm 1$ levels in Fig. 1.4, to the crystal ground state. In the absence of any observable higher-lying excited states above the X transition, it will be assumed that the internal strain splitting ε is large compared to the exchange splitting parameter Δ, and that the A and X line initial states therefore contain a negligible admixture of the $j=\frac{3}{2}$, $m_j=\pm\frac{1}{2}$ hole states. This assumption is somewhat of an approximation, as will be seen later in the section on Si:Tl stress results, but it greatly simplifies the calculation of the Zeeman splittings of the two lowest exciton states. In the local defect coordinates, the hole states are derived solely from p_x- and p_y-like orbital states, where the z axis is taken as the <111> defect axis. In the limit $\varepsilon >> \Delta$, the states 1 and 2 in [1.4] are given by (e.g. Davies, 1984)

A line ($m_J=\pm 2$):
$$|p_x+ip_y\rangle\uparrow\uparrow$$
$$-|p_x-ip_y\rangle\downarrow\downarrow$$

X line ($m_J=\pm 1$):
$$|p_x+ip_y\rangle\uparrow\downarrow$$
$$-|p_x-ip_y\rangle\downarrow\uparrow$$

where the first and second spinors denote the hole and electron spins respectively. In this basis, the exchange term, $-\Delta \underline{j}_h \cdot \underline{j}_e$ is diagonal, and the exciton ground state is split by an energy of $\frac{3}{4}\Delta$, to which the A to X line splitting is attributed. Note that this value corresponds to the exact expressions given in Fig. 1.4 in the limit $\varepsilon >> \Delta$. From the spectral data we have $\frac{3}{4}\Delta$ = 2.9 meV, and hence, Δ=4.0 meV. This value is somewhat larger than other values obtained in Si and GaP, which were on the order of 1–2 meV (Dean and Herbert, 1979). A small correction to this value will be given by the stress results.

The linear Zeeman Hamiltonian is of the form

$$H_{LZ} = \mu_B \underline{B} \cdot (\gamma \underline{L} + g_h \underline{s}_h + g_e \underline{s}_e) \qquad [4.1]$$

where γ is an orbital angular momentum reduction factor which is generally reduced from a value of unity in the vicinity of defects with strong vibronic coupling (e.g. Stoneham, 1975) and g_h and g_e are the spin g-factors for the electron and hole respectively, which should be close to the free electron value of 2.0. In principle there can be coupling from the basis states considered here to the $j=\frac{3}{2}$, $m_j=\pm\frac{1}{2}$ stress-split hole states, as well as to the $j=\frac{1}{2}$ split-off hole states, but since these states are assumed to lie at higher energy than the exchange and Zeeman perturbation energies, they are neglected. In this reduced representation, the Hamiltonian matrix is of the form

[4.2]

$$\begin{array}{cccc} |\tfrac{3}{2},\tfrac{1}{2}\rangle & |\tfrac{3}{2},-\tfrac{1}{2}\rangle & |-\tfrac{3}{2},\tfrac{1}{2}\rangle & |-\tfrac{3}{2},-\tfrac{1}{2}\rangle \end{array}$$

$$\begin{bmatrix} -\frac{3}{8}\Delta+(G+H+I)B_z & IB^- & 0 & 0 \\ IB^+ & \frac{3}{8}\Delta+(G+H-I)B_z & 0 & 0 \\ 0 & 0 & \frac{3}{8}\Delta+(-G-H+I)B_z & IB^- \\ 0 & 0 & IB^+ & -\frac{3}{8}\Delta-(G+H+I)B_z \end{bmatrix}$$

where $G=\mu_B\gamma$, $H=\frac{1}{2}\mu_B g_h$, $I=\frac{1}{2}\mu_B g_e$, and $B^{\pm}=B_x\pm iB_y$. Note that only $L_z=-i\hbar(\frac{\partial}{\partial y}-\frac{\partial}{\partial x})$ has non-zero matrix elements: L_x and L_y both project the orbital states onto p_z, which is orthogonal to these basis states. The full eigenvalues are given by

$$\begin{aligned} E_1 &= \mu_B B_z(\gamma+\tfrac{1}{2}g_h) \pm \tfrac{1}{2}\sqrt{\mu_B^2 g_e^2 B^2 + \tfrac{9}{16}\Delta^2 - \tfrac{3}{2}\Delta\mu_B g_e B_z} \\ E_2 &= -\mu_B B_z(\gamma+\tfrac{1}{2}g_h) \pm \tfrac{1}{2}\sqrt{\mu_B^2 g_e^2 B^2 + \tfrac{9}{16}\Delta^2 + \tfrac{3}{2}\Delta\mu_B g_e B_z} \end{aligned} \qquad [4.3]$$

where $B=|\underline{B}|$.

For the fields at which these measurements were taken (3.3 T), $(\mu_B g_e B)^2$ is considerably smaller than $\frac{9}{16}\Delta^2$, and hence to a good approximation the off-diagonal elements of the above matrix can be neglected. In this case, the approximate energies are given by

$$E_{A\ line}=\pm\mu_B(\gamma+\tfrac{1}{2}g_h+\tfrac{1}{2}g_e)B_z \qquad [4.4a]$$

$$E_{X\ line}=\pm\mu_B(\gamma+\tfrac{1}{2}g_h-\tfrac{1}{2}g_e)B_z. \qquad [4.4b]$$

The dependence on B_z implies a highly anisotropic dependence of

the Zeeman splitting and arises from the fact that only the L_z component of the orbital angular momentum operates on the basis states because of the strong axial crystal field. It is not clear how the model of Sauer and Weber would predict such an anisotropy. The splitting is seen to be a maximum when B is parallel to a given defect axis, and zero when perpendicular. The inclusion of the off-diagonal term in the above matrix does not alter the fact that the splitting is zero for the latter case; it merely shifts the energies of both components by the same small amount, roughly 10%, which is smaller than the error bars.

The apparent complexity of the Zeeman pattern arises from the fact that there are four equivalent orientations of a ⟨111⟩ oriented C_{3v} defect in a cubic lattice. For an arbitrary $\underline{B}$ field direction in the ⟨110⟩ plane, there are up to three inequivalent orientations of the ⟨111⟩ defect axes with respect to the field axis, resulting in up to three pairs of line splittings, the magnitude of which is determined by the component of $\underline{B}$ along the defect axis. The field splitting observed in Fig. 4.1 is simplest for $\underline{B} \parallel \langle 001 \rangle$, since for this field direction, all ⟨111⟩ axes are equivalent, resulting in a single doublet. Fig. 4.1 also shows that for $B \parallel \langle 110 \rangle$ there is one doublet resulting from centres oriented along the equivalent ⟨111⟩ and $\langle 11\bar{1} \rangle$ axes and an unsplit component due to centres oriented along the $\langle 1\bar{1}1 \rangle$ and $\langle \bar{1}11 \rangle$ axes, which are orthogonal to ⟨110⟩.

These designations are confirmed by the thermalization behaviour of the Zeeman spittings at various temperatures. Fig.

4.2 is a summary of the intensities of the magnetic field-split components of the A line at three representative temperatures, and with a field of 3.3 T aligned with each of the three principal crystal axes in turn. In the conventional IBE model, all splittings occur in the initial state. The relative intensities of the two components of a given pair of Zeeman lines originating from a set of equivalent centres should therefore show thermalization, whereas this should not be the case for lines originating from inequivalent centres. In Fig. 4.2 one can see a clear thermalization of the two subcomponents for $\underline{B}\|\langle 001\rangle$, for which all defect axes are equivalent. For $\underline{B}\|\langle 111\rangle$ there are two sets of inequivalent orientations corresponding to the inner and outer pairs of lines in Fig. 4.2, which thermalize within each pair. Similarly for $\underline{B}\|\langle 110\rangle$, there are two sets of inequivalent orientations, one of which is perpendicular to $\underline{B}$ and hence shows no splitting. The outer pair thermalizes within itself.

The solid lines in Fig. 4.1 were obtained using the simplified energy eigenvalues of [4.4a]. The best fit was obtained with $g_{eff}=2.2\pm0.1$, where

$$g_{eff}=\gamma+\frac{1}{2}g_h+\frac{1}{2}g_e. \qquad [4.5]$$

It is reasonable to assume that the electron and hole pure spin g-values will be close to 2.0. It is the orbital factor γ which can in principle be greatly reduced due to vibronic coupling. If we assume that $g_h=g_e$, then the orbital g-factor, γ is still underdetermined by [4.5]. According to the above simple model, the X line should also split in a magnetic

field, but with a reduced g'_{eff} given by

$$g'_{eff}=\gamma+\frac{1}{2}g_h-\frac{1}{2}g_e. \qquad [4.6]$$

Within the resolution of the measuring system no well-resolved splitting of the X line could be detected for field strengths of up to 7.6 T, as indicated in Fig. 4.3. The small splitting apparent in Fig. 4.3 is of the order of the instrumental resolution and therefore is not completely convincing. It is possible however to place an upper limit of $\Delta E'=\mu g'_{eff}B<0.2$ meV given that the instrumental resolution of the spectral lines was ~0.4 meV at the observation temperature of 15 K. For a 7.6 T field, this would require that $g'_{eff}\leq 0.45$. Combining [4.5] and [4.6] with the assumption that $g_h=g_e$ yields the limits $g_e=g_h\geq 1.75$ and $\gamma\leq 0.45$. The electron and hole spin g-values are consistent with those derived for other axial IBEs in GaP (Henry et al., 1968; Dean, 1971) and Si (Weber et al., 1979). In these references similar highly anisotropic Zeeman splittings were also attributed to a strong <111> oriented internal defect strain field. In these cases however, the Zeeman splitting of the $m_J=\pm 1$ transition was clearly resolved at lower fields than were employed in this study.

The small value of γ implied by the above analysis is an unusual result for a centre with such a small binding energy, but is consistent with the well known reduction of orbital angular momentum expectation values in defect systems with electronic degeneracy in the presence of strong vibronic coupling

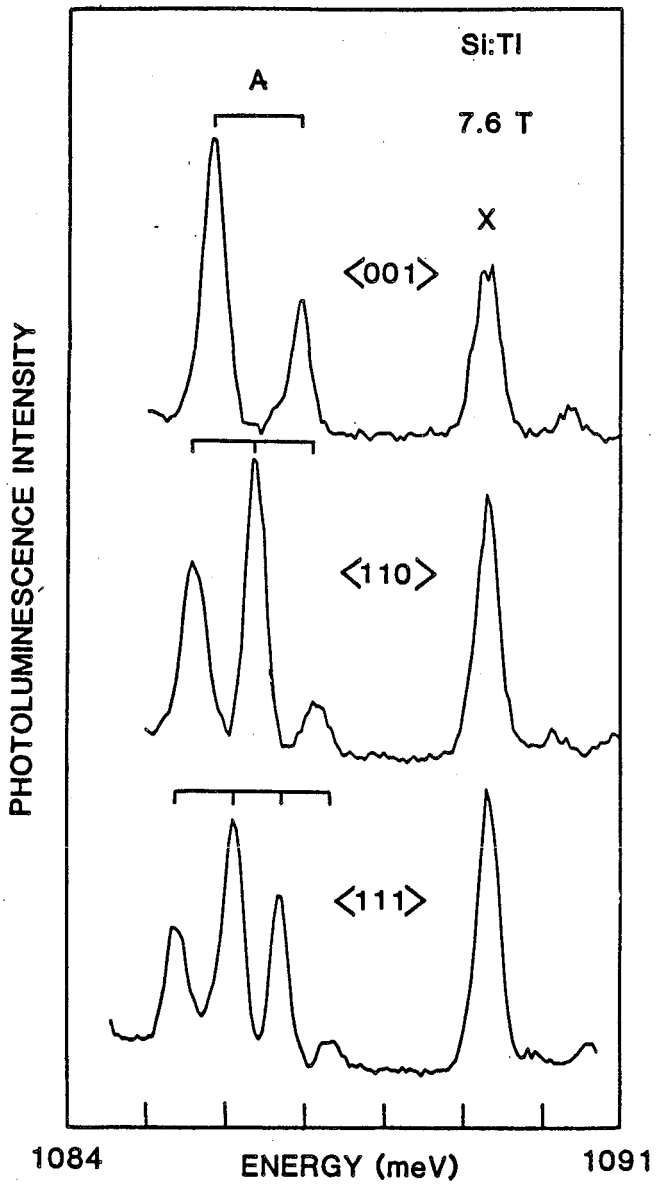

Fig. 4.3: The Si:Tl A and X line at a magnetic field of 7.6 T for the three principal stress directions. Note the absence of splitting of the X line. The slight doublet structure observed for $\underline{B} \parallel \langle 001 \rangle$ is expected according to the model described in the text, but may be a spurious result due to noise.

(e.g. Stoneham, 1975). Such effects are well known from the study of alkali halides and transition metal impurities in wide gap materials, but are virtually unknown from the study of bound exciton processes.

In the case of the A-centres, the electronic degeneracy is the p_x,p_y degeneracy of the C_{3v} hole states. The Jahn-Teller theorem states that for any state with degeneracy other than spin degeneracy there exists at least one degenerate phonon mode such that the total vibronic energy is lowered by coupling to this mode. For the A-centre the defect symmetry is C_{3v} which admits two-fold degenerate Γ_3 phonon modes. In this case the configuration coordinate diagram of Fig. 1.2 is no longer applicable. The vibronic surface now has two minima. Coupling to the degenerate mode causes the system to relax to either one of these minima. For strong coupling, the system relaxes to a single minimum with a consequent reduction in symmetry, the static Jahn-Teller limit. In the more usual case of a so-called dynamic Jahn-Teller interaction, the zero point motions of the defect allow reorientation between the different minima with the result that the symmetry is not reduced. The expectation values of off-diagonal operators however, such as the orbital angular momentum are reduced by a factor proportional to the overlap of the vibrational wavefunctions in the different minima (see Ham, 1967). The expectation value of such an operator among the full vibronic states can be written as the purely electronic expectation value multiplied by a reduction factor which accounts for the degree of overlap of the vibrational

states. This is the factor γ which appears in the Zeeman Hamiltonian of [1.12]. The reduction factor is of the form (Ham, 1965)

$$\gamma = e^{-3E_{JT}/2\hbar\omega}$$

where $\hbar\omega$ is the phonon energy , and E_{JT} is the Jahn-Teller energy, which describes the strength of the coupling to the degenerate phonon mode. The Zeeman data imply an upper limit of γ=0.4 which in turn gives $E_{JT}/\hbar\omega$=0.61. A full determination of E_{JT} and $\hbar\omega$ would require a detailed model for the vibrational modes of the defect which is beyond the scope of this work.

The Jahn-Teller mechanism accounts for the observed similarity in the oscillator strengths of the A and X transitions. In the absence of vibronic effects, the $m_J=\pm 2$ A transition is strictly dipole forbidden, whereas the $m_J=\pm 1$ transition X is partly allowed by mixing with the J=1 manifold of states (Chapt. 1). The observation that the A line is the dominant transition at all accessible temperatures is contrary to the expectation that this is the dipole forbidden transition. When the A/X intensity ratio is corrected for the appropriate Boltzmann thermalization ratio, one obtains the result that the oscillator strength of A is only a factor of at most ten lower than that of X. The oscillator strength of A is most likely increased by mixing with X due to the strong vibronic coupling responsible for the Jahn-Teller interaction.

4.2: Zeeman results: Si:In and Si:Tl P-centres

Fig. 4.4 shows the remarkable similarity of the Zeeman splittings of both the Tl- and In- related P-lines as observed in PL. Both were observed to split into highly isotropic triplet patterns with $g_{eff}=2.0\pm0.1$, in agreement with the data of Sauer and Weber (1983). Although the data presented are for $\underline{B}\parallel\langle 111\rangle$, the data for the other principal crystal axes were identical within the resolution of this study. Such an isotropic splitting indicates a total quenching of the orbital angular momentum of the hole. This could arise, for example, if the internal strain of the defect in the above analysis had a large negative (i.e. compressive) value, so that the hole state of lowest energy was derived from the non-degenerate p_z orbital state. Since $\langle p_z|\underline{L}|p_z\rangle=0$, there can be no orbital contribution to the Zeeman Hamiltonian [4.1] and the hole behaves like a pure spin $\frac{1}{2}$ particle. The total linear Zeeman Hamiltonian is then reduced to

$$H_{LZ}=\mu_B\underline{B}\cdot(\, g_h\underline{s}_h+g_e\underline{s}_e\,). \qquad [4.7]$$

This limit can only be reached if the hole spin-orbit coupling energy, ξ which tends to admix the various p_i states, is small compared with the internal strain energy, ε (Fig. 1.3, left side). If the hole state contains an admixture of more than one p_i state, the expectation value of the orbital angular momentum is no longer zero. Unfortunately, the isotropy of the Zeeman

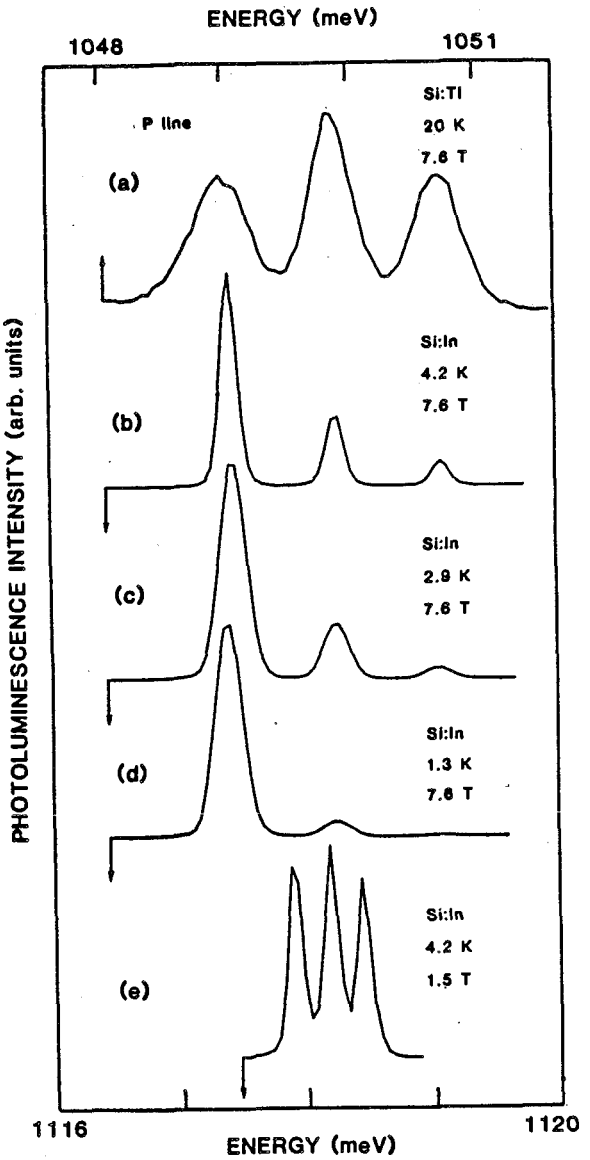

Fig. 4.4: The magnetic field splittings of the P line transition in Si:In, (b-e), and the P line transition in Si:Tl, (a), for B∥⟨111⟩. Splitting patterns were identical for all other crystal orientations. Note the thermalization of the Si:In P line subcomponents (b-d). (a) and (e) show the Si:In and Si:Tl P line splittings in the limit $\Delta < kT$.

splittings for such a centre precludes the determination of the defect symmetry from these data. In principle there should still exist small anisotropies in the g_h and g_e factors which are outside the resolution of PL measurements, but which have been observed using optically-detected magnetic resonance (ODMR), in a variety of other defect systems (e.g. Cavenett, 1981). Fortunately, uniaxial stress can provide detailed information about the defect symmetry in such cases. It will be shown that the defect symmetry of the Si:In and Si:Tl P-centres is C_{2v}.

The thermalization among all three subcomponents in Figs. 4.4b-d is well accounted for by assuming that all of the splitting occurs in a spin triplet IBE initial state. These data are not consistent with the designations of Sauer and Weber in terms of an ($|m_J|=\frac{1}{2}$ initial state)-to-($|m_J|=\frac{1}{2}$ final state) transition, nor are they consistent with their statement that only the two outer components thermalize. In their model, the central component should not freeze out at low temperature since it is due to two superimposed transitions, one of which originates from the lowest initial state level, in clear disagreement with the data of Figs. 4.4b-d.

It is interesting to compare the 4.2 K Si:In spectrum in Fig. 4.4b obtained with above-bandgap excitation, with the spectrum displayed in the inset of Fig. 5.3a, using bulk resonant excitation with a much lower energy input per unit volume, and operating at a similar field strength. This indicates that there may have been a small amount of sample

heating in the data of Fig. 4.4.

Thermalization measurements were not possible for the Si:Tl P-line, given the restricted range of temperatures over which the luminescence is observable (14-25 K). Figs. 4.4a and 4.4e show the splittings of the Si:Tl and Si:In P lines in the limit E<kT. The difference in peak height between the central and side peaks is probably due to the polarization dependence of the spectrometer which was not corrected for.

The magnetic field data for the Si:In centre have been greatly augmented by the excited state measurements discussed in Chapt. 5, which were obtained with the tunable laser system.

4.3: Stress results: Ground state splittings of the A-centres

Stress measurements undertaken on the Si:Tl A line luminescence system confirm the C_{3v} designation for the A-centre symmetry arrived at from the Zeeman data. As expected, the A line shows no splitting for <001> stress (Fig. 4.5), under which all <111> axes are equivalent. The twofold splitting observed for <111> and <110> stresses (Figs. 4.6 and 4.7) is ascribed to the removal of the orientational degeneracy of the axial centres as in the case of the Zeeman data. These doublets show no evidence of thermalization over the temperature range 1.5-10 K, yet for a given temperature the intensity of the upper components decreases rapidly to zero for both stress directions above 100 MPa. This effect may be due to a stress-induced

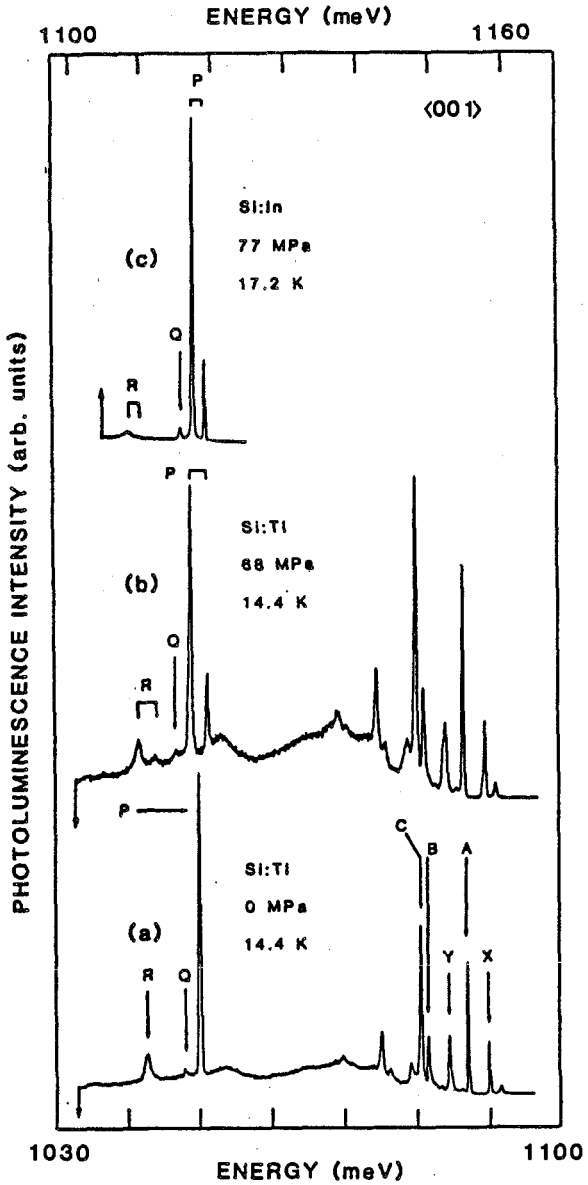

Fig. 4.5: (a) shows a zero stress Si:Tl spectrum at 14.4 K indicating the coexistence of both configurations of the binding centre. (b) shows a spectrum of the same sample with a 68 MPa stress directed along the ⟨001⟩ axis. Note the doublet splitting of both the no-phonon P line and the phonon replica R, and the absence of splitting of the A line. Also note the broadening of X and its replica Y. (c) shows the doublet splitting of the Si:In P line and the similarity in the behaviour of R and Q. The energy scales of (b) and (c) have been offset to emphasize the similarities between the Si:In and Si:Tl P-centres. No correction for the rapidly falling detector response has been made.

reorientation of the various inequivalent orientations of the ⟨111⟩ oriented defects. The lack of thermalization is indicated in Fig. 4.6 by the lack of change in the relative intensities of the two A line components between 4.2 and 14.5 K. In all cases, the behaviour of the phonon replicas C, D, etc. was identical to that of the A line.

The behaviour of the excited state luminescence line X and its phonon replica Y is more complex and is summarized in Fig. 4.7. For ⟨111⟩ and ⟨110⟩ stresses, X clearly splits into a triplet while for ⟨001⟩ stress it splits into a poorly resolved doublet, seen as a weak low energy shoulder on X and as a definite broadening of the phonon replica Y (Fig. 4.5). For each of the three stress directions the shift rates are very similar to those of the A line. However, the lowest energy X line component shows a small extra splitting which is considerably reduced fron the main splitting of the line. A clear example of the triplet splitting of X under ⟨111⟩ stress is given in Fig. 4.6c. This extra splitting will be shown to be due to the removal of some of the electronic degeneracy of the X-line.

The extra splitting of the X line components under all three stress directions provides evidence that the simplifying assumptions in the above Zeeman analysis are not strictly accurate. If the hole states of the two exciton transitions were derived only from the $j=\frac{3}{2}, m_j=\pm\frac{3}{2}$ hole subband, then the stress splittings of the $m_j=\pm 2$ and $m_j=\pm 1$ exciton levels (A and X) would be identical, assuming that the electron states are

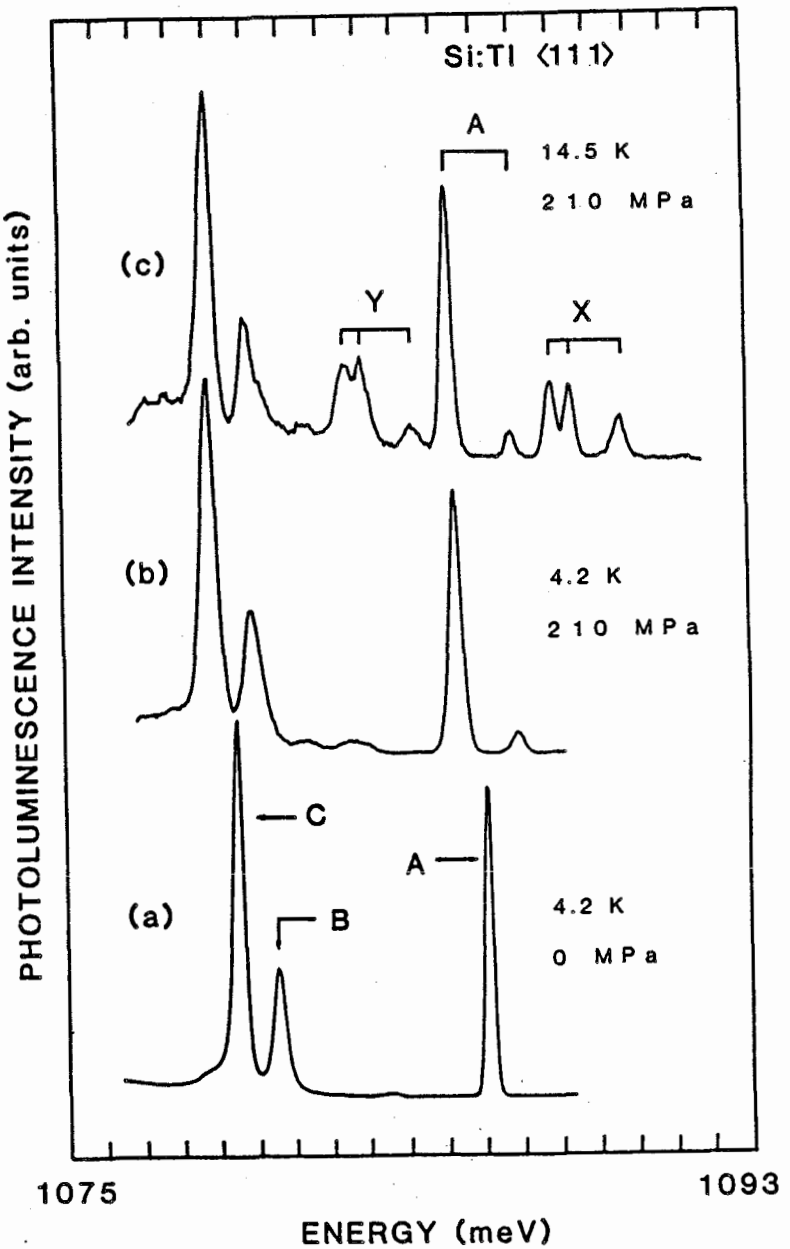

Fig. 4.6: (a) shows an expanded zero-stress spectrum of the Si:Tl A, B, C series. (b) and (c) show a spectrum of the same sample at 4.2 K and 14.5 K respectively, under an applied ⟨111⟩ stress of 210 MPa. There is no thermalization of the stress-split A line components. The excited state X and its phonon replicas are seen to split into a well-resolved triplet (c).

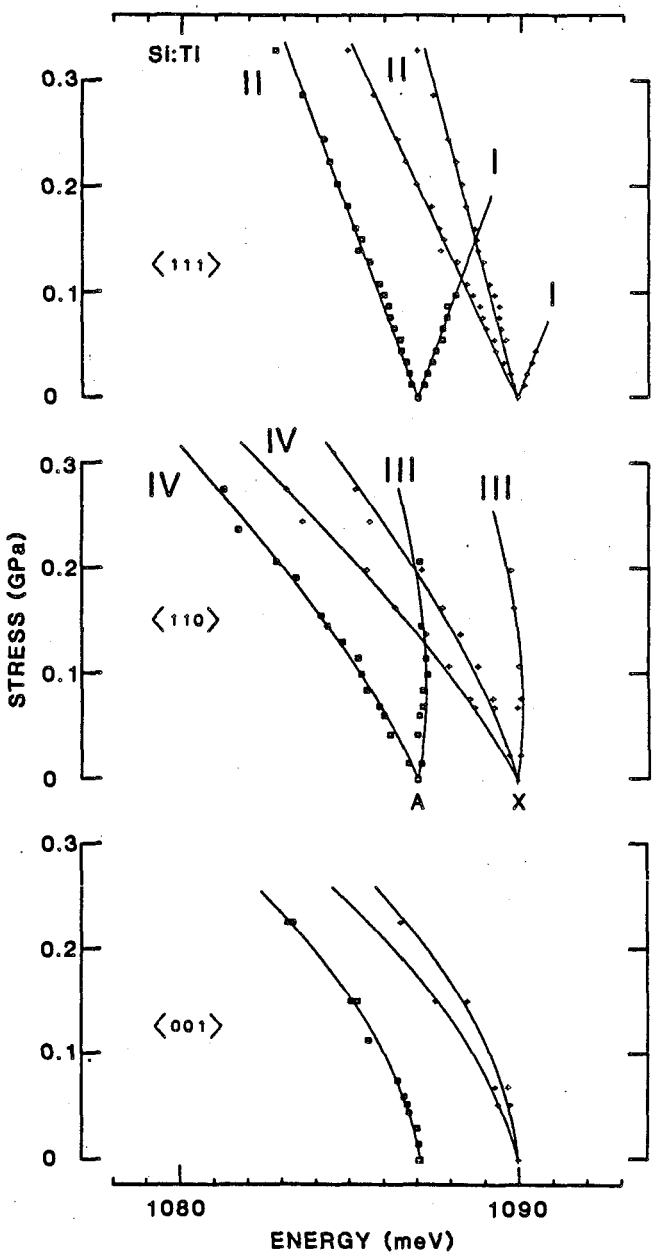

Fig. 4.7: A summary of the Si:Tl A and X transition stress splittings. For ⟨111⟩ stresses the splittings are highly linear, whereas the data show pronounced nonlinearity for ⟨110⟩ and especially for ⟨001⟩ stresses. This nonlinearity is attributed solely to the electron states. The solid lines represent fits using [4.8] in the text. The extra splitting of the lower X component is predicted by the model of Morgan and Morgan (1970). The roman numerals distinguish centres which belong to different orientations with respect to the stress axis.

identical in both cases. It turns out that the small splitting of the low energy stress component of the X line gives a measure of the degree to which the $j=\frac{3}{2}$, $m_j=\pm\frac{1}{2}$ hole substates are mixed in with the $j=\frac{3}{2}$, $m_j=\pm\frac{3}{2}$ states which were used in the simplified Zeeman analysis.

Morgan and Morgan (1970) have derived analytical expressions for the splittings of IBE bound to axial defects in the limit of low strains, where the shift rates are linear. This case is believed to apply to these data for two reasons: first, the high degree of linearity of the <111> data, and secondly, because of the low strains ($<10^{-3}$) which correspond to the maximum stresses applied in this study (300 MPa). It will be argued that the nonlinear stress splittings seen under <001> and <110> are due to the inequivalence of the conduction band valleys of Si under such stresses. The results of Morgan and Morgan depend only on three parameters: the exchange splitting parameter Δ, the axial strain splitting ε of the $j=\frac{3}{2}$ hole band, and a single parameter which describes the splitting rate of the $j=\frac{3}{2}$ hole band, and which is assumed to be isotropic. For the purpose of this analysis this isotropic splitting will be described by a term of the form KT where K is an experimentally determined constant, and T is the applied stress. For free excitons in Si it is well known (Laude et al., 1971) that the valence band splitting rates are similar in magnitude for each of the three stress directions. From the data of Laude et al. one can infer K values of 45.2, 35.0, and 37.5 meV/GPa for stresses in the <001>, <111>, and <110> directions respectively.

In the model of Morgan and Morgan, the hole band splitting rate K is entered as a single phenomenological parameter, to be determined by experiment.

The splitting rates for the $m_J=\pm 2$ and $m_j=\pm 1$ exciton levels of a defect oriented with an angle α between the direction of the external stress axis and the internal $\langle 111\rangle$ or equivalent strain axis, were given by Morgan and Morgan as

$$E_{\pm 2} = pKT \qquad [4.8a]$$

$$E^{S}_{\pm 1} = -\left[\frac{-p+\frac{1}{2}py-\frac{1}{2}\sqrt{3}ky}{\sqrt{(\ 1-y+y^2\ )}}\right]KT \qquad [4.8b]$$

$$E^{A}_{\pm 1} = -\left[\frac{-p+\frac{1}{2}py+\frac{1}{2}\sqrt{3}ky}{\sqrt{(\ 1-y+y^2\ )}}\right]KT \qquad [4.8c]$$

where $y=\Delta/2\varepsilon$, $p=\frac{1}{4}(1+3\cos 2\alpha)$, and $k=\frac{1}{4}\sqrt{(1-\cos 2\alpha)}$. The superscripts A and S refer to antisymmetric and symmetric exciton states which arise out of their model. As an example of the application of these expressions consider the case of a $\langle 111\rangle$ external stress. One quarter of the defects have their internal strain axes parallel to the stress axis and hence $\alpha=0$. No additional splitting is expected for this situation since it can be thought of as merely modifying the magnitude of the internal strain. This is the case for the upper line in Fig. 4.7, labelled I. For the remaining defects, oriented along the $\langle 1\bar{1}1\rangle$ and equivalent axes, $\cos\alpha=1/3$. For this case, a splitting of the $m_J=\pm 1$ state is predicted by [4.7b] and [4.7c], the magnitude of which can be seen to depend inversely on the ratio

of exchange to strain splitting, $y=\Delta/2\varepsilon$. This splitting is assumed responsible for the two lowest lying X line components, labelled II, seen in Fig. 4.7. The small magnitude of this splitting confirms the assumption made in the Zeeman analysis that $\Delta>>\varepsilon$ and that therefore the admixture of $j=\frac{3}{2}$, $m_j=\pm\frac{1}{2}$ hole band substates is relatively small. By comparing the magnitude of this splitting to the dominant splitting between the I and II components of the A line, it is possible to obtain an estimate of the value of ε. The difference in shift rates between the I and II components of the A line is given by $\frac{4}{3}KT$ while the splitting of the II component of the X line is

$$\frac{4}{3}\ \frac{y}{\sqrt{(1-y+y^2)}}\ KT$$

The experimentally observed ratio of these splittings of 22.1:6.3 (Table 4.1) gives the value $\Delta/\varepsilon=0.51$. Combining this result with the exact expression for the theoretical zero-field splitting of the $m_J=\pm2$ and $m_J=\pm1$ levels (Fig. 1.4) gives the values $\Delta=4.0$ and $\varepsilon=7.9$ meV. This value of Δ should be compared with the value of $\Delta=3.7$ meV which was derived in the Zeeman section with the approximation that $\varepsilon>>\Delta$. In the above analysis, specific knowledge of the hole band splitting rate K was not required, since it cancelled out in the above ratio. From these values of ε and Δ one can work backwards from the theoretical A line splitting to obtain K from the predicted A line splitting of $\frac{4}{3}KT$. This gives a value of K=16.6 meV/GPa which should be compared with the value obtained by Laude et al.

(1971) for free excitons, namely 35.0 meV/GPa.

Under a ⟨110⟩ stress, one half of the defects are oriented with $\cos\alpha=\sqrt{(2/3)}$, and the rest with $\cos\alpha=0$. These two classes are labelled III and IV respectively in Fig. 4.7. The III and IV components of the A line should split with a rate given by KT. The IV component of the X line should split with a rate of

$$\frac{3}{2}\,\frac{y}{\sqrt{(1-y-y^2)}}\,KT$$

while the III component should split with a value equal to one third of the above. In these experiments, only the splitting of the IV component was observed. It is possible that the small magnitude of the splitting of the upper component (<2 meV/GPa), combined with the lower intensity of the upper component, have obscured detection of this extra splitting. When the above analysis is applied to the ⟨110⟩ data, one obtains $\Delta/\varepsilon=0.50$, in excellent agreement with the value derived for the ⟨111⟩ data. A value of K= 19.4 meV/GPa was obtained from the shift rate of the III and IV components of the A line, which is also greatly reduced from the free exciton value of 37.5 meV/GPa.

For the case of a ⟨001⟩ external stress, the situation is simpler, in that all defects are equivalent. For this case, $\cos\alpha=1/\sqrt{3}$, and there is no splitting of the A line. Using the above values of ε, Δ, and the average of the two K values, one obtains an X line splitting of 5.2 meV, in excellent agreement with the experimentally observed value of 5.0 ± 0.5 meV.

Stress direction	Shift rate (meV/GPa)			
	A line		X line	
⟨001⟩	-5.7		-3.2 -8.2	ΔE=5.0±3.0 E_{avg}=5.8
⟨110⟩	6.5 -12.9	ΔE=19.4	5.2 -8.5 -16.4	 ΔE=8.0 E_{avg}=12.5
⟨111⟩	10.1 -12.0	ΔE=22.1	12.1 -8.4 -14.7	 ΔE=6.3 E_{avg}=11.6

Table 4.1. The linear shift rates of the A and X line components as determined by the least squares fits in Fig. 4.7. Note the close agreement of the average of the two lower X line shift rates in each case with the lower A line shift rate.

Table 4.1 gives a summary of the shift rates obtained in this study. The self-consistency of these data implies a remarkably good agreement with the simple phenomenological model of Morgan and Morgan, which has never been directly tested by experiment. In fact the close agreement is probably fortuitous to a large extent given that the assumption of isotropic shift rates is a rather crude approximation, especially in the vicinity of an axial defect. It is interesting to compare the above results with those of Onton and Morgan (1970) who observed an order of magnitude reduction in the hole deformation potentials for the isoelectronic donor GaP:Bi. The extreme reduction in the deformation potentials of this system were attributed to the strong vibronic coupling of the exciton to localized phonon modes of the defect. It is possible however that this reduction may just have been due to the extreme localization of the hole at the GaP:Bi defect, which invalidates the use of deformation potentials describing the behaviour of states at the valence band edge.

It is interesting to note that the reduction of the deformation potentials in the present case are roughly similar in magnitude to those reported by Henry et al. (1984) for the case of the Si:Be isoelectronic defect. In that study the effects of stress on the exciton states were described by two deformation potentials b' and d', similar in definition to those employed in studies of the free exciton (Laude et al., 1971). The use of two parameters models the anisotropy of the valence band splittings. Henry et al. found that the value of d', which

models the response to trigonal (<111>) deformations, was virtually identical to that of the free exciton, while b', which models the response to tetragonal (<001>) stresses was appprox-imately one half of the free exciton value. These results have been cited as confirmation of the isoelectronic acceptor model for this IBE which was put forward by Labrie et al.(1983), in which the hole is bound in an effective mass-like state, derived largely from band edge states. The fact that the deformation potentials of the Si:Tl A-centres are only reduced by a slightly larger factor indicates that the hole states are not as deep as one would expect considering the presence of Tl in the binding centre complex. This seems to suggest that the potential binding the hole in this case is more slowly varying than one would expect for the central cell of isolated Tl. In addition, the results of the next section show that the electron states are also relatively shallow. These two results are consistent with a more delocalized binding mechanism such as Allen's strain field model (1970).

Valley-orbit effects

The above analysis has completely ignored the stress dependence of the electron states. In the previous section it was assumed that the stress dependence of the hole states was in the linear region of the model of Morgan and Morgan (1970). This is the result of the relatively low applied strains, ($<10^{-3}$) as well as the relatively large value of the internal

strain energy (8 meV). It is the mixing of the $j=\frac{3}{2}$, $m_j=\pm\frac{3}{2}$ with the $j=\frac{3}{2}$, $m_j=\frac{1}{2}$ hole band which induces nonlinearities in the dependence of the hole energies, and this mixing will be small given the 16 meV splitting of the $j=\frac{3}{2}$ hole states implied by ε=8 meV. The starting point for what follows is the assumption that the electron in this IBE is effective mass-like i.e. derived from X conduction band edge electron states. The stress dependence is therefore expected to be similar to that of the common substitutional donors in Si.

It is assumed here that the electron states involved in the IBE ground state are derived from the totally symmetric 1S Γ_1 (T_d) electron state. Assuming that the electron states are less localized than the hole states, it seems reasonable to approximate the C_{3v} nature of these states by the T_d states to which they tend at large distances from the defect. This is probably an acceptable assumption for the higher lying Γ_3 and Γ_5 states which vanish at the core, but must have less validity for the Γ_1 state. Under ⟨111⟩ stress, all six conduction band minima of the perfect Si lattice shift by the same amount, proportional to the deformation potential Ξ_u of the X conduction band minima. Under ⟨001⟩ compressive stress ($s<0$), two of the bands are lowered by an amount $\frac{1}{3}\Xi_u s$, while the other four are raised by $-\frac{1}{6}\Xi_u s$. This causes a mixing of the Γ_1 and Γ_3 states, which contain different combinations of the different conduction band valleys. The Γ_1 state shifts to lower energy in a non-linear manner, asymptotically reaching a linear shift rate at high stress as the wavefunction becomes increasingly associated

with the lowest two conduction band valleys. Similar considerations apply for the case of <110> stress where there are four instead of two bands at lowest energy, with the result that the stress-induced nonlinearity is smaller. These qualitative features are seen to apply to the A-centre stress data shown in Fig. 4.7.

The fits to the <001> and <110> data in Fig. 4.7 were obtained by means of [1.7a], assuming that all of the nonlinearity was due to the electron states. The shift rate of each of the eight A line components under the three principal stresses was described by two parameters, a linear shift rate parameter unique to that component, and the parameter Δ_c which modelled the nonlinearity, and which was the same for all eight components. The fit was obtained by a least squares method using a simplex minimization algorithm. Note the close agreement of the X line nonlinearity with that of the A line. The X line slopes were also allowed to vary freely. Assuming the electron deformation constant Ξ_u=8.7 eV, the value obtained by Laude et al. (1971) from free exciton data, a value of Δ_c=5.8 meV was obtained. This implies a valley-orbit energy splitting $E_{vo}=6\Delta_c$ between the Γ_1 and Γ_3 states of 35 meV. This value is rather high compared to values obtained by Tekippe et al. (1972) for substitutional donors in Si. These authors observed a significant reduction of the deformation potential for Γ_1 electron states. It is reasonable to suppose that the response to stress would be somewhat "stiffer" in the vicinity of a large complex containing Tl. A reduction of Ξ_u to 7.0 eV would

decrease the value of E_{vo} implied by the data in Fig. 4.7 to ~20 meV, a value more comparable to that of the shallower substitutional donors. Evidence for such a reduction in Ξ_u will be presented in the section on the excitation spectra of the Si:In defect in Chapt. 5.

A knowledge of the energy of the Γ_3 electron state allows one to make a rough estimate of the hole binding energy. Assuming for the moment that 35 meV is the true valley-orbit splitting, this implies the existence of an excited state of the exciton at an energy of approximately 1122 meV, or 35 meV below the no-phonon free exciton edge of 1154.6 meV. The binding energy of the free exciton is known to be 14.7 meV which places the bandgap energy at 1169.3 meV. It is known from the study of shallow donors in Si (see e.g. Ramdas, 1981) that the position of the $\Gamma_{3,5}$ level with respect to the ionization limit agrees quite adequately in every case with the predictions of effective mass theory, even in the case of the more deeply-bound donors. This is because, unlike the symmetric Γ_1 state, the $\Gamma_{3,5}$ level has a node at the central cell. In all cases the Γ_3 level has been found to be bound by an energy very close to the 31.3 meV prediction of effective mass theory (Ramdas, 1981). It is worth noting that the above energy is expected for an electron bound to a point positive charge, and not to the smeared out charge distribution of a localized hole. The finite extent of the hole could reduce this value somewhat from 31.3 meV. Assuming that the A-centre behaves like an isoelectronic donor bound to a very localized electron, this 31.3 meV binding energy of the $\Gamma_{3,5}$

level places the ionization limit of the A-centre at ~66 meV above the A line, or 1153 meV. This energy corresponds to ionization of the electron with the hole remaining bound to the defect. The energy difference between this value and the bandgap energy of 1169.3 meV gives an estimate of the hole binding energy of ~17 meV. A smaller valley-orbit splitting of, say 20 meV would increase this value to ~30 meV. This would require a reduction of the electron deformation potential in the above analysis to a value around 7.0 eV. Such small binding energies for the primary particle have been directly observed before by Cohen et al. (1977) for the case of NN_i pairs with i>7. Unfortunately in the case of the A-centre it is has been impossible to determine the hole binding energy by more direct means. The electron binding energy cannot be determined from thermal activation measurements because of the configurational metastability which the centre exhibits above 10 K. In addition, it has not been possible to date to observe the excited state spectrum of the centre through excitation spectroscopy for reasons as yet unknown.

4.4: Stress results: Ground state splittings of the P-centres

The uniaxial stress splittings of the P lines in Si:Tl and Si:In are illustrated in Fig. 4.5 for the case of <001> stress. For both centres, the P line splits into similar doublets, in contrast to the Si:Tl A line, which does not split under this stress direction. The intensity ratio of the com-

ponents was observed to be independent of temperature, as in the case of the A-centre stress splittings. As in the ⟨111⟩ and ⟨110⟩ A-system data, the lack of thermalization between the components indicates that the splitting is due to an orientational, rather than electronic degeneracy. A rapid decrease in the intensity of the upper component with increasing stress was observed, and this suggests some form of reorientation of the centres as in the A-centre data. The ⟨111⟩ and ⟨110⟩ stress splittings, summarized in Figs. 4.8 and 4.9, also display quite similar behaviour. The ⟨110⟩ data in Fig. 4.8 give a clear example of the reorientation to the lower energy stress component at high stress. It is evident from these data that the symmetries of the P- and A-centres are quite different.

Fig. 4.8 gives a comparison of the Si:In and Si:Tl P-type spectra at representative ⟨110⟩ stresses. These defects show strong similarities in the form and magnitude of the stress splittings, indicating that the same defect symmetry is present in both cases. The Si:In P line was observed to split into a nonthermalizing triplet at stresses above 20 MPa (Figs. 4.8b and 4.7c), offering further evidence of a lower symmetry for the P-centre configuration. For the Si:Tl P line there is no evidence of a higher energy component up to stresses of ~150 MPa, beyond which the upper component begins to broaden substantially. It should be emphasized that this broadening is probably not due to inhomogeneous stress since such effects should have a much greater broadening effect on the lower energy component, which is displaced much further from the zero stress energy. Above

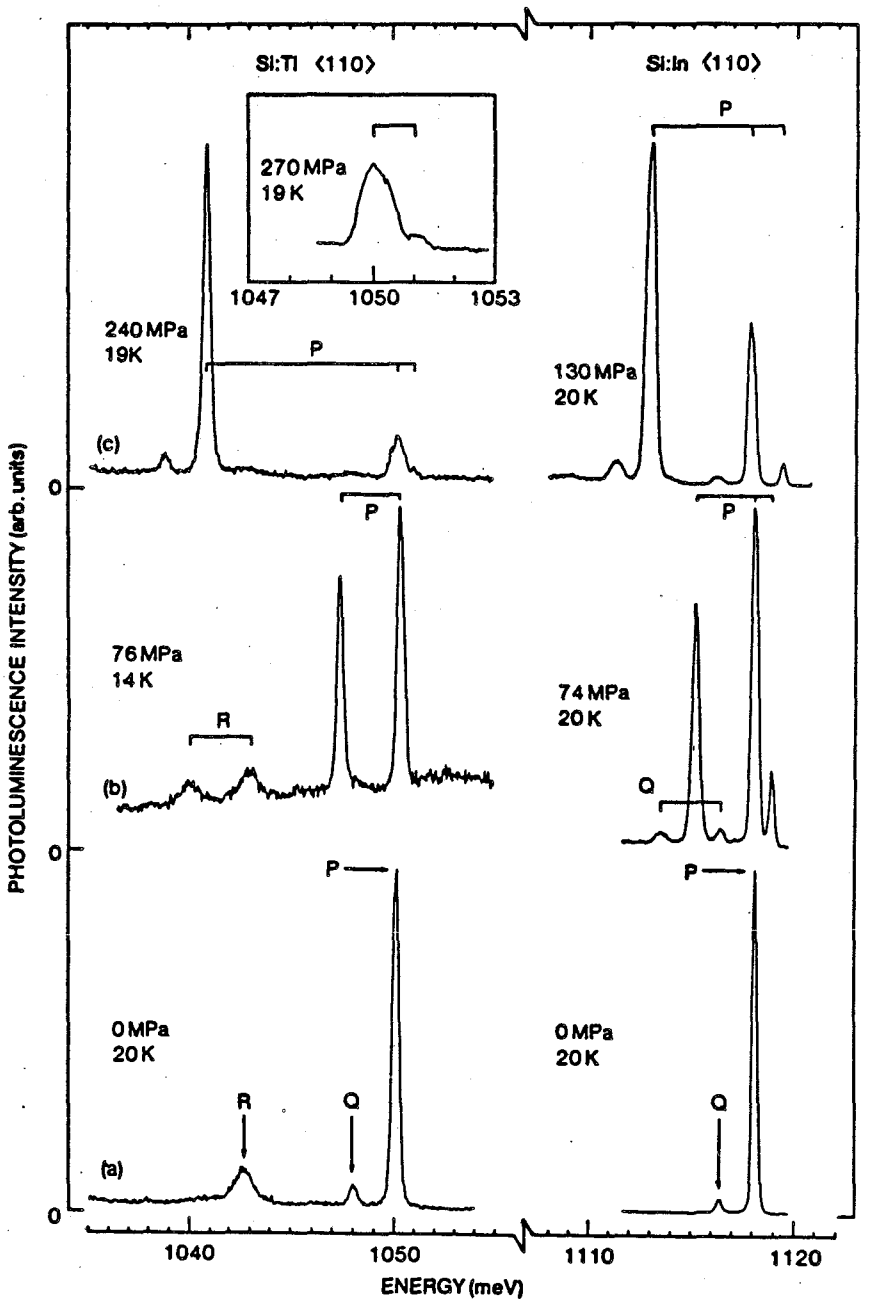

Fig. 4.8: A comparison of the Si:Tl and Si:In P, Q, R spectra under ⟨110⟩ stresses. (a) shows the zero stress spectra. (b) indicates the splittings at 76 and 74 MPa for Si:Tl and Si:In respectively. At this stress the Si:In P line splits as a doublet. Note the similarities in the intensities and energy splittings of the two lower components in each case. (c) indicates the stress splittings at higher stress, showing the appearance of a weak third component in the Si:Tl spectrum at 270 MPa (inset, Fig. 4.5c). The relative intensity ratios show the same qualitative behaviour in both samples.

200 MPa the intensity of the upper component is greatly reduced, but nonetheless the appearance of a weak third component is evident on the high energy side of the upper component (see inset in Fig. 4.8c). Similar spectra were observed in other samples. Note that for both Si:Tl and Si:In there is a similar shift in intensity from the central peak as the stress is increased.

From Fig. 4.8 it is evident that in both Si:In and Si:Tl the excited state Q transition and the local mode R transition have the same stress behaviour as the no-phonon P line. This was also the case for <001> and <111> stresses.

The stress splitting patterns summarized in Fig. 4.9 are consistent with a C_{2v} defect symmetry for the Si:In and Si:Tl P-centres. For the moment a detailed discussion of this result will be deferred until the Si:In excitation spectra are presented in Chapt. 5.

It is interesting to note that the P lines also exhibit nonlinear shift rates for <001> and <110> stresses, although to a lesser degree than the Si:Tl A line. An analysis similar to that used in modelling the nonlinear shift rate of the A-centre data, using [1.7a], yields valley-orbit splittings of ~40 and 60 meV for the Si:In and Si:Tl P-centres respectively if the free electron deformation potential of Ξ_u=8.7 eV is used. The least squares fits to the P-centre stress data are given by the solid lines in Fig. 5.9. In this analysis the linear shift rates of each component were again modelled by a single parameter unique to that component, while the nonlinearity was modelled solely by

the valley-orbit energy Δ_c and the deformation potential Ξ_u. It will be shown in the next section that the effective deformation potential for the Si:In Γ_1 state is actually considerably reduced from this value, and a similar effect is expected for the Si:Tl centre. This has the result of significantly reducing the magnitude of the valley-orbit energies derived by the fits to the data in Fig. 4.9.

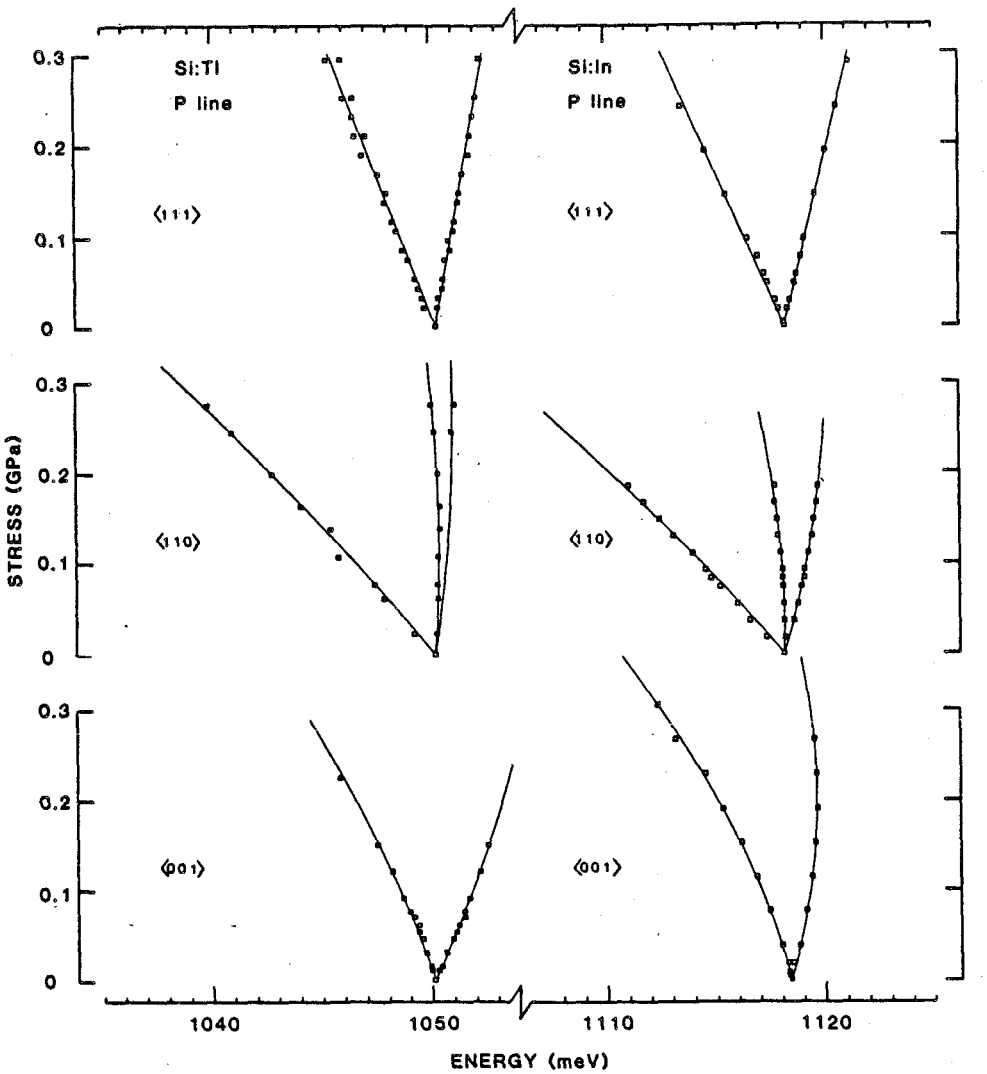

Fig. 4.9: A summary of the P line splittings under uniaxial stress for both Si:Tl and Si:In. The splittings show nonlinearities which are qualitatively similar to, but slightly reduced from, those of the Si:Tl A line.

Chapter 5: Excitation spectroscopy of the Si:In centre with stress and Zeeman perturbations

5.1: Zeeman Results

The zero field excitation spectrum for the Si:In isoelectronic centre is shown by the lower spectrum in Fig. 5.1, which was obtained using the previously described OPO system. This spectrum is identical to the one first observed by Wagner and Sauer (1983). The spectrum represents the emission intensity of the dominant P line transition (Fig. 5.1, lower curve) as a function of excitation energy. Following the labelling convention of Wagner and Sauer this line is henceforth referred to as P_0^0. The subscript identifies the electronic state, while the superscript denotes the number of Stokes or anti-Stokes phonon modes which are excited.

Because of the long 200 μs luminescence lifetime of these centres at 4.2 K, it was possible to scan the laser energy over the P_0^0 luminescence transition by rejecting scattered laser light during the actual firing of the laser pulse by means of a chopper wheel synchronized to the laser pulse train. In addition to the P_0^0 line, which is the predominant PL transition, two even stronger no-phonon excited states labelled P_2^0 and P_3^0 are observed at energies 11.4 and 36.4 meV above P_0^0. The P_3^0 transition energy of 1154.3 meV is almost exactly coincident with the free exciton no-phonon energy of 1154.6 meV, so this state is only bound by a few tenths of an meV. The anti-Stokes replicas P_0^{-1} and P_2^{-1} are derived from the coupling of

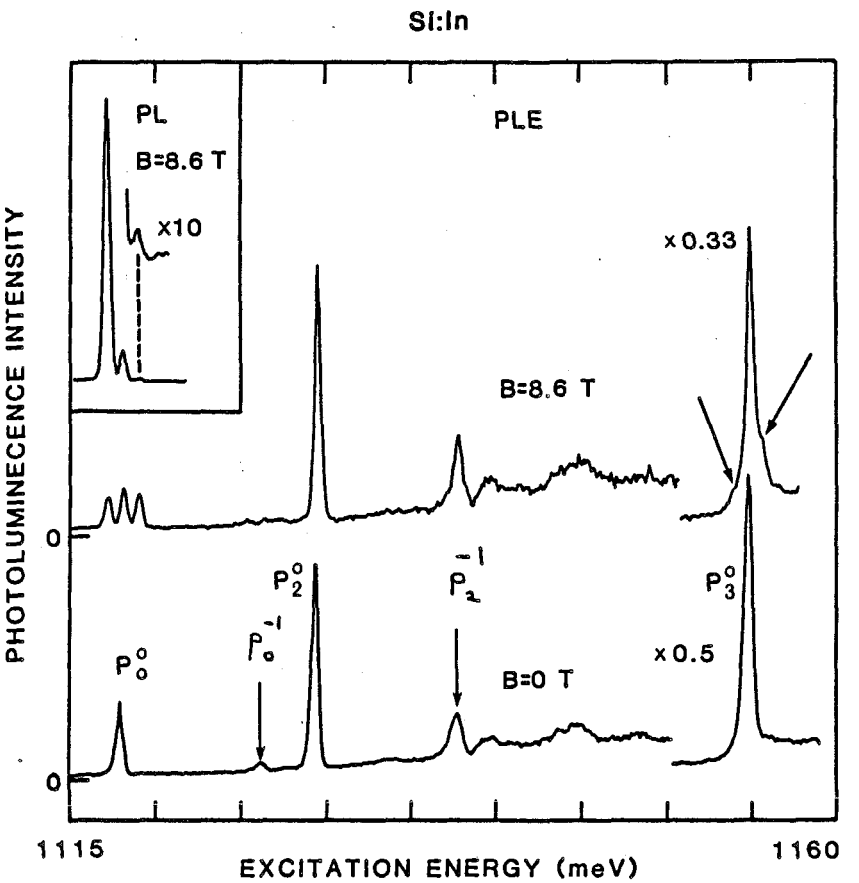

Fig. 5.1: Excitation spectrum of the In isoelectronic bound exciton with magnetic fields of zero and 8.6 T, monitoring the total PL intensity of the ~1118 meV P_0^0 no-phonon lines. Note the weak shoulders on the P_3^0 line upon application of the field. The inset shows the PL spectrum obtained at the observation temperature of 4.2 K showing the strong thermalization of the Zeeman subcomponents of P_0^0, which is of course not observed in the excitation spectrum. P_0^{-1} and P_2^{-1} are anti-Stokes replicas of P_0^0 and P_2^0 respectively generated by coupling to the same local mode responsible for the R transition in Fig. 4.1c.

P_0^0 and P_2^0 to the 8.3 meV phonon mode responsible for the Stokes transition R in Fig. 4.1c. That line is denoted P_0^1 by Wagner and Sauer. The value of 8.3 meV is somewhat reduced from the 9.0 meV value observed for the Stokes replica, indicating a softening of the vibronic coupling for the exciton state.

This spectrum is quite different from any of the shallow acceptor-like or donor-like spectra observed in other isoelectronic centres in Si to date, which consist of a set of absorption lines decreasing in intensity with increasing energy, and converging to an ionization limit of 30-40 meV above the ground state transition (Wagner et al., 1981; Wagner and Sauer, 1982; Thewalt et al., 1982; Thonke et al., 1985).

The magnetic field dependence of the P_0^0 line has been discussed in a previous work which involved only PL measurements (Watkins and Thewalt, 1985). In that work it was demonstrated that the P_0^0 line split into a triplet with a splitting that was independent of the direction of the applied field, and this fact was used to argue that the hole orbital angular momentum was quenched by a low symmetry defect field. The upper excitation spectrum in Fig. 5.1 shows the effect of an 8.6 T magnetic field on the excited states. The P_0^0 line splits with an effective g-value of 2.0, while the P_2^0 line does not split for fields up to 8.6 T. This behaviour is consistent with the coupling of two spin $\frac{1}{2}$ particles to form a spin triplet and a spin singlet with a j-j coupling interaction energy of 11.4 meV. This spectrum was obtained by monitoring the PL intensity at the zero field P_0^0 energy, with the spectrometer slits opened wide

enough to accept all three PL transitions. Identical spectra were obtained by selectively monitoring any of the three magnetically split P_0^0 subcomponents, the only difference being due to the different signal strengths caused by the extreme thermalization of the PL subcomponents (see inset, Fig. 5.1). This behaviour is expected for a purely electronic splitting, and differs from the case of the stress splittings discussed below, which are due solely to orientational effects.

Although P_3^0 at first appeared to remain essentially unsplit in an 8.3 T field, a closer examination revealed evidence of shoulders forming on either side of the zero field energy, consistent with an effective g-value close to 2.0, but with a rather low intensity (see upper excitation spectrum, Fig. 5.1). It will be argued below that the nature of the electron state responsible for P_3^0 results in a negligible j-j coupling splitting, leading to a superposition of a strong singlet and a weak triplet transition, thus explaining the low intensity of the shoulders.

Fig. 5.2 is a summary of the polarization dependence of the magnetic subcomponents of the P_0^0 triplet transition for the case in which the polarization of the excitation beam is either parallel or perpendicular to the magnetic field. Excitation was in all cases approximately along the ⟨110⟩ crystal axis. It is interesting to note that this polarization dependence is the opposite of that expected for electric dipole transitions from a spin triplet state to a spin singlet state in a system with full rotational symmetry. This feature will be explained below.

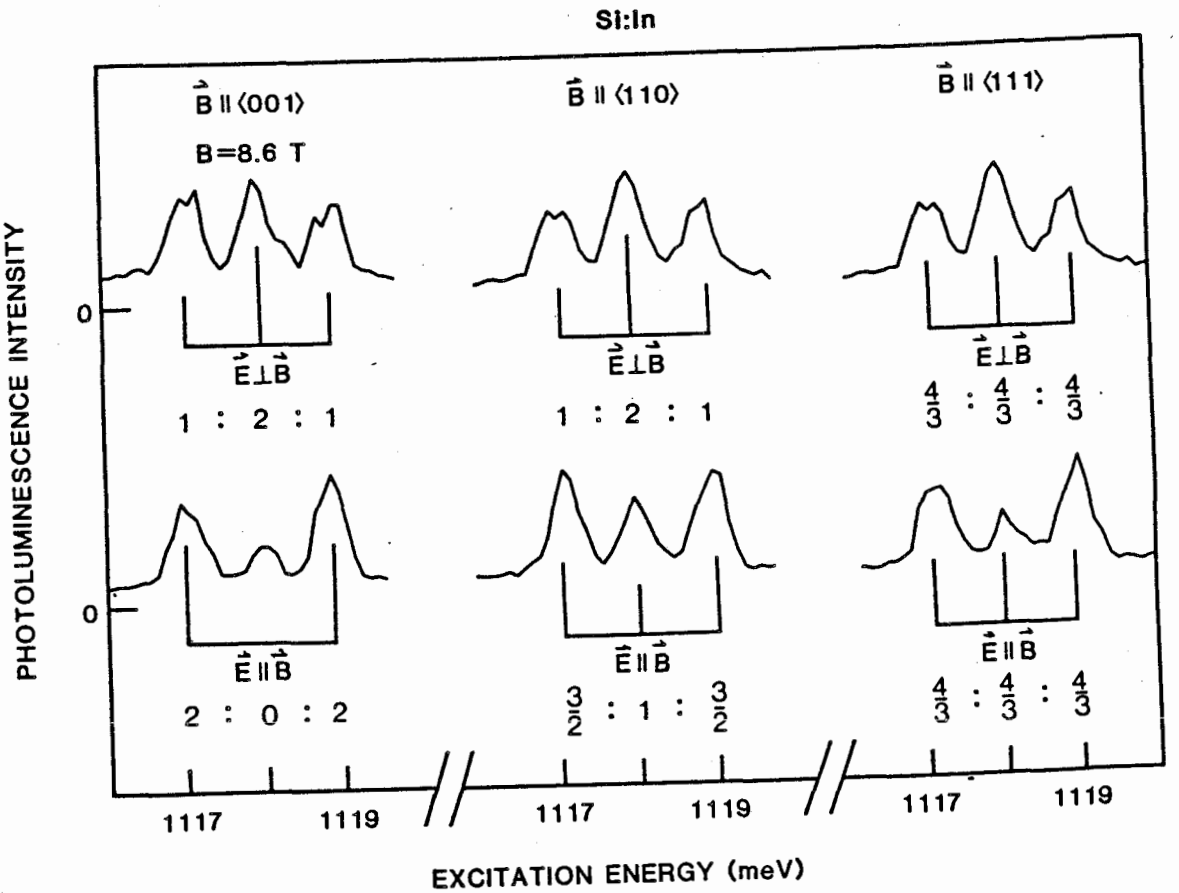

Fig. 5.2: Excitation spectrum of the P_0^0 line with the electric field of the exciting radiation alternately parallel or perpendicular to the 8.6 T magnetic field. The polarization dependence is the opposite of that expected for a pure spin triplet with full rotational symmetry. The length of the bars under each component is proportional to the relative strength of that component as calculated using the model described in the text.

It is unfortunate that no PLE spectra could be obtained for either of the Si:Tl IBE configurations. Attempts were made to resonantly excite the Si:Tl A- and P-centre excitons while monitoring various PL transitions. No exciton absorption could be detected however due to the presence of a strong featureless absorption band which was observed from the monitor energy right up to the transverse acoustic free exciton edge. This is believed to be due to the generation of free carriers by some two photon absorption process. A similar, but weaker process was observed in the Si:In system. This process is could be due to the high peak intensity of the pulsed OPO excitation, and is likely reduced by the use of continuous excitation sources, such as a colour centre laser.

5.2: Stress results

Fig. 5.3 summarizes the important features of the PLE spectrum under a uniaxial stress of 95 Mpa in the ⟨111⟩ direction. Inset (a) shows the splitting of the P_0^0 line as observed in PL with above-gap excitation under the same conditions. The stress dependence of this line was previously investigated by means of PL, and on the basis of a lack of thermalization of the subcomponents for stress along any of the three major axes, it was concluded that the splittings were purely orientational (Watkins and Thewalt, 1985). This is confirmed in a convincing fashion by the PLE spectra of Figs. 5.3b and 5.3c in which the PL emission is monitored at the upper and lower stress-split P_0^0

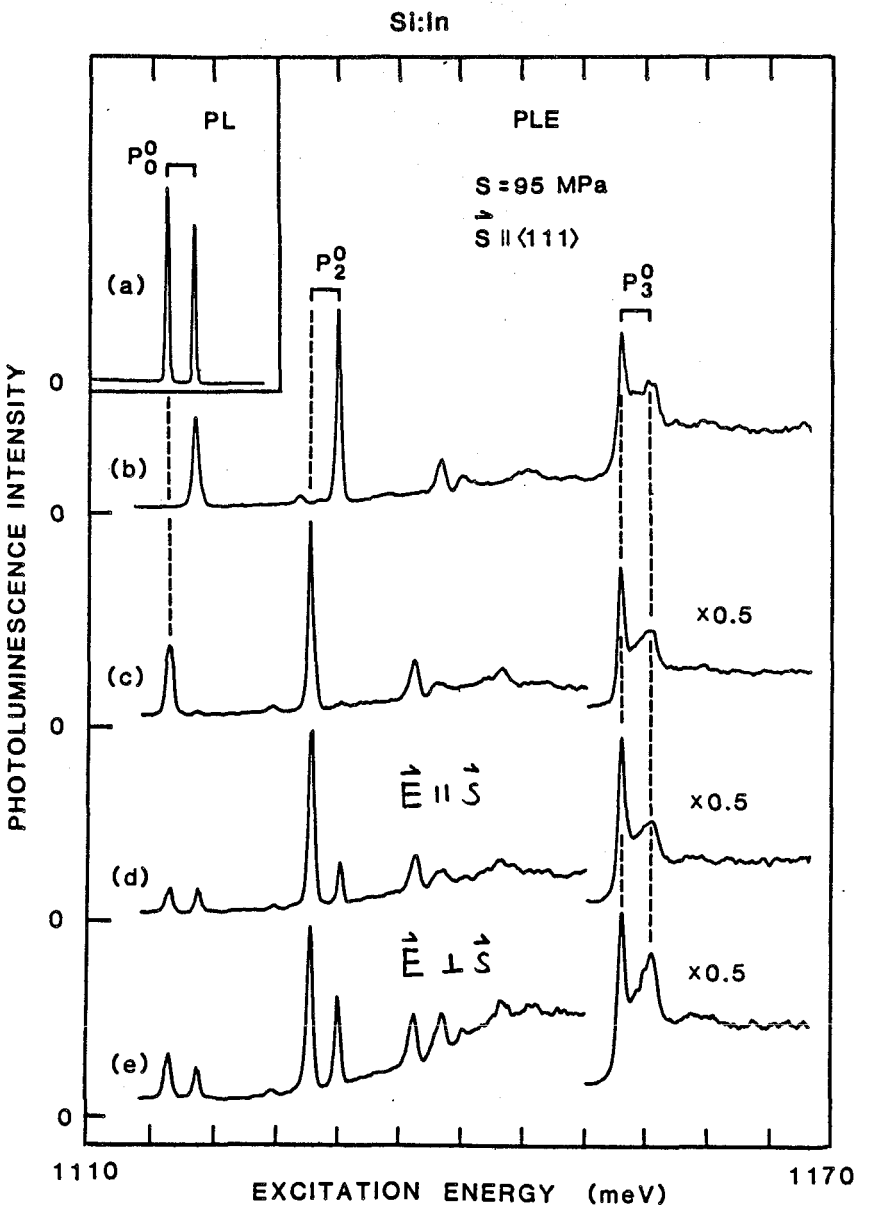

Fig. 5.3: Inset (a): PL spectrum of the P_0^0 line under a 95 MPa stress along the ⟨111⟩ axis showing the lack of thermalization at 4.2 K. (b) and (c): The excitation spectra obtained when monitoring the upper or lower PL subcomponents of P_0^0 respectively. These spectra confirm that the splittings of P_0^0 and P_2^0 are due solely to orientational degeneracy. (d) and (e): The excitation spectra obtained by polarizing the excitation beam respectively parallel or perpendicular to the stress axis. In these spectra the spectrometer bandpass was greatly increased in order to collect signal from both P_0^0 PL components simultaneously.

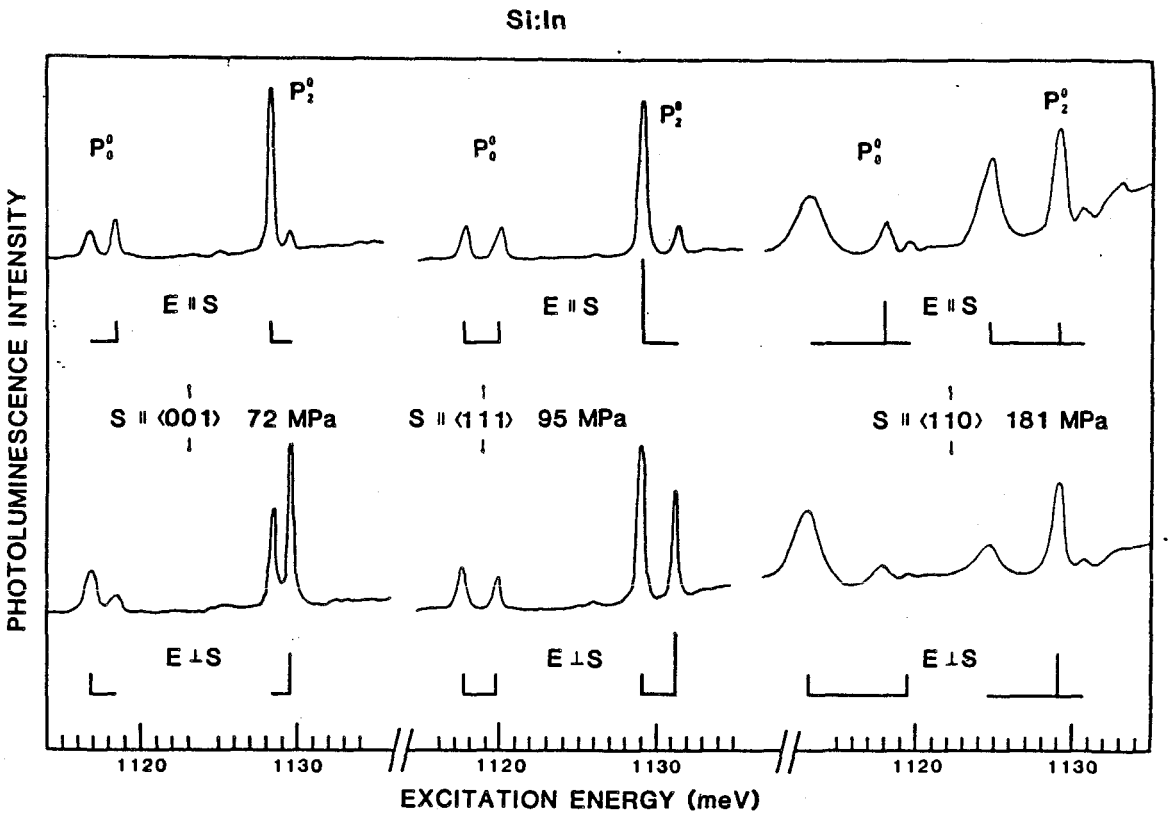

Fig. 5.4: Summary of the polarization dependence of the P_0^0 transition for all three stress directions. Vertical bars represent the relative intensities predicted for a "π" (P_2^0) or "σ" (P_0^0) oscillator (Kaplyanski), for the two orientations of the electric vector. Results for ⟨110⟩ stress are the least reliable given the somewhat inhomogeneous stress obtained.

components respectively. For the case of the P_0^0 and P_2^0 resonances, excitation only occurs into the defect orientation corresponding to the PL energy being monitored. The behaviour of P_3^0 is more complicated. Under <111> stress P_3^0 splits into two components with the same shift rates as P_0^0 and P_2^0, but the upper component becomes quite broad. In addition, both components are observed simultaneously while monitoring either of the P_0^0 subcomponents. This is probably due to the fact that P_3^0 is essentially resonant with with the free exciton no-phonon energy, permitting excitation transfer from one class of defect orientations to the other via free exciton generation and subsequent recapture. It is interesting to note that there is nonetheless a small enhancement of the lower P_3^0 absorption strength when monitoring at the lower P_0^0 PL energy. In Figs. 5.3d and 5.3e, the entrance and exit slits of the spectrometer were opened up to the point where the spectral bandpass of the spectrometer exceeded the splitting of the P_0^0 components. In this way both P_0^0 components could be monitored in the same scan and the relative effect of polarization of the excitation beam could be determined. The polarization dependences of the other principal stress directions are summarized in Fig. 5.4 and will be discussed below.

Fig. 5.5 is a summary of the stress splittings for all three principal stress directions. The P_0^0 stress splittings agree well with the PL data presented in Chapt. 4. As in the case of the PLE data under <111> stress, excitation into a given P_0^0 or P_2^0 stress-split component only occured if the

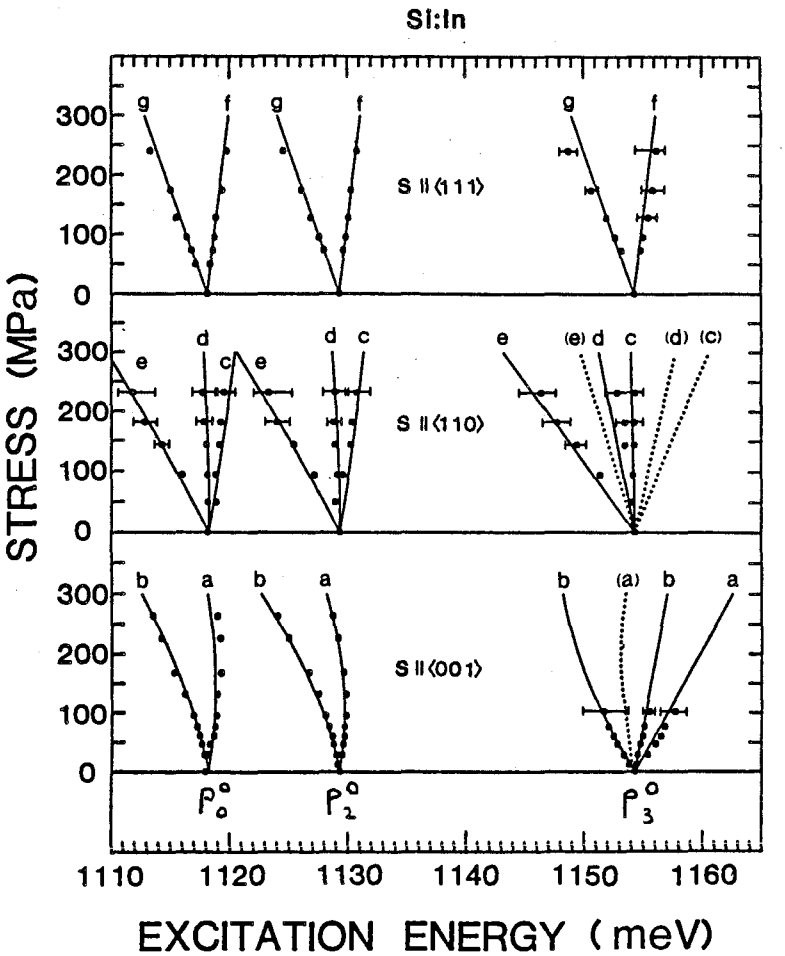

Fig. 5.5 : Summary of the stress splittings of the three principal lines for stresses along the three main crystal axes. For ⟨111⟩ stress all three lines split with roughly the same shift rate. For ⟨001⟩ stress P_0^0 and P_2^0 split in a similar fashion, although the P_2^0 splitting is more nonlinear. In addition, P_3^0 shows extra degeneracy consistent with a Γ_3 (T_d) electron excited state. Lines represent fits using the simple valley-orbit model described in the text. Dotted lines are predicted lines which are not observed in practice, probably due to the large broadenings due to the resonance or near resonance of P_3^0 components with free exciton states.

corresponding P_0^0 PL component was monitored, confirming that these splittings are purely orientational. Unfortunately the <110> stress data were somewhat broadened by inhomogeneous stress, which is reflected in the broad linewidths indicated by the error bars, but comparison with the previous PL data do not indicate a large discrepancy in the energy splittings. For the other stress directions, the stress homogeneity was very good and yielded P_0^0 PL linewidths of no greater than 0.4 meV up to the maximum applied stress.

The similarities of the splitting patterns for the P_0^0 and P_2^0 lines are consistent with the proposal of this thesis that these two lines originate from the recombination of excitons with the same electron and hole states, but with symmetric and antisymmetric total spin functions respectively.

It was shown that the <111> stress splittings of the P_3^0 line are essentially the same as those of the two lower energy lines. Under <001> stress however the P_3^0 transition splits into three readily observable components: a sharp central peak whose absorption strength is enhanced when monitoring the lower P_0^0 PL transition, and two broader lines to higher and lower energies. The extra degeneracy of this line is clearly revealed in the spectra of Fig. 5.6 in which the P_0^0 emission is monitored with the spectrometer slits opened to include both PL components. Given the similarity in splitting rate of the upper two P_3^0 components to the P_0^0 and P_2^0 rates it is likely that these two P_3^0 components correspond to the lifting of the same orientational degeneracy but with an additional upward shift of

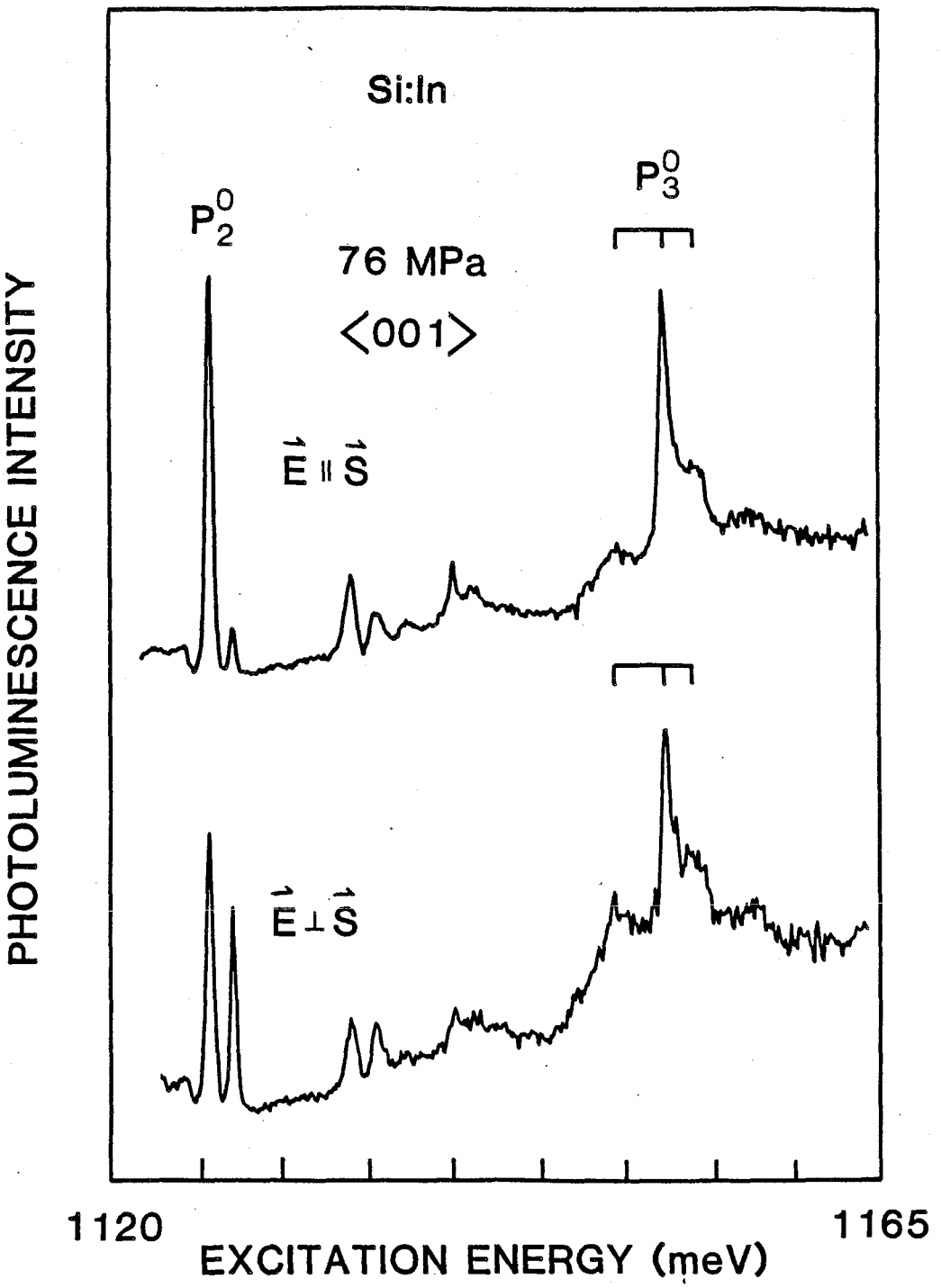

Fig. 5.6: Si:In excitation spectra under <001> stress showing the appearance of three components for P_3^0 rather than two for P_0^0 and P_2^0. In these spectra the P_0^0 line was monitored with the spectrometer slits opened to include both stress components.

their centre of gravity, and that the extra line represents a splitting due to an additional electronic degeneracy of the bound electron. At stresses above 100 MPa the P_3^0 line is soon lost in the rapidly shifting free exciton edge.

The ⟨110⟩ splittings of P_3^0 were rather obscured by the broadening of these lines due to stress inhomogeneities. Nevertheless three principal components were observed, and their shift rates correlate fairly well with those of P_0^0 and P_2^0, except for a centre of gravity shift to lower energy. In addition there is some weak structure to higher energy that again indicates extra electronic degeneracy.

5.3: Defect symmetry

The stress splittings of the P_0^0 and P_2^0 transitions in Fig. 5.5 are consistent with the removal of the orientational degeneracy of a rhombic I defect imbedded in a cubic lattice. The point group of such a defect is C_{2v}, consisting of a two-fold axis labelled Z along an ⟨001⟩ or equivalent axis and two reflection planes whose normals, labelled X and Y, are perpendicular to that axis and lie along the ⟨110⟩ and ⟨1$\bar{1}$0⟩ or equivalent axes. Such a defect has six equivalent orientations in an unstrained crystal. Under external stress some of these orientations become inequivalent. For ⟨111⟩, ⟨110⟩, and ⟨001⟩ stresses there are respectively two, three, and two inequivalent classes, in agreement with the number of components observed for the P_0^0 and P_2^0 transitions. Kaplyanski (1964) has derived

phenomenological shift expressions which parametrize the shift rates of optical transitions between nondegenerate levels of centres with orientational degeneracy, based solely on the kind of symmetry arguments presented in Chapt. 1.4, and the assumption that the perturbing potential is a-linear function of the stress tensor. For a rhombic I centre all seven shift rates were shown in Chapt. 1.4 to depend linearly on only three parameters, A_1, A_2, and A_3. The shift rate expressions are given in Table 5.1 together with the P_0^0 components to which they correspond. Also listed are the number of equivalent orientations within each subcomponent. These should be reflected in the relative intensities of the PL subcomponents of the P_0^0 line. This is observed to be the case for low stresses although some stress induced reorientation to the lower energy configurations appears to occur at higher stresses (Watkins and Thewalt, 1985). The experimental shift rates listed in Table 5.1 represent the linear component of the least squared fits to the data in Fig. 5.5. The method by which these fits were obtained will be described below. The A_i values quoted in the Table are those which best reproduce the observed shifts. The relatively close agreement confirms the correctness of the C_{2v} designation. It is interesting to note that these shift rates are very close to those obtained by Clifton et al. (1984) for the case of the 875 meV Ga-related PL transition in electron-irradiated Si:Ga, for which C_{2v} symmetry was also deduced.

Stress	Component	Energy	Shift Rate (meV/MPa)	
			Measured	Calculated
<001>	a (2)	A_1	7.5	7.0
	b (4)	A_2	-10.4	-11.3
<110>	c (1)	A_2-A_3	9.0	6.4
	d (4)	$(A_1+A_2)/2$	0.0	-2.2
	e (1)	A_2+A_3	-27.0	-29.1
<111>	e (3)	$(A_1+2A_2-2A_3)/3$	5.9	6.6
	f (3)	$(A_1+2A_2+2A_3)/3$	-17.8	-17.1

Table 5.1: This table shows the shift rates predicted on simple symmetry grounds for a rhombic I (C_{2v}) center in a cubic crystal. The letters "a" to "g" label each of the stress components in Fig. 5.5. The best fit to the seven experimentally observed shift rates was obtained with A_1= 7.0 meV/MPa, A_2= -11.3 meV/MPa, and A_3= -17.8 meV/MPa.[1]

5.4: Lowest-lying exciton states

The Zeeman data obtained with PLE confirm that the hole behaves essentially like a spin $\frac{1}{2}$ particle in its coupling to the electron states. This was shown in Chapt. 4 to imply that the orbital angular momentum of the hole is "quenched" (Dean and Herbert, 1979). This requires that the lowest hole state is derived from a single p-state with negligible admixture of the others. It is often stated (Gislason et al., 1982; Monemar et al., 1982) that a compressional sign of the local strain field is required to produce such a hole state at lowest energy, but this is true only for strain fields with relatively high symmetry e.g. C_{3v} or D_{2h}. A C_{2v} strain field of sufficient strength will always produce such a hole state at lowest energy regardless of the sign of the field, guaranteeing that the hole orbital angular momentum will be quenched, assuming that the spin-orbit coupling constant is relatively small compared with the internal strain perturbation.

The particular p-state which lies lowest in hole energy is determined by the relative magnitudes of the shear components of the C_{2v} biaxial crystal field. In order to reproduce the polarization results of Figs. 5.2 and 5.4, it was assumed that the hole state is derived from either the p_X or p_Y hole states, i.e. not from the hole state which is associated with the two-fold Z axis of the defect. Specifically, it was assumed that the hole state was p_X, which transforms as the group representation Γ_2 in C_{2v}, while the electron was assumed to transform

as the Γ_1 (C_{2v}) state derived from the lowest valley-orbit electron state. The spin of both particles transforms as the Γ_5 (C_{2v}) double group. Coupling of the two spin functions together with the electron and hole Γ_1 and Γ_2 orbital wavefunctions according to the prescription of Koster et al. (1963) leads to the following exciton product states which transform as the four 1-d representations of C_{2v} namely:

$$\Gamma_2: \quad \Psi_2 = p_X(\uparrow\downarrow - \downarrow\uparrow) \qquad (P_2^0) \qquad [5.1a]$$

$$\begin{aligned} \Gamma_1: &\quad \Psi_1 = p_X(\uparrow\uparrow + \downarrow\downarrow) \\ \Gamma_3: &\quad \Psi_3 = p_X(\uparrow\uparrow - \downarrow\downarrow) \qquad (P_0^0) \\ \Gamma_4: &\quad \Psi_4 = p_X(\uparrow\downarrow + \downarrow\uparrow). \end{aligned} \qquad [5.1b]$$

j-j coupling is included by a term of the form:

$$E_{jj} = \Delta \underline{S}_h \cdot \underline{S}_e$$

where $\underline{S}_h$ and $\underline{S}_e$ are the hole and electron spin operators and Δ is a constant. This leads to a splitting of the exciton ground state into a Γ_2 antisymmetric singlet and the remaining three symmetric basis functions which are partners of a nearly degenerate spin triplet. The orthorhombic splitting of this triplet state, which is in principle possible, must be so small as to be unobservable by optical measurements alone. This splitting could possibly be resolved by optically detected magnetic

resonance (e.g. Cavenett, 1981), as was done for the closely related 1911 meV centre in GaP (Gislason et al.,1982). The j-j coupling energy, Δ is given by the P_2^0-to-P_0^0 singlet-to-triplet splitting of 11.4 meV.

In the absence of external fields, transitions from the Γ_2 singlet bound exciton state to the Γ_1 crystal ground state are dipole-allowed for radiation with the electric vector parallel to the X axis. Transitions from the Γ_1 and Γ_4 components of the bound exciton triplet state are allowed for radiation with the electric vector parallel to the Z and Y axes while transitions from the Γ_3 component are dipole-forbidden. To obtain the selection rules under an applied magnetic field, one treats the triplet levels as strictly degenerate and looks for the linear combinations of the three unperturbed basis functions in [5.1b] which diagonalize the linear Zeeman Hamiltonian. In the case of quenched hole angular momentum that Hamiltonian is just $H_{LZ}=\mu_B g_h \underline{B}\cdot\underline{S}$, where $\underline{S}$ is the total spin angular momentum, $\underline{S}=\underline{S}_h+\underline{S}_e$, and $g_h\sim 2$. In the [5.1] basis the Zeeman Hamiltonian for the P_0^0 triplet is given by

$$\begin{array}{c} \quad |\Psi_1\rangle \quad\quad |\Psi_3\rangle \quad\quad |\Psi_4\rangle \\ \mu_B\hbar \begin{bmatrix} 0 & \gamma B_z & \gamma B_x \\ \gamma B_z & 0 & -i\gamma B_y \\ \gamma B_x & i\gamma B_y & 0 \end{bmatrix} \end{array} \qquad [5.2]$$

The linear combinations of the Ψ_i states which diagonalize [5.2] are easily calculated for an arbitrary $\underline{B}$-field direction and

yield the standard energy eigenvalues, $+\mu_B B\hbar$, 0, and $-\mu_B B\hbar$. For an arbitrary $\underline{B}$-field direction, there are up to six inequivalent orientations of a C_{2v} defect, each with different admixtures of Γ_1, Γ_3, and Γ_4. Computation of the polarization dependence of the Zeeman splittings of the P_0^0 triplet ground state consists of evaluating the squared matrix elements, $|\langle\Gamma_1|e\underline{E}\cdot\underline{r}|\underline{\Psi}_i\rangle|^2$, where $\underline{\Psi}_i$ are the linear combinations of the Ψ_i states in [5.1b] which diagonalize the Zeeman Hamiltonian for a particular defect orientation. The results of this calculation are indicated in Fig. 5.2 by vertical bars under the experimental data. This simple theory predicts the qualitative behaviour of the data, namely that the central component has a higher oscillator strength for transitions with the E-vector perpendicular to the field than with it parallel, while the reverse obtains for the outer components. This behaviour is the opposite of that expected for transitions from a pure spin triplet to a spin singlet in a system with full rotation symmetry. It is also at variance with the result obtained by assuming a p_z hole state in the calculation.

The treatment of the stress polarization data is simpler since the stress field cannot mix states which differ only in their spin functions. The simplest case is the Γ_2 singlet (the final state of the P_2^0 absorption transition), which has no spin degeneracy. In this case, the linear combination of states which diagonalizes the stress perturbation is just the Γ_2 state itself. The transition probability for absorption of light with the electric vector $\underline{E}$ at a given defect is proportional to the

square of the component of $\underline{E}$ along the dipole axis of the centre, which is the X axis for the case of Γ_1 to Γ_2 transitions. Kaplyanski (1964) has compiled tables of the expected polarization dependences of optical transitions between nondegenerate levels at orientationally degenerate centres in cubic crystals using the above method. For a rhombic I defect, two different polarization dependences are predicted depending on whether the dipole axis of the final state level (i.e. the exciton) is parallel (σ) or perpendicular (π) to the n-fold rotation axis of the defect (a Γ_1 initial state is assumed here). The Γ_1 to Γ_2 transition corresponds to a π transition in Kaplyanski's terminology. The experimental polarization results for the P_2^0 transition are given in Fig. 5.4 for the electric field vector parallel and perpendicular to the applied stress direction. Also shown are the predicted relative intensity ratios based on the above simple model. These are summarized in Table 5.2. All data are shown for an excitation beam propagating approximately parallel to the ⟨110⟩ axis. The qualitative features of the predicted splittings are observed. There is some enhancement of the low energy ⟨111⟩ and ⟨110⟩ components which may be due to the stress induced reorientation which is observed in PL. The agreement is quite poor for the ⟨110⟩ data, for which direction the stress was known to be somewhat inhomogeneous.

The stress dependence of the P_0^0 transition is complicated by the fact that it has a triplet final state (in absorption) consisting of two representations Γ_1 and Γ_4, transforming

as Z and Y, to which transitions from the Γ_1 crystal ground state are dipole-allowed, and a Γ_3 state, to which transitions are dipole-forbidden. The two allowed transitions should show the polarization dependence of a σ and a π dipole respectively in the terminology of Kaplyanski (1964) (see Table 5.2). The polarization data of Fig. 5.4 however are more consistent with the behaviour of a σ transition alone i.e. with the behaviour of a single Γ_1 to Γ_1 transition. There appears to be no explanation for this discrepancy at the moment, but the important point is that the P_0^0 polarization dependence is substantially different from that of P_2^0, and the change is in the direction predicted by the above simple model. It is worthwhile to point out that the measurement of stress-induced polarization dependences in Si with its high index of refraction are notoriously difficult due to multiple internal reflections and can often be misleading.

Oscillator strengths under zero field

The above simple model makes definite predictions about the oscillator strength ratio between the P_0^0 and P_2^0 transitions. The observation that these two transitions couple identically to the same 8.3 meV anti-Stokes phonon mode confirms the conclusion that these two lines are derived from the same electronic states and differ only in the symmetry of their total spin functions, since otherwise one might expect markedly different coupling to phonons. The relative intensities of the two

(a) Dipole-allowed transitions in C_{2v}

Transition	Transforms as	Kaplyanski designation
(P_2^0) $\Gamma_2 \rightarrow \Gamma_1$	X	π
(P_0^0) $\Gamma_1 \rightarrow \Gamma_1$	Z	σ
(P_0^0) $\Gamma_4 \rightarrow \Gamma_1$	Y	π

(b): Polarization properties

	⟨001⟩		⟨111⟩		⟨110⟩	
	Energy	$I_{\parallel}:I_{\perp}$	Energy	$I_{\parallel}:I_{\perp}$	Energy	$I_{110}:I_{001}:I_{1\bar{1}0}$
σ:	A_2	0:1	$\frac{1}{3}(A_1+2A_2+2A_3)$	1:1	A_2+A_3	0 : 1 : 0
	A_1	1:0	$\frac{1}{3}(A_1+2A_2-2A_3)$	1:1	$\frac{1}{2}(A_1+A_2)$	2 : 0 : $\pm$2
					A_2-A_3	0 : 1 : 0
π:	A_2	2:1	$\frac{1}{3}(A_1+2A_2+2A_3)$	4:1	A_2+A_3	1 : 0 : 0
	A_1	0:1	$\frac{1}{3}(A_1+2A_2-2A_3)$	0:3	$\frac{1}{2}(A_1+A_2)$	1 : 2 : 0
					A_2-A_3	0 : 0 : 1

Table 5.2: (a) shows the designations of the experimental lines within the simple theory of Kaplyanski (1964). (b) shows the predicted polarization dependence of "π" and "σ" transitions for the three principal stress axes. The A_i parameters are the same as in Table 5.1. The behaviour of P_0^0 is expected to be a superposition of a π and a σ transition. In fact its behaviour as shown in Fig. 5.4 is more in line with a σ transition alone.

transitions under zero field can therefore be modelled by considering only electronic matrix elements.

The transition probability for dipole-allowed transitions is of the form

$$|\langle\Gamma_1|\underline{E}\cdot\underline{r}|\Psi_i\rangle|^2$$

where $\langle\Gamma_1|$ is the crystal ground state whose orbital and spin parts belong to the totally symmetric representation, $\underline{E}$ is the electric vector of the incident light, $\underline{r}$ is the dipole operator, and the $|\Psi_i\rangle$ are as in [5.1]. There can be only two kinds of nonzero matrix elements. For the singlet these are of the form

$$|\langle\Gamma_1|X|p_X\rangle|(\uparrow\downarrow-\downarrow\uparrow)\rangle|^2|E_X|^2$$

where X is referred to the defect axes. For the triplet the nonzero elements are of the form

$$|\langle\Gamma_1|Z|p_X\rangle|(\uparrow\uparrow+\downarrow\downarrow)\rangle|^2|E_Z|^2$$
$$|\langle\Gamma_1|Y|p_X\rangle|(\uparrow\downarrow+\downarrow\uparrow)\rangle|^2|E_Z|^2$$

which are considerably reduced from the singlet. These elements have been calculated here for the case of an unpolarized beam normal to a <110> plane of the crystal. When all possible defect orientations are included, one obtains a transition probability ratio $I_{singlet}/I_{triplet}= 4.9$ which is in reasonable agreement with the observed ratio of ~3. This is different from the case of singlet-triplet transitions at a centre with full rotational symmetry, for which the ratio is very large since transitions from a spin triplet would be dipole-forbidden.

The observed photoluminescence lifetime of the Si:In defect is 230 μs (Thewalt et al, 1982). If this is taken as the radiative lifetime of the P_0^0 transition then the above indicates a lifetime for the P_2^0 transition of 40-70 μs. This is rather large for a supposedly dipole-allowed transition. Similar discrepancies are observed in other isoelectronic centres in Si and GaP.

5.5: Valley-orbit effects

In the PL stress measurements on the P_0^0 line of Chapt. 4, a definite nonlinearity in the shift rate of the <001> data was observed. This was ascribed to the effects of valley-orbit mixing of the Γ_1 electron state of the exciton ground state with a higher-lying, at that point unidentified, Γ_3 (T_d) electron excited state. Based on the assumption of the free electron deformation potential, Ξ_u, and the use of unperturbed T_d electron states, a valley-orbit splitting energy $6\Delta_c$ of the order of 60 meV was derived. In view of the stress data obtained with PLE, it is now proposed that the P_3^0 transition may be identified with the Γ_3 (T_d) excited state of the electron, and that the reduced valley-orbit energy which this implies is consistent with a reduced value of the deformation potential in the vicinity of the defect.

For the moment, it will be assumed that all the electron states have T_d symmetry. This is a reasonable approximation if the P_3^0 line is due to a Γ_3 electron, since such a state has a

node in the central cell and would not feel the C_{2v} defect field too strongly. For the P_0^0 and P_2^0 states, which are assumed to derive from Γ_1 electron states, this approximation probably has less validity. The difference in the extent to which the Γ_1 and Γ_3 electron states sample the core immediately explains the presence of the large j-j coupling splitting between the P_0^0 triplet and the P_2^0 singlet, and the apparent lack of any such splitting of the P_3^0 level. If it is assumed that the no-phonon oscillator strength for these transitions derives largely from the high localization of the bound hole, then the increased strength of the P_3^0 transition is just a reflection of the much higher degeneracy of this level due to the absence of an exchange splitting and the extra electron degeneracy. The above model for the Si:In energy levels is summarized in Fig. 5.7.

The similarity of the splitting patterns of all three lines under ⟨111⟩ stress (Fig. 5.5) agrees with the fact that such stress shifts all conduction band valleys linearly by the same amount. The solid lines through the ⟨111⟩ data in Fig. 5.5 have slopes given by a simultaneous least squares fit to the P_0^0 and P_2^0 data, and are seen to give an adequate fit to the P_3^0 data. Under ⟨001⟩ stress, a stress-induced mixing should occur between the Γ_1 and Γ_3 levels (Wilson and Feher, 1961). This mixing introduces a nonlinearity into the ⟨001⟩ shift rates which increases with decreasing valley-orbit interaction energy. This nicely accounts for the increase in curvature of the P_2^0 shift rates relative to those of P_0^0. According to the above model the measured spectroscopic splitting between P_3^0 and the

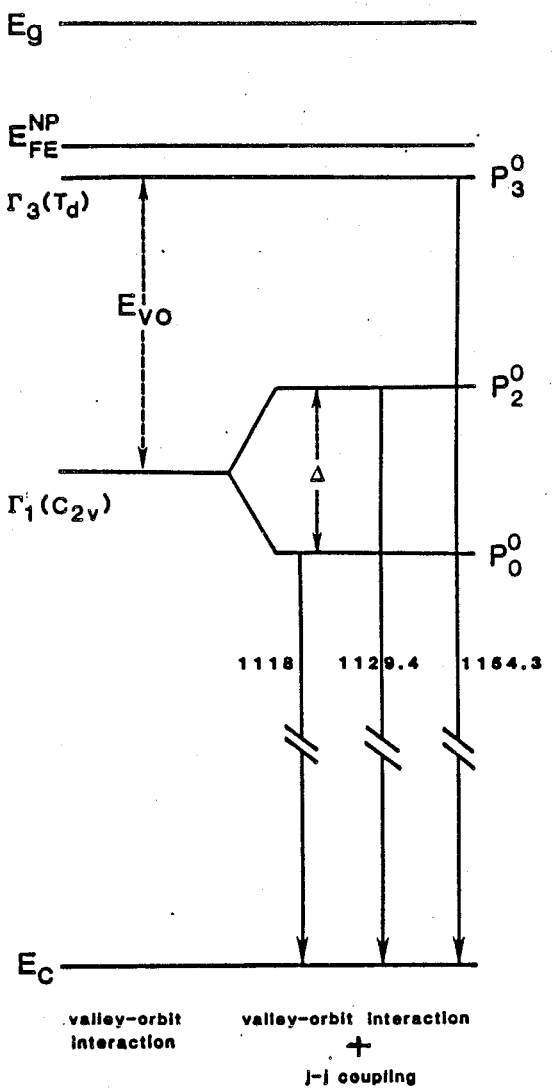

Fig. 5.7: Energy levels of excitons bound to the Si:In P-centre, measured relative to the crystal ground state energy, E_c=0. The P_0^0 and P_2^0 lines are derived from the 1s Γ_1 valley-orbit electron state, while P_3^0 is derived from the 1s Γ_3 state. The Γ_3 state is in principle split by the internal axial field of the defect, but this effect is presumed to be negligible since this state has a node at the central cell. P_0^0 and P_2^0 are the singlet-triplet partners of the exciton ground state, split by j-j coupling of the hole and electron. No such coupling is observed for the P_3^0 transition, since the electron has no amplitude at the central cell. The energy of the P_3^0 transition is just 0.3 meV below the free exciton no-phonon energy E_{FE}^{NP}, or 15 meV below the 4.2 K bandgap energy, E_g. The energies of the predominant PLE transitions are given in meV.

other two lower energy transitions directly gives the valley-orbit splitting energy, $6\Delta_c$ of the electron bound in either the antisymmetric P_0^0 ground state, or the symmetric P_2^0 state. In this model, the j-j coupling interaction between the electron and the hole is included into the central cell potential which scatters the electron into the various conduction band valleys.

The lines through the <001> data in Fig. 5.5 represent fits to the data points based on the shift expressions of Wilson and Feher (1961) for the valley-orbit states of electrons bound to substitutional donors in Si. The only free parameters in the fit are the orientational shift rates A_1 and A_2 from the preceding analysis, and the deformation potential for the conduction band electrons. The parameters A_1 and A_2 largely model the orientational shift rates of the hole state, and this is assumed to be a constant for all three exciton transitions. The A_i values thus obtained are the experimental <001> shift rates quoted in Table 5.1. The values of $6\Delta_c$ were derived from the spectroscopic splittings of the P_0^0 and P_2^0 states relative to the P_3^0 transition, respectively 36.3 meV and 24.9 meV, giving a mean value of 30.6 meV in the absence of the j-j coupling interaction. In this simple model the two upper components of the P_3^0 line which are observed under <001> stress are assumed to arise from the two different defect orientations of a rhombic I defect, labelled 'a' and 'b' in Fig. 5.5. The upward shift of these levels reflects the fact that they are derived solely from the four upward-shifting conduction band valleys. This model predicts two additional lines at lower energy, but

only one is unambiguously identified. The expected position of the extra line is indicated by the dotted line in Fig. 5.5. Like the upper P_3^0 component, the lower one is so broad that it could easily contain a weak unresolved extra component (see Fig. 5.6). Cohen and Sturge (1977) also reported considerable broadening of excitation lines of excited states of the NN_i pairs in GaP for i>7. These excitation lines also overlapped the free exciton continuum. The value of the electron deformation potential Ξ_u which produces the best fit is 6200 meV, which is considerably reduced from the value deduced from the far-infrared spectroscopy of shallow odd-parity donor levels, namely 8770 meV (Tekippe et al., 1972). This value is consistent with an observed reduction of Ξ_u for Γ_1 states in the deeper substitutional donors in Si (Tekippe et al., 1972). This reduction suggests that the lattice is somewhat "stiffer" in its response to stress in the vicinity of the defect.

A <110> stress is similarly expected to remove some of the electronic degeneracy of the P_3^0 electron state. The lines through the P_3^0 data in Fig. 5.5 represent the predictions of the above simple model in the case of <110> stress, using the same deformation potential but using three different orientational shift parameters to model the linear shift rates. These are the experimental shift rates quoted in Table 5.1. As in the case of the <001> data, each of the three classes of orientationally distinct centres, labelled "c", "d", and "e", should show an additional two-fold splitting corresponding to the removal of some electronic degeneracy, but in practice only

the lowest components are clearly seen. There is evidence of some additional splitting at higher energies but the inhomogeneous stress coupled with the intrinsic wide linewidths of the P_3^0 components precludes positive identification.

It can be argued that the above description in terms of T_d symmetry is too simple and that, at the very least, one should attempt to include the effects of the local C_{2v} defect symmetry on the lowest lying electron states. The data have also been modelled, as a part of this study, assuming as an additional fitting parameter a constant internal strain field of the order of 10^{-3}, in the spirit of Davies (1984), and more recently Thonke et al. (1985). This procedure complicates the electron valley-orbit interaction matrix (Wilson and Feher, 1961) somewhat, and does not offer a significantly better fit to these data. The response of the Γ_1 states is still linear under <111> stress and nonlinear under <001> stress, but the nonlinearity differs for the two classes of defects under <001> stress. The data of Fig. 5.5 do not show this behaviour to a significant degree within the scatter of the data points.

Lack of an isolated hole bound state

The above data allow one to determine whether or not the Si:In isoelectronic defect is capable of binding an isolated hole, as required by the HTL model. It is known that the central cell potential of the acceptor is important in the binding of excitons to these defects. Presumably the excess

charge of the deep acceptor is neutralized by a nearby constituent, e.g. an interstitial donor, rendering the whole defect electrically neutral as in the case of the isoelectronic GaP:Cd-O, Zn-O defects. In the simple HTL binding scheme one might expect to see a shallow donor-like excited state spectrum of an electron bound in the Coulomb field of the hole, which is tightly bound by the hole attractive central cell potential of the defect. This is certainly not observed in the case of the Si:In defect. The average value of $6\Delta_c$=30.6 meV obtained for the valley-orbit energy of the electron should be compared to values of 13.01, 22.5, and 37.11 meV for P, As, and Bi donors respectively (Ramdas and Rodriguez, 1981). Thus the short-range attractive potential for the electron is relatively deep by comparison with the simple substitutional donors in Si. The designation of P_3^0 as due to an excited valley-orbit state of the 1S-like electron places the donor ionization limit very close to 31 meV above the P_3^0 energy according to effective mass theory, which is expected to give useful predictions for the higher lying electron states. This is well above the no-phonon free exciton edge and accounts for the observation that the thermal dissociation energy of the exciton is identical to the spectroscopic localization energy with respect to the free-exciton energy (Thewalt et al., 1982). This is different from the usual case of isoelectronic centres as described by Hopfield et al. (1966) in which the first bound particle has a bound state even in the absence of the second particle. In such centres e.g. the NN_i pairs in GaP with $i<8$, the binding energy

of the first bound particle is given by the difference between the total binding energy of the exciton ground state and the binding energy of the weakly bound particle as determined from the series limit of its excited states (Cohen and Sturge, 1977; see also Fig. 1.1). For the case of the In isoelectronic centre this binding energy would be negative, so it appears that the central cell potential of the In-related isoelectronic binding centre is not strong enough to bind a hole alone, and the HTL model is clearly not applicable. Similar effects are observed by Cohen and Sturge (1977) for the NN_i pairs with $i>7$.

Chapter 6: Discussion

Some of the conclusions obtained by performing excitation spectroscopy on the Si:In centres can be generalized to the Si:Tl P-centre data, for which PLE spectroscopy was not possible. By means of PL and PLE in conjunction with uniaxial stress, the defect symmetry of the Si:In defect was unambiguously determined to be C_{2v}. The stress splittings of the Si:Tl P-centres were quite similar in magnitude and form to those of the Si:In defect, implying C_{2v} symmetry also. The Zeeman behaviour of both systems was also quite similar, confirming a high degree of hole localization at a low symmetry C_{2v} defect which results in a complete quenching of the hole orbital angular momentum.

The model which emerges from these data is similar in some respects to that of the nearest-neighbour donor-acceptor pair IBE, GaP:Zn-O and Cd-O. The strong central cell potential provides a high degree of localization for the hole. The excess charge of the substitutional deep acceptor In or Tl is presumably neutralized by the presence of a nearby "donor" constituent which will be labelled *, which renders the whole complex electrically neutral. As in the case of the Zn-O defect (Chapt. 1), the isolated hole binding energy of the acceptor complex is reduced by an amount which can be thought of as the electrostatic potential energy between the bare acceptor-"donor" pair. Jaros and Brand (1976) have shown that this binding energy is extremely sensitive to axial displacements of the pair, and that

for small enough separations, the single particle bound state leaves the forbidden gap entirely. The Si:In excitation data showed that the In-* complex is not capable of binding a single hole, whereas the hole binding energy of substitutional In is known to be 157 meV.

In contrast to the above case, there is strong evidence for the existence of a single hole bound state for the Si:Tl P-centre. From measurements of the thermal quenching of the luminescence, Thewalt et al. (1982) deduced an electron binding energy to the localized hole of 47 meV. From the 104.5 meV spectroscopic binding energy of the exciton this implies a 72 meV binding energy for an isolated hole at the defect. This is considerably reduced from the 248 meV binding energy of a hole at an isolated Tl acceptor. In this case the electrostatic energy of the Tl-* pair is not large enough to completely offset the deep central cell potential of the Tl, contrary to the Si:In case.

Evidence for a strain field contribution to exciton binding

The Si:In data show clear evidence of the breakdown of the usual HTL exciton binding picture. In addition to the lack of a single particle bound state for the localized hole, the large value of the j-j coupling interaction implied by the singlet-triplet splitting, combined with the large valley-orbit splitting of the electron imply considerable localization of the electron as well. The large electron attractive potential is

most likely generated by the strain field which is expected to exist around such an extended defect. Monemar et al. (1982) and Gislason et al. (1982) have invoked a strain mechanism to account for the extreme localization of both particles which they observe in excitons bound to Cu-related isoelectronic defects in GaP. Gislason et al. (1982) reported an unusually large electron-hole j-j coupling energy of 91 meV, which can only be accounted for by a defect potential in which both particles are quite deeply bound.

A strain field can be attractive to both particles and could provide the extra binding energy which the above data require. Such a field arises from the internal hydrostatic and shear components generated by the relatively large defect components. In addition, lattice relaxation after exciton capture could enhance the effect of such a strain well. The phonon sidebands observed in PL (Fig. 3.3) are indicative of substantial lattice relaxation, especially for the Si:Tl A-centre for which virtually all of the binding energy is due to lattice relaxation. It is important to note however that a strain field is typically long-ranged, with a $1/r^3$ dependence, and it is not clear whether such a field could cause the large valley-orbit splitting indicated by the above data.

Unfortunately, the absence of excitation spectra for the Si:Tl centre precludes the direct determination of the j-j coupling splitting or valley-orbit energy for the P-centre configuration of this defect. At 20 K, an excited state denoted S is observed in PL (see Fig. 3.1) at 6.8 meV above the Si:Tl P_0^0

line (Thewalt et al., 1982). Thewalt et al. (1982) measured the thermal dependence of this line relative to the P_0^0 line. The intensity ratio followed an Arrhenius behaviour with an activation energy equal to the spectroscopic separation of the lines. Extrapolation of the thermal data to 1/T=0 shows that this line has an oscillator strength roughly 2-5 times that of the P_0^0 line, and it is therefore most likely the equivalent of the singlet transition P_2^0 in Si:Tl. This implies a reduced value of the j-j coupling energy Δ=6.8 meV. This value cannot be taken as firm however given that the magnetic behaviour of this line is not known.

Defect constituents

The observation of C_{2v} point group symmetry for the P-centres places rather severe constraints on any model for the microscopic structure of these defects. It is unlikely that the defect contains more than two binding centre components because this would, in general, lead to a point group symmetry lower than C_{2v}. The simplest model consists of substitutional In or Tl with some as yet unknown nearest neighbour donor impurity in the nearest T_d interstitial site (Fig. 6.1). This constituent must be quite mobile given the stress-induced reorientation observed in PL at 4.2 K (Fig. 4.8). This is not an unreasonable requirement. Haller et al. (1980) have shown that shallow donors and acceptors in Ge can complex with single and multiple hydrogen atoms which can tunnel between various interstitial

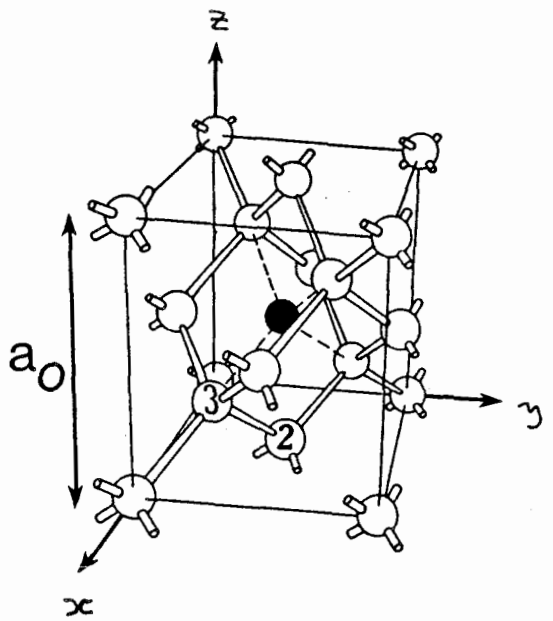

Fig. 6.1: Simple model which results in the observed C_{2v} and C_{3v} symmetries of the Si:In and Si:Tl IBE. For simple visualization the interstitial "donor" is fixed at a tetrahedral site with coordinates $a_0(1/2,1/2,1/2)$ where a_0 is the lattice parameter. Positioning the acceptor at the substitutional sites labelled 2 or 3 generates a defect with C_{2v} or C_{3v} symmetry respectively. Physically, it is the interstitial which moves a distance close to the bond length $\sqrt{3}a_0/4$ during the reorientation. In the absence of lattice relaxation the pair separation is $0.5a_0$ for the C_{2v} case and $0.43a_0$ for the C_{3v} case.

sites in the vicinity of the defect. In the present case the extra binding centre constituent is presumed to be less mobile and largely confined to a single interstitial site. The role of hydrogen in the In isoelectronic defects was briefly investigated in the present study by diffusion of atomic deuterium but without any observable result. Prior speculations by Sauer and Weber (1982) that extra component was an interstitial Fe donor were not supported by Schlesinger et al. (1983) who observed no isotope shift after doping with Fe^{54} and Fe^{56}.

The above model provides a plausible explanation for the structure of the A-centre configuration of the defect since a simple reorientation of the interstitial to another T_d interstitial site results in the observed C_{3v} symmetry of the A-centres as indicated in Fig. 6.1. The unrelaxed pair separations are similar for the two configurations, respectively $\sqrt{\frac{3}{4}}a_o \sim 0.43a_o$ for the C_{3v} defect and $\frac{1}{2}a_o$ for the C_{2v} defect, where a_o is the lattice parameter. The smaller pair separation for the case of the C_{3v} defect may explain the higher vibronic coupling of the A-centres compared with the P-centres, since the hole binding energy would be more sensitive to axial displacements.

A simple model for the Si:Tl rearrangement process is indicated in Fig. 6.2. Before exciton capture, the C_{3v} arrangement is preferred, perhaps because the electrostatic energy of the Tl-* pair is minimized for this configuration. The C_{2v} bare centre configuration is at higher energy, and is separated by a vibronic barrier, representing the barrier to movement of the interstitial (Fig. 6.2a). After exciton capture however, the

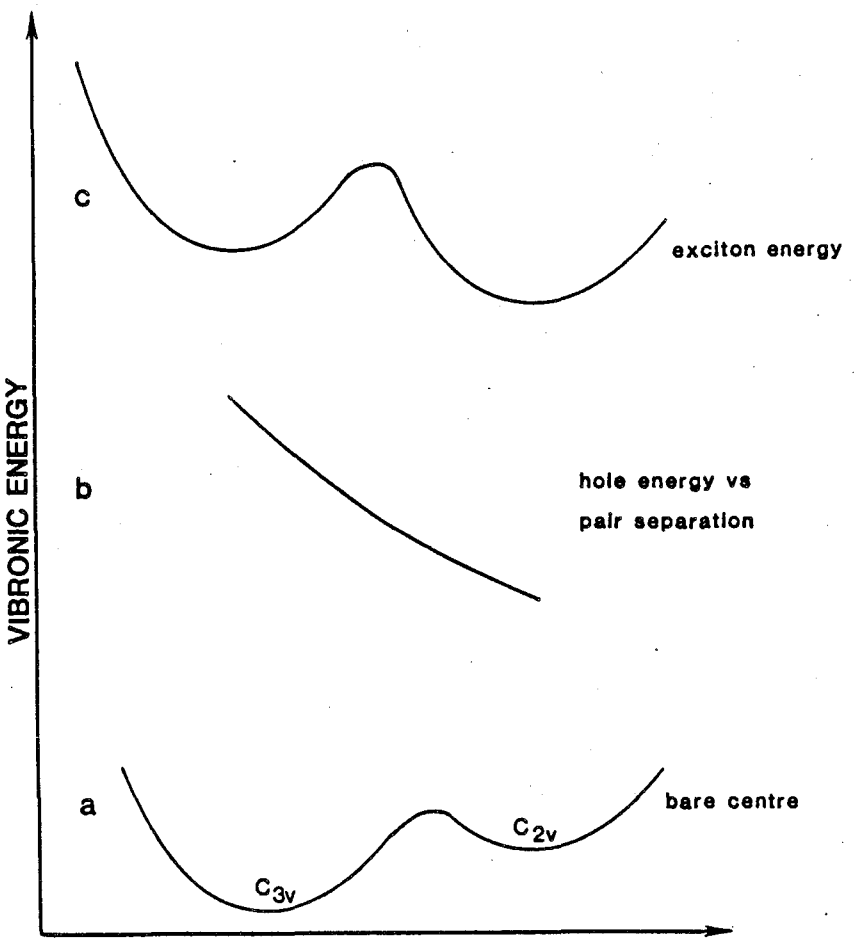

Fig. 6.2: Model for the Si:Tl bistability. In this model the C_{3v} configuration of the bare centre is favoured because the separation between the Tl-* pair, and hence their coulomb energy, is minimized (curve a). After Jaros and Brand (1976), curve b shows how the hole binding energy of the Tl impurity would depend on the Tl-* separation. This results in a reversal of the minima (curve c), with the result that the p-type exciton now has lowest energy. The energy barrier E_B is related to the barrier to movement of the interstitial from one T_d interstitial site to the other.

situation could be reversed because of the increase in hole binding energy (Fig. 6.2b) which can be achieved by an axial dilation of the Tl-* pair separation toward the C_{2v} configuration. Thus excitons are initially created in the C_{3v} configuration but can thermally overcome the vibronic barrier in Fig. 6.2c and relax to the C_{2v} configuration as indicated by the transient and spectral data of Thewalt et al. (1982), Watkins et al. (1984), and Watkins and Thewalt, (1985). The resulting configuration coordinate surface for the exciton is shown in Fig. 6.2c.

The situation is clearly different for the case of the Si:In defect given that there is no direct evidence for the existence of the C_{3v} defect configuration in this case. The transient data of Watkins et al. (1984) suggest that A- and P-type excitons are essentially degenerate (Chapt. 3) and that reorientation between the A- and P-configurations can proceed in both directions above 10 K. It appears that for the bare Si:In centre, the C_{2v} configuration is the lowest in energy, in contrast to the Si:Tl case. Indeed it is not clear whether there is a metastable C_{3v} configuration for the bare Si:In binding centre, and if there is, it must have an energy greater than or equal to that of the bare P-centre. This does not fit in with the above simple argument that the relative energies of the bare A- and P-centres should vary according to the electrostatic energy of the acceptor-* pair. This is not a serious objection however, since it is by no means proven that the electrostatic mechanism is operative in the Si:Tl case,

given the lack of knowledge of the other binding centre constituents.

Clifton et al. (1984) have recently reported on a defect observed in electron irradiated Ga-doped Si which also exhibits C_{2v} symmetry, with stress shift rates which are almost identical to those of the Si:In isoelectronic defect, even though the exciton is bound by the much larger energy of 295 meV. The presence of carbon has been determined by Thonke et al. (1985) by isotope doping. It is quite likely that these lines are due the recombination of isoelectronic bound excitons with a microscopic structure similar to that of the In- and Tl-related centres. Since the binding energy of the hole, and subsequently, the exciton, is very large, this centre could allow the opportunity to observe the entire range of excited electron states, beyond the 1S levels observed for the Si:In case. Unfortunately initial attempts to observe PLE spectra with the OPO system described in this work have been unsuccesful.

In conclusion, the stress, Zeeman, and excitation spectroscopy measurements undertaken in this study allowed for the first time a simple model of both the electronic states and the structure of the unusual In- and Tl-related isoelectronic bound excitons. There is enough evidence now, even in the absence of exact knowledge of the other binding centre constituent(s), to warrant detailed theoretical modelling of the defect. The Si:Tl defect is one of the few bistable semiconductor defects for which a wealth of experimental evidence regarding the structure

and electronic states is available. The understanding of bistable defects is presently very limited.

References

Allen J W, 1971, J. Phys. C 4, 1936.

Bains S K and Banbury P C, 1985, J. Phys. C, 18, L109.

Belt R F, Gashurov G, and Liu Y S, 1985, Laser Focus, October.

Boyd G D and Kleinman D A, 1968, J. Appl. Phys., 39, 3597.

Byer R L, 1975, in "Quantum Electronics", edited by H. Rabin and C.L. Tang,(Academic Press, New York).

Cavenett B C, 1981, Adv. Phys., 30, 475.

Chandrasekhar H R and Ramdas A K, 1975, Phys. Rev. B12, 5780.

Chromatix Inc., 1976, CMX-4/IR reference manual.

Clifton P, Davies G, and Lightowlers E C, 1984, J. Phys. C 17, 1889.

Cohen E and Sturge M D, 1977, Phys. Rev. B15, 1039.

Davies G, 1984, J. Phys. C 17, 6331.

Dean P J, Henry C H, and Frosch C J, 1968, Phys. Rev. 168, 812.

Dean P J, Cuthbert J D, and Lynch R T, 1969, 179, 754.

Dean P J, Faulkner R A, and Shonherr E G, 1970, Proc. 10th Int. Conf. on the Physics of Semiconductors (Springfield VA, US Atomic Energy Commission) p286.

Dean P J, 1971, Phys. Rev. B4, 2596.

Dean P J, and Herbert D C, 1979, in "Excitons", edited by K. Cho (Springer-Verlag,New York)

Faulkner R A, 1968, Phys. Rev. 175, 991.

Gil B, Camassel J, Merle P, and Mathieu H, 1981, Phys. Rev. B25, 3987.

Gislason H P, Monemar B, Dean P J, and Herbert D C, 1982, Phys. Rev. B 26, 827.

Haller E E, Joos B, Falicov L M, 1980, Phys. Rev. B21, 4729.

Ham F S, 1965, Phys. Rev. A138, 1727.

Henry C H, Dean P J, and Cuthbert J D, 1968, Phys. Rev. 166, 754.

Henry M O, Lightowlers E C, Killoran N, Dunstan D J, Cavenett B C, 1981, J. Phys. C 14, L255.

Henry M O, Moloney K A, Treacy J, Mulligan F J, and Lightowlers E C, 1984, J. Phys. C 17, 6245.

Hopfield J J, Thomas D G, and Lynch R T, 1966, Phys. Rev. Lett., 17, 312.

Hughes A E and Runciman W A, 1967, Proc. Phys. Soc., 90, 827.

Hung N and Brechignac P, Optics Commun., 1985, 53, 405.

Jaros M, and Brand S, 1976, Proc. 13th Int. Conf. Physics of Semiconductors, Rome (North-Holland, New York), p1090.

Jaros M, and Brand, S, 1979, J. Phys. C 12, 525.

Jaros M, 1982, "Deep levels in semiconductors" (Adam Hilger Ltd., Bristol).

Kaplyanski A A, 1964, Opt. Spectrosc. 16, 329.

Killoran N, Dunstan D J, Henry M O, Lightowlers E C, Cavenett B C, 1982, J. Phys. C 15, 6067.

Kohn W , Luttinger J M, 1955, Phys Rev. 98, 915.

Koster G F, Dimmock J O, Wheeler R G, and Statz H, 1963, "Properties of the thirty-two point groups" (M.I.T. Press, Cambridge, Massachusetts)

Labrie D, Timusk T, and Thewalt M L W, 1983, Phys. Rev. Lett., 52, 81.

Laude L D, Pollak F H, and Cardona M, 1971, Phys. Rev. B3, 2623.

Levinson M, 1983, Phys. Rev. B28, 3660.

Lightowlers E C, Canham L T, Davies G, Thewalt M L W, Watkins S P, 1984, Phys. Rev. B29, 4517.

Littman M G, 1978, Optics Lett., 3, 138.

Littman M G, 1984, Appl. Optics, 23, 4465.

Litton-Airtron Company, 1984, KTP specifications sheet, 200 E. Hanover Avenue, Morris Plains, N.J. 07950, Tel.:(201)-539-5500.

Mitchard G S, Lyon S A, Elliott K R, and McGill T C, 1979, Solid State Commun. 29, 425.

Mollenauer L F, 1980, Opt. Lett., 5, 188.

Monemar B, Gislason H P, Dean P J, and Herbert D C, 1982, Phys. Rev. B 25, 7719.

Morgan J W and Morgan T N, 1970, Phys. Rev. B1, 739.

Morgan T N, 1970, J. Luminescence, 1,2, 420.

Onton A, and Morgan T N, 1970, Phys. Rev. B1, 2592.

Ramdas A K, and Rodriguez S, 1981, Rep. Prog. Phys. 44, 1298.

Rome J J, Spry R J, Chandler T C, Brown G J, Covington B C, Harris R J, 1982, Pys. Rev. B25, 3615.

Sauer R, and Weber J, 1982, Proc. 12th Int. Conf. on Defects in Semiconductors, Amsterdam (North-Holland, Amsterdam, 1983).

Schlesinger T E, Hauenstein R J, Feenstra R M, McGill T C, 1983, Solid State Commun. 46, 321.

Shoshan I, Danon N, and Oppenheim U, 1977, J. Appl. Phys. 48, 4495.

Shoshan I and Oppenheim U P, 1978, Optics Commun., 25, 375.

Smith R G, 1973, IEEE J. Quantum Electron., QE-9, 530.

Stavola M, Levinson M, Benton J L, Kimerling L C, 1984, Phys. Rev. B30, 832.

Steiner T, 1986, Ph.D. thesis, unpublished.

Stoneham A M, 1975, "Theory of Defects in Solids", (Clarendon Press, Oxford).

Sturge M D, 1967, "Solid State Physics", (Academic Press, New York), vol. 20.

Tekippe V J, Chandrasekhar H R, Fisher P, and Ramdas A K, 1972, Phys. Rev. B6, 2348.

Thewalt M L W, Ziemelis U O, Parsons R R, 1981a, Solid State Commun., 39, 27.

Thewalt M L W, Ziemelis U O, Parsons R R, 1981b, Phys. Rev. B24, 3655.

Thewalt M L W, Watkins S P, Ziemelis U O, Lightowlers E C, and Henry M O, 1982a, Solid State Commun. 44, 573.

Thewalt M L W, Ziemelis U O, Watkins S P, and Parsons R R, 1982b, Can. J. Phys. 60, 1691.

Thomas D J and Hopfield J J, 1966, Phys. Rev. 150, 680.

Thonke K, Hangleiter A, Wagner J, and Sauer R, 1985, J. Phys. C. 18, L795 (1985).

Toyazawa Y, 1983, Physica 116B, 7.

Trumbore F A, Gershenzon M, and Thomas D G, 1966, Appl. Phys. Lett., 9, 4.

Wagner J, and Sauer R, 1982, Phys Rev. B 26, 3502.

Wagner J, and Sauer R, 1983, Phys. Rev. B 27, 6568.

Wagner J, Dornen A, and Sauer R, 1985, Phys. Rev. B 31, 5561.

Wallace R W, 1972, IEEE J. Quantum Electronics QE-8, 819.

Watkins S P, 1983, M.Sc. thesis, unpublished.

Watkins S P, Thewalt M L W, and Steiner T, 1984, Phys. Rev. B29, 5727.

Watkins S P and Thewalt M L W, 1985, Can. J. Phys. 63, 1074.

Weber J, Schmid W, and Sauer R, 1979, Phys. Rev. B, 21, 2401.

Wilson D K and Feher G, 1961, Phys. Rev. 124, 1068.

Yariv A, 1985, "Optical Electronics", (Holt, Rhinehart, and Winston, New York).